2014-06-12

Evaluation of Passive Force Behavior for Bridge Abutments Using Large-Scale Tests with Various Backfill Geometries

Jaycee Cornwall Smith
Brigham Young University - Provo

Evaluation of Passive Force Behavior for Bridge Abutments Using Large-Scale Tests with Various Backfill Geometries

Jaycee Cornwall Smith

A thesis submitted to the faculty of
Brigham Young University
in partial fulfillment of the requirements for the degree of

Master of Science

Kyle M. Rollins, Chair
Fernando S. Fonseca
Kevin W. Franke

Department of Civil and Environmental Engineering

Brigham Young University

June 2014

ABSTRACT

Evaluation of Passive Force Behavior for Bridge Abutments Using
Large-Scale Tests with Various Backfill Geometries

Jaycee Cornwall Smith
Department of Civil and Environmental Engineering, BYU
Master of Science

Bridge abutments are designed to withstand lateral pressures from thermal expansion and seismic forces. Current design curves have been seen to dangerously over- and under-estimate the peak passive resistance and corresponding deflection of abutment backfills. Similar studies on passive pressure have shown that passive resistance changes with different types of constructed backfills. The effects of changing the length to width ratio, or including MSE wingwalls determine passive force-deflection relationships. The purpose of this study is to determine the effects of the wall heights and of the MSE support on passive pressure and backfill failure, and to compare the field results with various predictive methods.

To compare the effects of backfill geometries, three large-scale tests with dense compact sand were performed with abutment backfill heights of 3 ft (0.91 m), 5.5 ft (1.68 m), and 5.5 ft (1.68 m) confined with MSE wingwalls. Using an existing pile cap 11 ft (3.35 m) wide and 5.5 ft (1.68 m) high, width to height ratios for the abutment backfills were 3.7 for the 3ft test, and 2.0 for the 5.5ft and MSE tests. The failure surface for the unconfined backfills exhibited a 3D geometry with failure surfaces extending beyond the edge of the cap, increasing the "effective width", and producing a failure "bulb". In contrast, the constraint provided by the MSE wingwalls produced a more 2D failure geometry. The "effective width" of the failure surface increased as the width to height ratio decreased. In terms of total passive force, the unconfined 5.5ft wall provided about 6% more resistance than the 5.5ft MSE wall. However, in terms of passive force/width the MSE wall provided about 70% more resistance than the unconfined wall, which is more consistent with a plane strain, or 2D, failure geometry. In comparison with predicted forces, the MSE curve never seemed to fit, while the 3ft and 5.5ft curves were better represented with different methods. Even with optimizing between both the unconfined curves, the predicted Log Spiral peak passive forces were most accurate, within 12% of the measured peak resistances. The components of passive force between the unconfined tests suggest the passive force is influenced more by frictional resistance and less by the cohesion as the height of the backwall increases.

Keywords: passive force, bridge abutment, large scale, skew, pile cap, lateral resistance, MSE wingwalls, mechanically stabilized earth, PYCAP, backwall height, geometry

ACKNOWLEDGEMENTS

I would like to acknowledge the following people who provided assistance in the completion of this thesis. Dr. Kyle M. Rollins who provided the project and secured the funds with which to make this study possible. With both of our busy lives, it is amazing that we actually got this thesis finished. His encouragement, support, feedback and insights for the past two years have been a tremendous help in analyzing data and composing this thesis. Dave Anderson and Rodney Mayo provided the field know-how for the summer work. They were both very willing to allow Katie and me opportunities to learn new skills, such as working with hand tools, electronics, and soldering.

I would also like to thank my research team: Bryan Franke, Aaron Marsh, and Katie Palmer. We all worked manual labor together in the field and data reduction in the lab. Due to their advice and help, analyzing and writing was much more enjoyable. The discussions and arguments in the grad lab on how to reduce certain data were very helpful; I learned to think for myself and to defend my assumptions and analysis procedures.

I know I would not have finished my degree without the support of my husband Charles Smith. He knew I could not give up what I started, even though my degree took longer than we planned. Through my schooling, we have had a wonderful marriage and love our little boy Austin who was born November 2013, in the middle of my last year in grad school. Also, my parents who, while they did not completely understand my thesis work, continued to ask about and encourage my progress. I also want to thank my Father in Heaven for giving me the opportunity to attend the Masters program at BYU; for allowing my life to be led by His hand and not my own. I have grown as a student, person, citizen, wife and mother.

TABLE OF CONTENTS

LIST OF TABLES

LIST OF FIGURES

1 INTRODUCTION

This document provides further analysis of the skewed bridge abutment tests performed over the summer of 2012. The effects of a skew angle on abutments with MSE walls, and with both 5.5ft and 3ft heights were previously analyzed by Franke (2013), Marsh (2013), and Palmer (2013), respectively. While skew angles were a large part of this research study, a lot of information can come from comparing the backfill heights as well. This thesis compares the different backfill types of the abutment tests with no applied skew angle. Due to the excessive comparisons and reference to the backfill heights as the names of the tests, the 3ft, 5.5ft, and MSE tests will be referred to as such without metric units. When height descriptions are needed, metric units will be provided. While the zero skew results can be found in the corresponding skewed abutment tests, the analysis provides distinct comparisons between different length-to-width abutment ratios and between unconfined and confined backfills.

1.1 Background

Bridge abutments are used to support a bridge crossing. Usually, the abutments consist of driven pile groupings overlain with a thick concrete block, or pile cap. A soil backfill is then compacted behind the cap to provide lateral resistance. Due to loads from thermal expansion, earthquakes, and strong winds, passive earth pressures may develop within the backfill. Passive pressures exceeding the soil resistance can cause failure of the bridge structure. Passive earth pressure equations commonly used to predict passive earth pressures include the Rankine,

Coulomb, and Log Spiral theories. Testing of non-skewed abutments on various backfills have shown that the Log Spiral theory comes closest to observed soil failure (Duncan and Mokwa 2001, Lemnitzer, et al. 2009, Rollins and Cole 2006, Rollins and Sparks 2002). Peak passive pressures were also seen to occur between 3% and 5% of the backwall (abutment) height (Rollins and Sparks 2002). Design criteria (AASHTO 2011, Caltrans 2010) for bridge abutments have been based on the results of previous tests. In most design criteria, skew angles are ignored and non-skew designs are implemented. Some specifications limit skew angles not to exceed 30° or less (Kunin and Alampalli 1999). Recent examples have shown that these predictions are overestimating the lateral resistance of the backfill and bridge failures are occurring with skewed bridges (Apirakyorapinit, et al. 2012, Elnashai, et al. 2010, Shamsabadi, et al. 2006, Unjohn 2012).

Recently, testing has been completed to analyze the effects of skew angles on bridge abutments. Rollins and Jessee (2012) conducted lab-scale tests which established passive force-deflection curves for bridge abutments at zero, fifteen, thirty, and forty-five degree skew angles. Numerical models were also analyzed by Shamsabadi, et al. (2006). Results of both studies warranted further research and so large-scale tests were conducted to validate the results. Tests were established to analyze various backfill mechanisms at skew angles of 0°, 15°, and 30°. Detailed analyses of the 3 ft (0.91 m) backfill, 5.5 ft (1.68 m) backfill, and 5.5 ft (1.68 m) backfill with mechanically stabilized earth (MSE) walls are discussed by Palmer (2013), Marsh (2013), and Franke (2013), respectively.

To further validate the large-scale skew tests and discover similarities between the heights of the backfill and the effects of MSE walls, a comparison of the backfill mechanisms

was also completed. This comparison is to provide information about the behavior of bridge abutments as abutment length vs. height ratios are changed and as MSE walls are implemented.

1.2 Research Objectives

The objectives of the research conducted are to:

(1) Determine and compare the failure geometry of abutment backfills with varying heights and with the effects of MSE wingwalls.

(2) Provide comparisons of the measured passive force of abutments with varying backfill heights and with the effects of MSE walls.

(3) Validate the developed procedures for predicting passive resistance for bridge abutments.

(4) Determine and compare the measured and computed passive force-displacement curves for bridge abutments with varying backfill types from large-scale tests.

1.3 Scope of Research

The research project focused on the effects of different skew-angled bridge abutments at different backfill heights and with the placement of MSE walls. To analyze this research effectively, the project included 10 large-scale tests with various skew degree (0°, 15°, 30°), and backfill height (3ft, 5.5ft, and with MSE wingwalls). Data were obtained with repetition and overlap to compare and validate the results. Recorded data included: passive force-deflection curves, pile cap displacement and rotation, pressure distribution, soil strain, and backfill failure surfaces. The data was then analyzed and reduced to be presented in multiple papers. Specific skewed abutment test results can be found in Marsh (2013), Palmer (2013), and Franke (2013).

This thesis will focus on the zero skew tests performed including the 3ft, 5.5ft, and MSE wall tests. Without including the skew angles, the effects of changing backfill parameters will be

compared. The three zero skew tests will be analyzed but most comparisons will be made between the two unconfined tests with different heights (3ft and 5.5ft), and between the 5.5ft unconfined and confined tests. To better relate with the other presented theses, some data and assumptions may overlap. However, the passive force analysis was determined with new parameters to better match the given curves as a whole. Finally, the developed passive force design curves and peak values are compared with the measured passive force-deflection curves. Expectations are to have similar failures between the height differences, and an increase in both force and displacement with backfill confinement. Also, the Log Spiral prediction method is expected to align most accurately with the measured curves.

2 LITERATURE REVIEW

This chapter covers the research that has previously been completed relating to the scope of this thesis. This includes multiple theories to predict passive earth pressures, analysis methods of the Log Spiral theory (Duncan and Mokwa 2001), previous testing and results on similar studies with pile caps and MSE wingwalls, seismic bridge design, and reports on skewed bridge abutments including recent examples of performance.

2.1 Passive Earth Pressures: Governing Factors, Theories, and Methods

Passive earth pressures develop when a body of soil is compressed. The resistance of the soil against the compelling force can be measured with displacement. The failure surface of the soil occurs along the shear, or weakest, plane when the soil inadequately resists the applied pressure. Differing theories have been established to predict the soil resistance and the location of the failure plane, including the Coulomb, Rankine, and Log Spiral theories. For this study, a large-scale pile cap was pushed into a soil backfill providing a compressive force to determine the soil resistance and failure surface of the backfill. The field values resulting from this test are compared with the predictive methods in Chapter 5.

2.1.1 Governing Factors

The published studies of lateral earth pressures began in 1776 with Coulomb and due to the unpredictability of soil behavior and recent considerations, new findings are still being published today. A paper published by Duncan and Mokwa (2001) pinpoints factors that affect the passive resistance of a soil as: the magnitude and direction of structure movement; soil strength and stiffness; structure to soil relationships, including friction and adhesion; and structure shape.

The magnitude and direction of the structure movement affects how the backfill soil behaves. Simultaneous horizontal and vertical soil movement occurs when passive resistance is not large enough to cause the structure to move upwards as well. Small structures, such as anchor blocks, tend to follow vertical soil movement (Ovesen 1964). Upward movement of the structure is prevented by using a heavy weight or supporting the structure with underlying piles, such as used with a pile cap. Figure 2.1(a) shows how the soil moves in this case. Restricted vertical movement was provided for the results of this project and as such, the same force assumptions were made as seen in Figure 2.1(b) and (c). The upward movement of the soil causes upward and downward shear forces on the structure and soil, respectively, resulting in a passive earth pressure E_p both acting in the direction of push and downward at an angle δ_{mob} from the horizontal (Duncan and Mokwa 2001). Loose, compressible soils require more movement to reach the passive state than dense, relatively incompressible soils (Clough and Duncan 1991, Cole and Rollins 2006).

The strength and stiffness of a soil also affects the forces needed to mobilize the backfill. Stronger soil resists a larger maximum passive force, where stiffer soil increases the passive

pressure at any given displacement. Shear strength depends on the effective stress and density of the soil, which can be defined by field compaction.

Interface friction depends on the roughness of the structure face and the properties of the soil (friction, density, cohesiveness). This is the angle δ_{mob} from the horizontal at which the passive pressure force is acting on the soil, causing the soil to separate from the structure. On large, stable structures such as a pile cap, the slip occurs at the interface. Based on a relationship study between soil friction angles ϕ and interface wall friction angles δ by Potyondy (1961), a range of $\delta/\phi = 0.6$ to 0.8 is used in current practice.

Another factor is the shape of the structure. Most theoretical methods – including Coulomb, Rankine, and Log Spiral – assume a 2-dimensional failure plane, assuming that the length of the structure-soil interface is indefinite. But most often this is not the case; the structure has boundary limits, such as a measured 11 ft (3.35 m) wide pile cap, which increases the amount of load that the soil can withstand. For finite wall lengths, the failure surface extends beyond the length of the backwall, mobilizing more backfill and resulting in a greater passive resistance (Cole and Rollins 2006). The Ovesen (1964) and Brinch Hansen (1966) method corrects for this with a 3D correction factor R_f. This value is limited to twice the calculated passive pressure.

The conducted project tested the shape of the structure by changing the backwall height and confining the backfill. All other governing factors were left the same: the pile cap was pushed at the same load increments; the backfill used throughout testing consisted of the same soil, compacted to similar values; and the friction and adhesion for interface between concrete and sand were assumed similar between tests. Each of these factors is addressed in each predictive method.

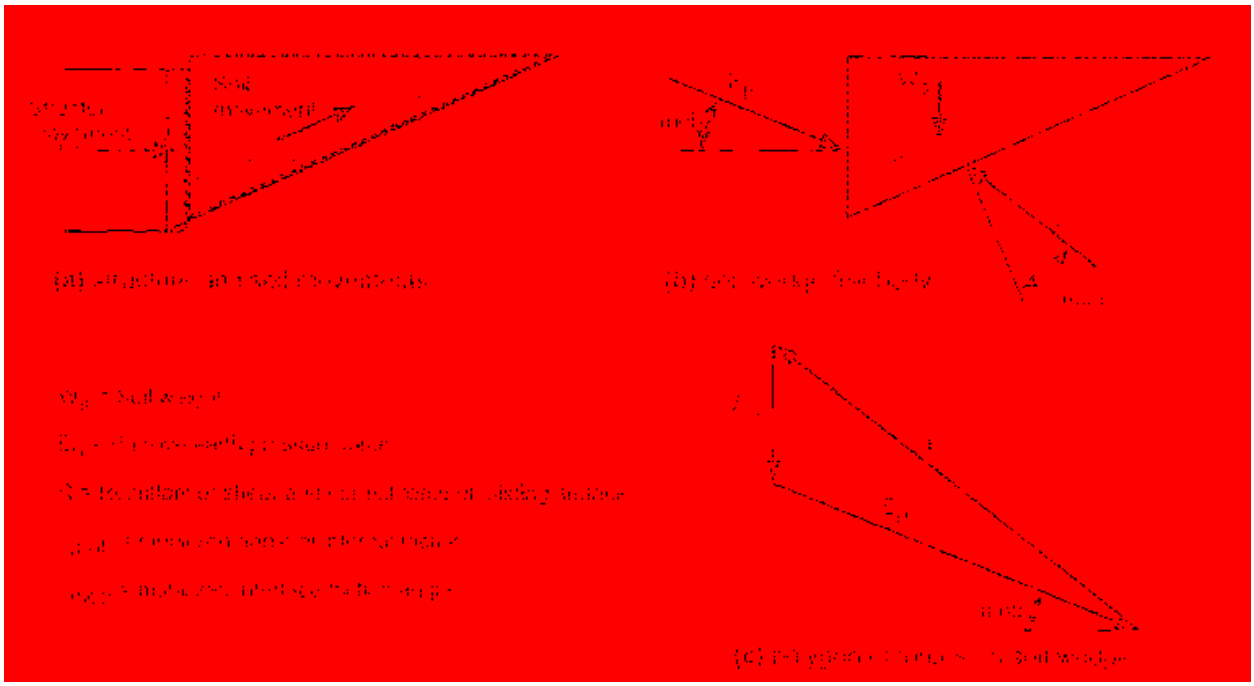

Figure 2.1: Movement of structure affecting soil movement (Duncan and Mokwa 2001)

2.1.2 Coulomb Method

Coulomb was the first to theorize the passive earth pressure on retaining structures in a paper he published in 1776 (Coulomb 1776). Coulomb's work is well-known and was summarized from a Principles of Geotechnical Engineering text book (Das 2010). The Coulomb method, as described in Figure 2.2, assumes a linear failure surface behind the backwall. Using parameters such as the interface friction angle δ', soil friction angle ϕ', soil unit weight γ, and height of the backwall H, the peak passive force P_p can be estimated, as exhibited in Equation (2.1). Studies over the years have limited the Coulomb method to low angles of interface friction (Terzaghi et al., 1996). Large angles over $0.4\phi'$ tend to overestimate the passive force.

$$P_p = \frac{1}{2} K_p \gamma H^2 \qquad \textbf{(2.1)}$$

where

P_p = passive force per unit length of wall; inclined at an angle $\delta'$to the normal of the

wall face that supports the soil
δ' = interface friction angle between soil and wall
K_p = Coulomb's passive earth-pressure coefficient, described as

$$= \frac{\cos^2(\phi' + \theta)}{\cos^2\theta \cos(\delta' - \theta)\left[1 - \sqrt{\frac{\sin(\phi'+\delta')\sin(\phi'+\alpha)}{\cos(\delta'-\theta)\cos(\alpha-\theta)}}\right]^2} \quad \textbf{(2.2)}$$

γ = the unit weight of the soil

H = the height of retaining wall

α = angle of inclined backfill

W = the weight of the soil wedge

F = the resultant of shear and normal forces on failure surface, *BC*; inclined at an angle of φ' to normal of *BC* plane

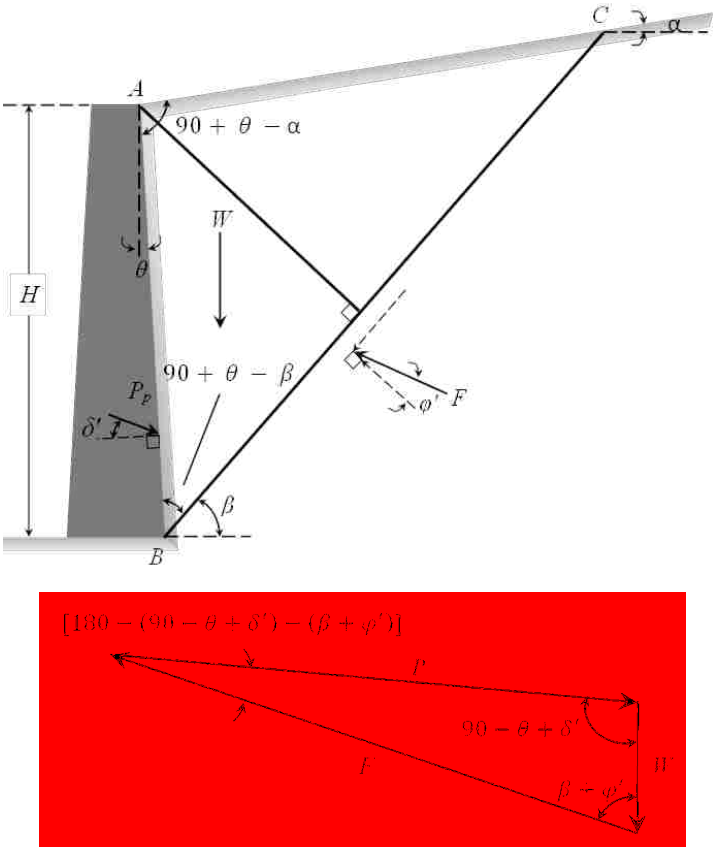

Figure 2.2: Coulomb's passive pressure trial failure wedge (top) and force polygon (bottom) (Das 2010)

2.1.3 Rankine Method

Rankine's theory is the simplest to calculate using many simplifying assumptions (Rankine 1857). Rankine's passive pressure is calculated using P_p as given in Equation (2.1) using a simpler K_p, when there is no inclined backfill ($\alpha = 0$), given as Equation (2.3). The soil friction angle ϕ is the only parameter needed to calculate Rankine's coefficient K_p, where Coulomb's coefficient also requires the interface friction angle δ', referred to in Equation (2.2).

$$K_p = \tan^2\left(45 + \frac{\phi}{2}\right) = \frac{1 + \sin\phi}{1 - \sin\phi} \quad \textbf{(2.3)}$$

where

$K_p =$ Rankine's passive earth pressure coefficient
$\phi =$ internal friction angle of soil

Rankine's theory has proven conservative for determining active pressure values and is regularly used in practice. In determining passive pressures, however, Rankine's theory greatly underestimates the passive pressure making the theory unsuitable for use in these circumstances (Duncan and Mokwa 2001).

2.1.4 Log Spiral Method

The Log Spiral theory does not assume a planar failure surface as do the Coulomb and Rankine theories. As seen in Figure 2.3, Terzaghi (1996) assumes a log spiral or circular arc curve beneath the base of the structure. Line *ab* is assumed to be a structure pushed into the soil mass behind it. The surface slides along *bde*. This line is separated into two zones, the curved *bd* and straight *de*. The linear wedge is the Rankine zone where the soil is in the passive Rankine state and there are no shearing stresses in the vertical direction at *f*, leaving the horizontal force E_{PR}. The curved side near the wall is the Prandtl zone, which incorporates the log spiral failure of the soil.

Assuming log spiral or arc of circle shape simplifies the means of obtaining the real sliding surface. Although this does not find the real surface plane, Terzaghi (1996) reports that after performing the more complicated equations, the accuracy is sufficient. The error between using the log spiral or arc of circle methods is negligible. For either method, Equation (2.4) can be used to determine the log spiral failure surface.

$$r = r_0 e^{\theta \tan \phi'} \quad \textbf{(2.4)}$$

Using the center of the spiral *O* on line *ad* at an angle of $45° - \frac{\phi'}{2}$ from the horizontal, every force *F*, ϕ' from the vertical, passes through point *O*. Using this assumption, Terzaghi (1996) then created a graphical method to determine the forces on the soil to overcome the normal P_p and shear C_a forces.

Though more complicated to compute, the Log Spiral method has proven to give a more accurate passive pressure estimation (Duncan and Mokwa 2001). To simplify the computational process, charts and computer programs were developed to apply and solve for passive earth pressures using the Log Spiral theory. For example, AASHTO (2011) uses charts in the LRFD code to estimate the K_p value used in the passive force Equation (2.1). Duncan and Mokwa (2001) established PYCAP, an Excel module which calculates and plots the passive force as a function of displacement. Shamsabadi, et al. (2007) developed another program entitled ABUTMENT to determine backfill soil capacity. These Log Spiral method applications are further explained in the following sections and compared to field results in Chapter 5.

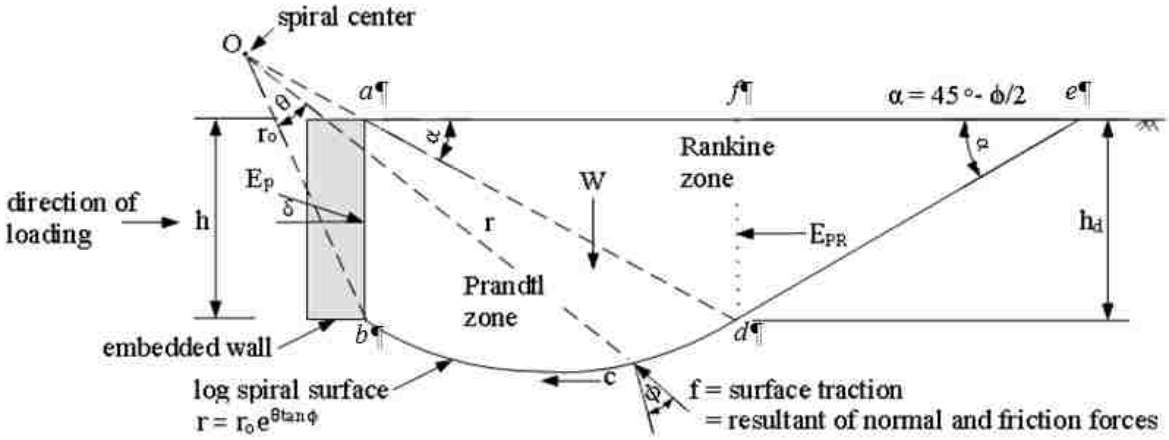

Figure 2.3: Log Spiral Passive Pressure Failure (Duncan and Mokwa 2001)

2.1.5 AASHTO LRFD Approach

The AASHTO (2011) method uses Equation (2.5) to determine the peak passive pressure for bridge design. The coefficient K_p is determined from Figures 3.11.5.4-1 or 3.5.11.4-2 in the 2011 Bridge Specification manual. For more information refer to the AASHTO LRFD Bridge Design Specification (2011) manual.

$$P_P = \left(\frac{1}{2}K_P\gamma_s H w_1 + 2c\sqrt{K_P}w_2\right)H\cos\delta \qquad \textbf{(2.5)}$$

where

P_p = horizontal component of the passive lateral earth pressure (ksf)
γ_s = unit weight of soil (kcf)
w_1 = effective width of failure wedge [see Ovesen (1964)]
w_2 = abutment width (ft)
c = soil cohesion (ksf)
H = abutment height (ft)
K_p = coefficient of passive earth pressure calculated as specified above

2.1.6 Caltrans Approach

The Caltrans (2010) method uses a bilinear approximation, as shown in Figure 2.4. Based on large-scale passive force tests on bridge abutments by Maroney (1995) and Stewart, et al. (2007), and analyzed by Shamsabadi, et al. (2007), the initial stiffness K_i for appropriate soils (given in the Standard Specifications) was determined to be 50 kip/in/ft (28.70 kN/mm/m) or half for non-standard fill material [25 kip/in/ft (14.35 kN/mm/m)]. This value is adjusted for height with Equation (2.6).

$$K_{abut} = K_i \times w \times \left(\frac{h}{x}\right) \quad \textbf{(2.6)}$$

where w is the width of the abutment backwall, h is the height of the abutment backwall, and x is a height proportionality factor of 5.5 ft (1.7 m) based on the heights of the previous tests. The passive pressure force is determined by the ideal bilinear Equation (2.7).

$$P = A_e \times y \times \left(\frac{h}{x}\right) \quad \textbf{(2.7)}$$

where

$A_e = h \times w_e =$ effective abutment wall area **(2.8)**
$h =$ the effective height of the backwall
$w_e =$ the effective width corrected for skew (see Figure 2.5)
If the abutment design is skewed, w_{abut} is taken as the width of the abutment.
$y =$ 5.0 ksf (239 kPa); the maximum passive pressure determined by the ultimate static force from previous testing
$x =$ 5.5 ft (1.7 m); height proportionality factor based on heights of previous testing

For more information on the design of shear keys and elastic response of the abutment, see the Caltrans 2010 Seismic Design Criteria manual. The design to account for transverse movement of the abutment due to skew is suggested to use a seat type abutment which resists lateral loads with an elastic response. Caltrans (2010) also suggests that the lateral resistance

should be placed on the bridge bent rather than on the abutment itself. Diaphragm type abutments are conservatively estimated, but not recommended.

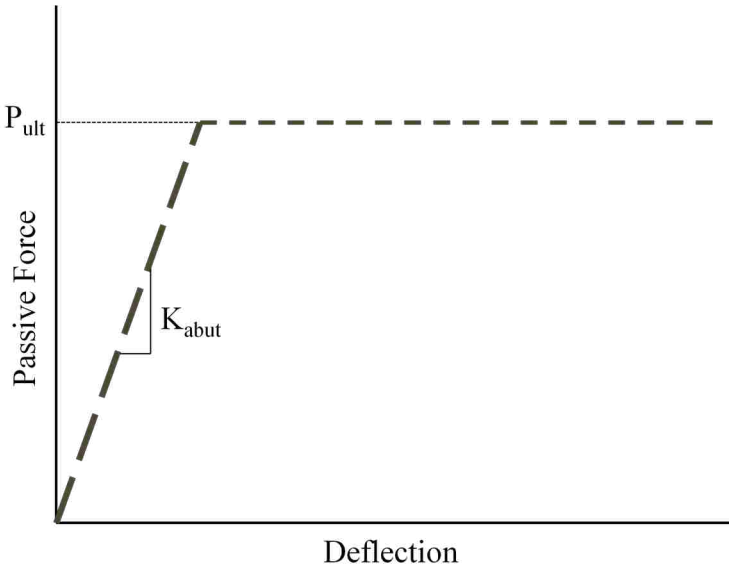

Figure 2.4: Passive force - deflection curve developed by Caltrans bilinear method

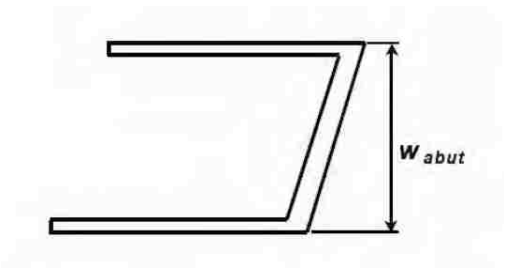

Figure 2.5: Effective abutment width corrected for skew (Caltrans 2010)

2.1.7 Development of Passive Earth Pressure with Deflection

As passive pressures develop with deflection, methods have also been developed to predict the shape of the passive force curves. Both the AASHTO (2011) and the Caltrans (2010) approaches assume a conservative bilinear failure as seen in Figure 2.4. After reaching the

ultimate passive pressure, P_{ult}, the force is considered constant with more deflection. Another theory is the hyperbolic model developed by Duncan and Mokwa (2001). The curve follows the calculated line given in Equation (2.9) and displayed in Figure 2.6.

$$P = \frac{\Delta}{\frac{1}{K_{max}} + R_f \frac{\Delta}{P_{ult}}} \tag{2.9}$$

where

P_{ult} = maximum passive resistance
P = mobilized passive resistance
Δ= deflection
R_f = failure ratio
K_{max} = initial stiffness of the load-deflection curve

This hyperbolic curve is used when estimating the passive force - deflection with both PYCAP (Duncan and Mokwa 2001) and ABUTMENT (Shamsabadi, et al. 2007). Field results seem to more closely follow the hyperbolic model (Cole and Rollins 2006, Lemnitzer, et al. 2009, Rollins and Sparks 2002).

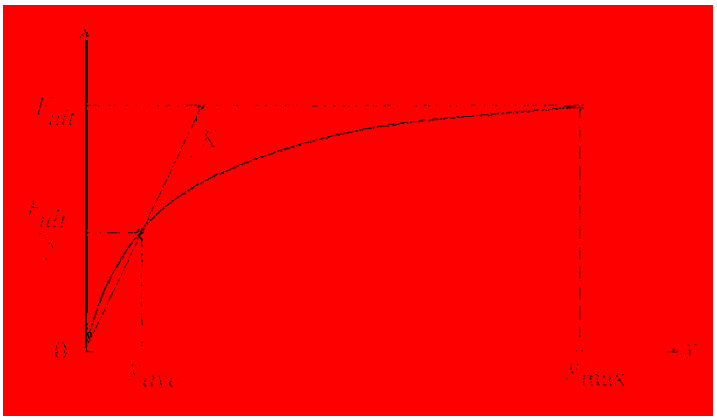

Figure 2.6: Example of hyperbolic curve taken from Shamsabadi, et al. (2007)

2.2 Passive Force-Displacement Tests for Non-Skewed Abutment Walls

Various tests have been performed incorporating abutment backfills and passive force - displacement curves. Each test or series of tests has added information to the way soils behave in passive pressure situations. Different variables tested include backfill material, wall heights, pile configurations, and including MSE wingwalls. Some tests were also compared to the predictive design methods listed in Section 2.1 giving insight to the accuracy of those methods.

2.2.1 Tested Variables and Results

Scopes of research included pushing a solid mass into backfill soil, measuring force and displacement. With different types of backfill soil used, tests developed a variety of peak resistance values. Tests were comprised of assorted wall heights and pile cap configurations. Dynamic tests on pile caps also provided information on earth pressure behavior. While the operation and mechanics varied, the tests yielded comparable results.

Among the various studies conducted on passive earth pressures, similar trends were observed. Most studies recorded lateral deflection of the wall as it was pushed into the backfill. Measurements of displacement indicated that maximum passive earth pressures developed between 2 and 6% of the wall height (Lemnitzer, et al. 2009, Rollins and Cole 2006, Rollins and Sparks 2002). In comparison to unconfined backfills, MSE wingwalls slightly increased the deflection at which maximum passive force occurred (Rollins, et al. 2010). Mokwa and Duncan (2001) concluded that the passive resistance directly related to the stiffness and strength of the backfill. As they compared backfill heights, they noted that lateral deflections can be reduced with increased cap thickness or depth of embedment. Compared to an unconfined backfill, the MSE walls provided a decrease in the overall resistance while increasing the passive force per unit width of the backwall (Rollins, et al. 2010).

The measured peak passive earth pressures were often compared to the predictive methods. The Coulomb and Rankine methods regularly over- and under-estimated, respectively, the measured force. Most studies agree that the Log Spiral method best predicts the peak passive pressure measured in the field (Duncan and Mokwa 2001, Lemnitzer, et al. 2009, Rollins and Cole 2006, Rollins and Sparks 2002). Cole and Rollins (2006) specifically identified the Log Spiral theory to be accurate among differing types of soil. With MSE walls, the Log Spiral method overestimates the passive resistance. To accurately predict the backfill resistance using MSE walls, the 3-dimensional reduction needed to be neglected and the friction angle increased in the Log Spiral method equations (Rollins, et al. 2010, Strassburg 2010). The shear planes recorded from the varying tests also repeatedly correlated with the Log Spiral estimated failure surface (Lemnitzer, et al. 2009, Rollins and Cole 2006). Computer models of failure zones also indicated Log Spiral profiles (Nasr and Rollins 2010).

2.3 Passive Force-Displacement Tests for Skewed Abutments

The skew angle on a bridge abutment causes passive pressures to develop differently than with the previously tested and predicted square bridges. Few tests have been completed to determine the earth pressure distribution and behavior of skewed bridges. As further studies have been conducted, similar results validate the loss of passive resistance with increased skew angles. Recent earthquakes have also demonstrated that skewed bridges are more apt to failure than those with non-skewed abutments.

2.3.1 Skewed Bridge Behavior

Differences in skewed and non-skewed bridges have been recently noticed and researched. Lateral earth pressures, assumed 2D in bridge design, seem to behave in a 3D fashion

when forces are applied at a skewed angle. The lateral pressure on the obtuse side of skewed bridges was observed to be significantly higher than on the acute side (Palmer 2013, Sandford and Elgaaly 1993). Tests also indicated rotation of the abutment which could account for the increase in pressure on the obtuse end (Marsh 2013, Palmer 2013, Sandford and Elgaaly 1993, Shamsabadi, et al. 2006). The worst effect of skew is the loss of passive resistance behind the bridge. In Figure 2.7, PLAXIS computer models demonstrate the capacity of the abutment backfill with increased skew (Shamsabadi, et al. 2006). As the skew angle increases, passive resistance drops dramatically.

To further validate the conclusions of the models, both small-scale laboratory and large-scale field tests were completed. Both series of tests found the same trends in the loss of resistance with increased skew. The results from Rollins and Jessee (2012) are displayed in Figure 2.8. Using the resulting data, Rollins and Jessee (2012) developed a reduction factor to predict the passive resistance of backfills against skewed abutments, as shown in Figure 2.9. The equation to determine the skew correction factor R_{skew} depends on the skew angle θ, as seen in Equation (2.10).

$$R_{skew} = 8.0 * 10^{-5}\theta^2 - 0.018\theta + 1.0 \quad \textbf{(2.10)}$$

The large-scale test results from this study also showed a decrease in passive force when the skew angle was increased. Each of the 5.5ft, 3ft, and MSE wall passive resistances decreased with increased skew (Franke 2013, Marsh 2013, Palmer 2013). The large-scale tests are plotted in Figure 2.9 along with Shamsabadi's numerical analysis, and generally follow the suggested reduction curve.

The effects of earthquakes on skewed bridges have also been analyzed. The dynamic loading produces similar results to the static loading of the tests. Studies concluded that skewed bridges tended to incur more damage than their non-skewed counterparts (Toro, et al. 2013,

Unjohn 2012). The cause of the damage was attributed to rotation of the skewed bridges. The cases found an increase in stress on the obtuse side of the abutments and unseating of the bridge deck on the acute side (Apirakyorapinit, et al. 2012, Unjohn 2012). With these recent considerations, suggestions have been made to improve the design of skewed bridges (Toro, et al. 2013).

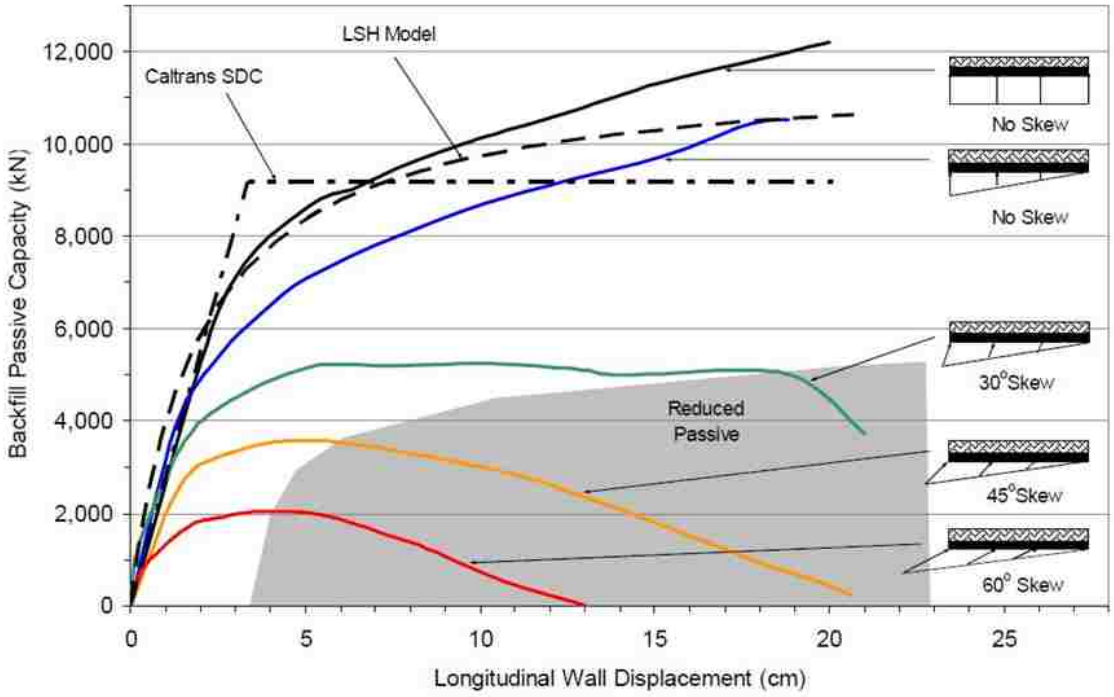

Figure 2.7: Effect of bridge skew angle on passive backfill capacity based on PLAXIS models (Shamsabadi, et al. 2006)

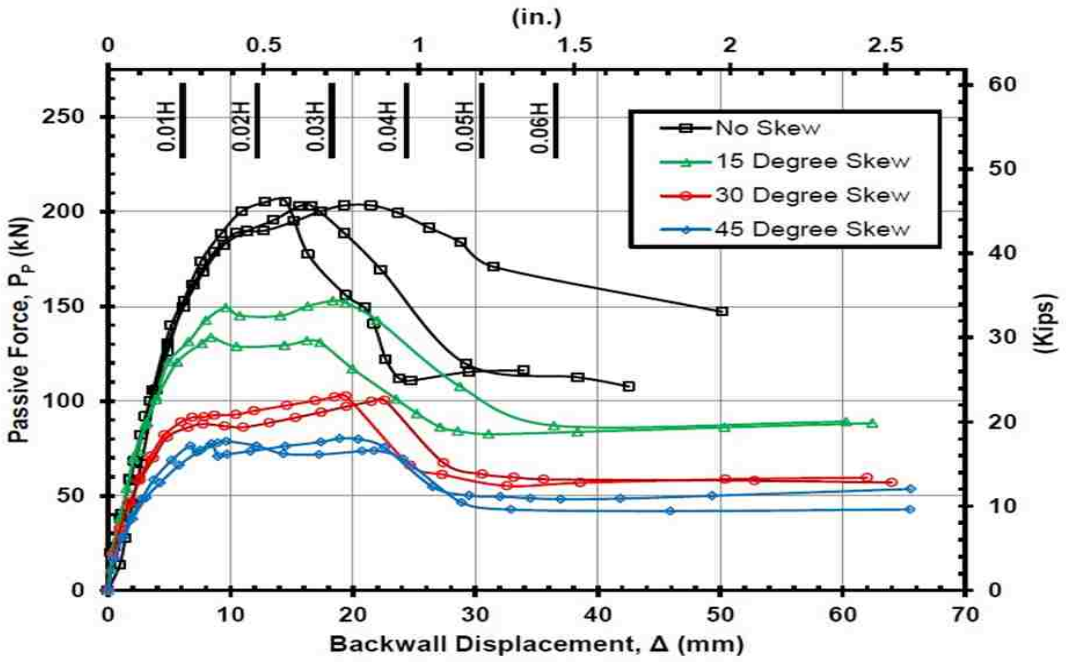

Figure 2.8: Passive force-deflection curves for lab tests (Rollins and Jessee 2012)

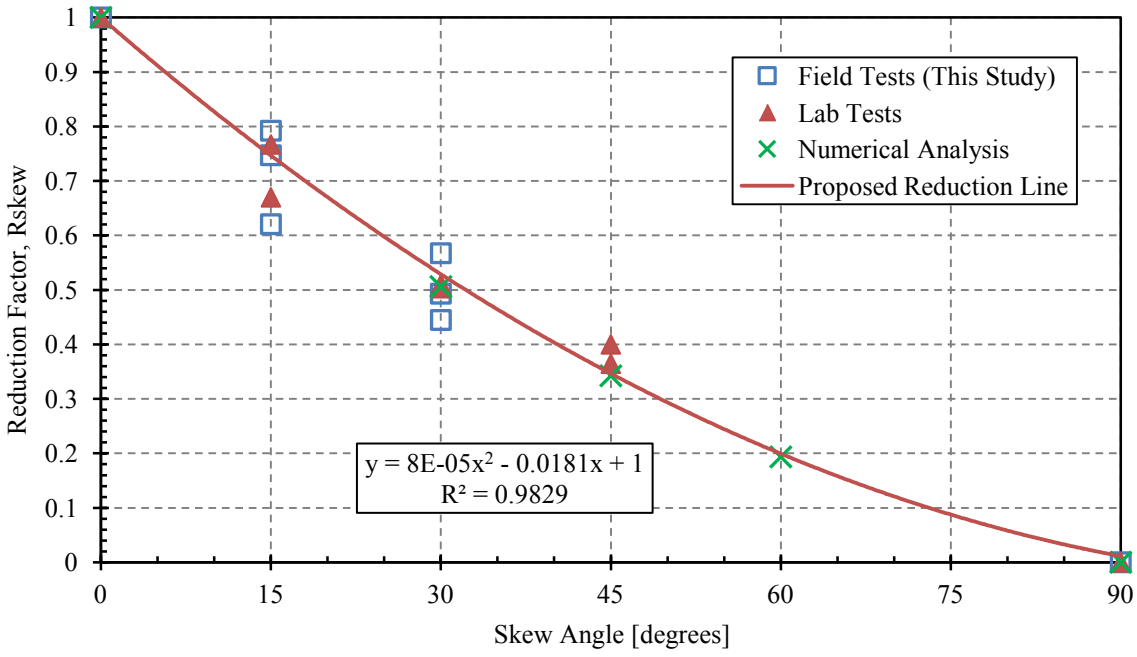

Figure 2.9: Reduction factor based on skew angle, compared to field, lab, and numerical tests [adapted from Rollins and Jessee (2012)]

3 TESTING METHODS

This section describes the methods of testing, including: the test site description and history, and geotechnical characteristics of the test site. Also described are the methods used for this research: the testing layout, backfill properties, measurement instrumentation, and the general test procedure.

3.1 Site Description

The Salt Lake Airport test site was originally built in 1995 and used for multiple tests throughout the years, being altered and adapted for new test scopes. Large-scale lateral load tests on pile groups and caps were conducted at the site (Christensen 2006, Johnson 2003, Peterson 1996, Snyder 2004, Walsh 2005). The previous testing provided a source for expected results. Many tests were also previously conducted to determine the soil profile and these results were used for current soil properties.

All testing occurred on unused land located near the Salt Lake City (SLC) International Airport. The site is located approximately 1000 ft (300 m) north of the airport control tower. A recent Google Map aerial photograph of the test site is provided in Figure 3.1. Figure 3.2 shows how the unused land is flat and open, clear of vegetation, structures, or any obstructions. It is a gated area, safe from vandalism and interference. Also, over the 2012 test course, Granite Construction Company shared the gated area but nothing conflicted with the testing.

Figure 3.1: Location of test site (2012 Google Map)

Figure 3.2: Plan view of test site location

3.1.1 Geotechnical Site Characterization

From past research, geotechnical site information is available from tests during the construction of the airport control tower (in 1995) and tests done specifically on the test site. Previous testing includes: standard penetration (SPT), vane shear (VST), pressuremeter (PMT), cone penetrometer (CPT); 3 new CPT tests and 2 drilled holes were conducted and compared in 2003 (Christensen 2006). Lab tests from disturbed samples were also conducted to determine particle size distribution, soil classification (USCS), consolidation characteristics, shear strength, and Atterberg limits. More lab tests were completed in 2003. A diagram is provided in Figure 3.3 locating each in-situ test and the year it was performed throughout the test site. No further tests were conducted for this study. The pile cap used for this study is located 26 ft (7.92 m) north of the drilled shafts in Figure 3.3.

3.1.2 Soil Profile Results

Previous testing resulted in a soil profile of imported gravel fill on the top 5 ft (1.5 m). Underlying soils alternate between lean clay, sandy silt, and silty sand layers to approximately 50 ft (15 m) as shown in Figure 3.4. The gravel fill surrounding the pile cap and drilled shafts was replaced with clean sand for the tests. Figures 3.4 and 3.5 consist of an idealized soil profile of the site and other measured soil characteristics. Additional subsurface soil information can be found in Christensen (2006), Snyder (2004), and Peterson (1996).

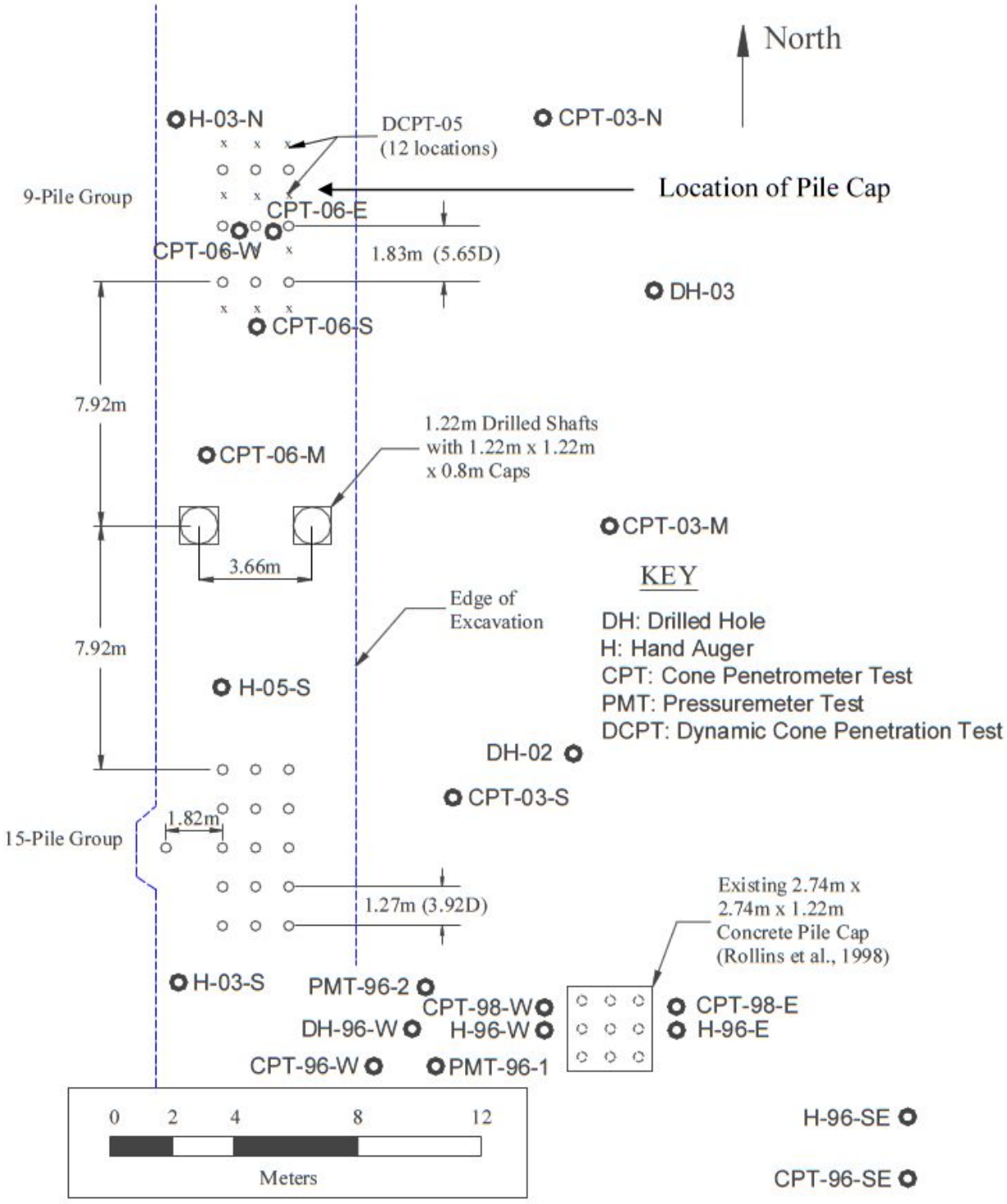

Figure 3.3: Locations and years of site in-situ tests (Christensen 2006)

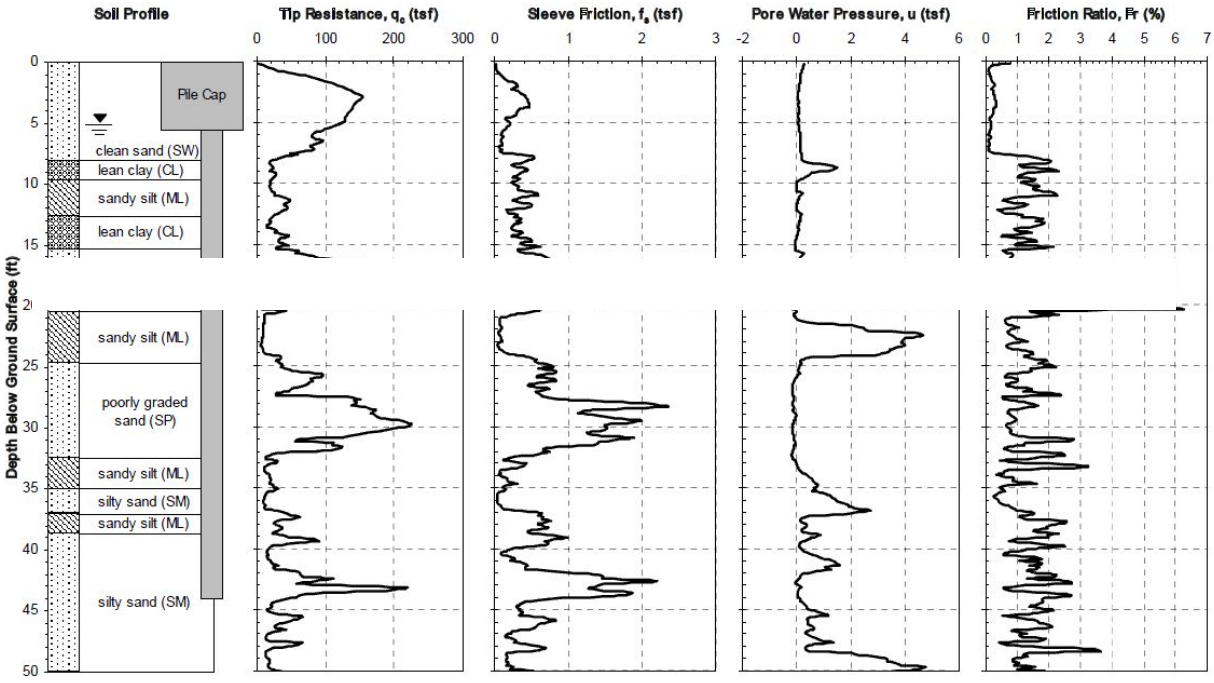

Figure 3.4: Idealized soil profile from lab and in-situ tests (Christensen 2006)

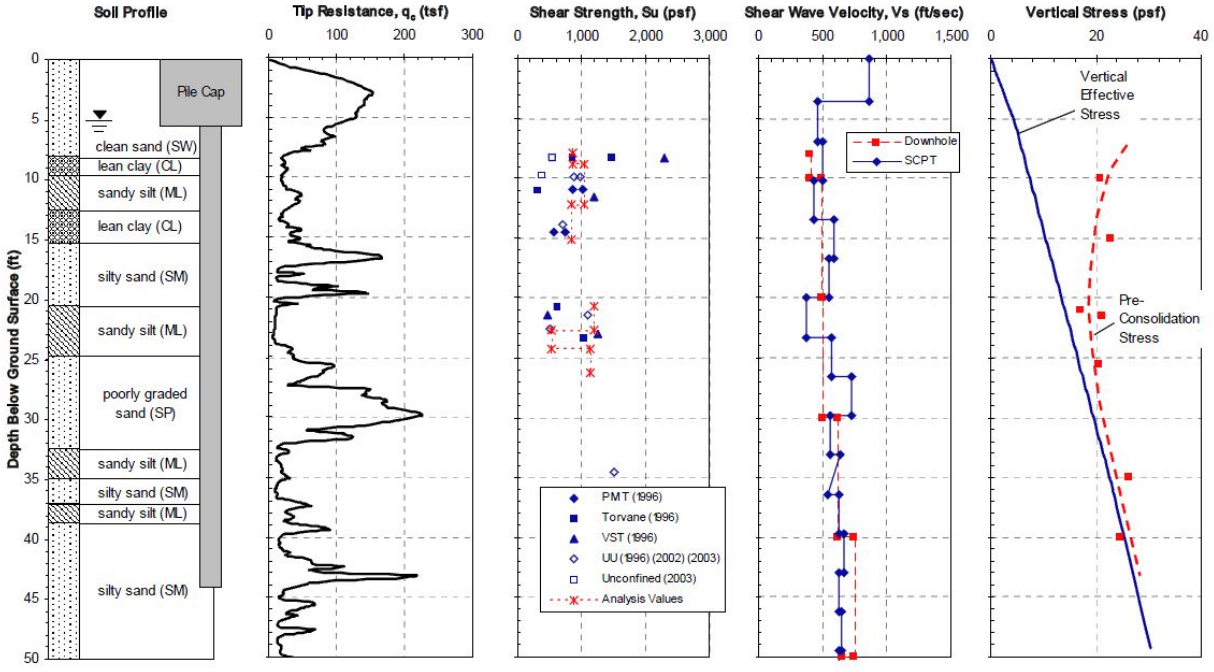

Figure 3.5: Idealized soil profile from CPT data (Christensen 2006)

3.2 Test Layout

Four major components provided the general testing layout: a reaction foundation, pile cap, loading apparatus, and backfill zone. Detailed descriptions of each component follow in the next sections. Figure 3.6 shows a complete drawing of the general testing setup.

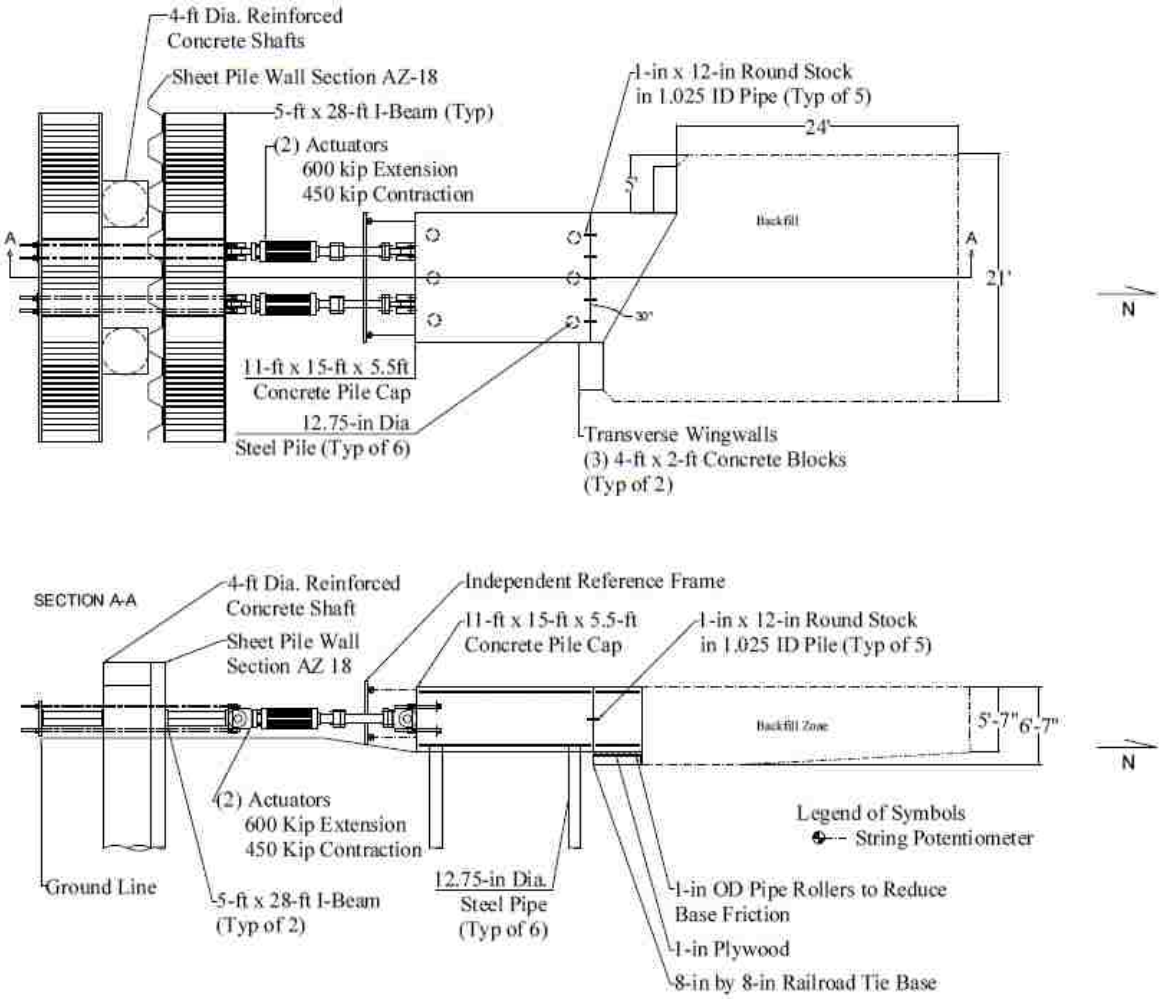

Figure 3.6: Plan and cross-section views of the general testing layout (Marsh 2013)

3.2.1 Reaction Foundation

The reaction foundation was constructed for previous testing and consists of two drilled shafts, a sheet pile wall, and two large steel I-beams. Figures 3.7 and 3.8 show the reaction foundation setup. The setup provides resistance as the actuators push against the pile cap.

The 4-ft (1.22-m) diameter drilled shafts are spaced apart 12 ft (3.66 m) center-to-center. The west shaft is 55.2 ft (16.8 m) deep and the east shaft is 70.0 ft (21.35 m) deep. The reinforcement in the top 35 ft (10.67 m) of each shaft consists of 18 #11 (#36) vertical bars, spiral reinforcement of #5 (#16) bars with a 3- in (75-mm) pitch. From 35 ft (10.67 m) and below only 9 #11(#36) vertical bars were used and the spiral pitched increased to 12 in (0.305 m). The top two feet of the shafts consist of a 4-ft (1.22-m) square cap. Throughout the lengths of the shafts, a 4.75-in (120-mm) concrete cover was maintained. The concrete compressive strength was 6000 psi (41 MPa).

The sheet pile wall was previously installed against the north sides of the drilled shafts. Installation was completed by driving the sheet pile sections with a vibratory hammer alternating depths from 33.6 to 35.6 ft (10.24 to 10.85 m) below the ground surface. As the piling is designed to support the drilled shafts, installation was kept as vertical and as close to the shafts as possible. The material for the wall consists of AZ-18 sheet piling constructed of ASTM A-572, Grade 50 steel.

The two I-beams were 28 ft (8.53 m) long, 64 in (1626 mm) high with 16 in (406 mm) wide flanges. They were reinforced with parallel stiffeners along the web to prevent buckling. Each beam was previously laid horizontally on both sides of the drilled shafts to provide additional lateral resistance, distribute loading, and unify the system. Between testing projects, the north beam settled in the soil and was thus raised to a level position and realigned with the

actuator connections. The I-beams were attached to the reaction foundation with eight 1.75-in (44-mm) DYWIDAGs which extended through the reaction foundation to connect to the actuators. Minimal post-tensioning was used as no dynamic testing was conducted.

Figure 3.7: South side of reaction foundation

Figure 3.8: North side of reaction foundation

3.2.2 Loading Apparatus

Two MTS hydraulic actuators, shown in Figure 3.9, were used to load the pile cap. They were positioned between the reaction foundation and the pile cap. They were held in place with the DYWIDAGs on the reaction foundation and DYWIDAGs embedded in the pile cap. Two 4-ft (1.22-m) extension beams connected the actuators to the pile cap. Each actuator has a compressive capacity of 600 kips (2.67 MN) (north direction) and a tensile capacity of 450 kips (2.00 MN) (south direction). Swivel heads located at both the north and south ends of the actuators eliminate bending moment effects on the pile cap loading. Care was taken to install the actuators level and attached at a height of 2.75 ft (0.84 m) above the base of the pile cap.

Figure 3.9: MTS hydraulic actuators

3.2.3 Pile Cap and Piles

The pile cap and piles setup was previously installed before the project and only minor changes to the pile cap (i.e., skew construction) and the reaction foundation were needed. The pile cap is located 16.4 ft (5.0 m) north of the reaction foundation above six piles. Each pile has

an outside diameter of 12.75 in (324 mm), a wall thickness of 0.75 in (9.5 mm), and is constructed with ASTM A252 Grade 3 steel pipe with average yield strength of 57 ksi (393 MPa). All piles were driven closed-ended to a depth of approximately 43 ft (13.1 m) below the ground surface.

Construction of the pile cap involved removing the center row of piles from an existing 9-pile group which increased the (north-south) center-to-center spacing to 12 ft (3.66 m). The east-west center-to-center spacing of the piles remained at 3.5 ft (1.07 m). To ensure a rigid connection between the piles and the cap, the piles were embedded into the cap at a 6 in (150 mm) minimum. Rebar cages, 18 ft (5.49 m) long, consisting of 6 #8 (#25) vertical bars and a #4 (#13) spiral at a pitch of 6 in (152 mm), were lowered 13.2 ft (4.02 m) into the steel piles with the remaining 4.8 ft (1.47 m) extending into the pile cap to support the upper horizontal reinforcing mat. Horizontal reinforcing mats consisting of #5 (#19) bars in the longitudinal and transverse direction 8 in (203 mm) on center were installed on both top and bottom of the pile cap. The connections and the cap were constructed of 6,000-psi (41.37-MPa) concrete. Final cap dimensions are 15 ft (4.57 m) long (north-south direction), 11 ft (3.35 m) wide, and 5.72 ft (1.74 m) high. During construction, inclinometer and shape array pipes were cast into the center pile of each row, along with eight DYWIDAGs cast horizontally into the pile cap to provide a connection point between the pile cap and the loading apparatus.

3.2.4 Concrete Wedges

While the zero skew tests did not utilize the skew wedges, a basic understanding of the pile cap modifications is useful. To establish the 15 and 30 degree skew angles for testing, concrete wedges were formed and cast adjacent to the existing pile cap backwall face, as shown in Figure 3.10. Construction occurred after the zero degree testing was completed. Concrete

reinforcement was conservatively designed for both a vertical and horizontal triangular pressure distribution along the face of each wedge. Wedge construction provided a rigid connection between the cap and both wedges and also allowed for simple removal of the skewed faces after testing was completed for the 30° and 15° tests. The wedges were constructed atop a railroad tie foundation with a series rollers as illustrated in Figure 3.11 to reduce friction at the base of the wedges. The wedges were effective for testing, providing the necessary solid resistance as the pile cap was pushed into each backfill. For a more detailed explanation of the set up and installation of the 15° and 30° skew wedges refer to Marsh (2013).

Figure 3.10: Construction of 15° and 30° wedges (Marsh 2013)

Figure 3.11: Roller foundation for 15° and 30° wedges (Marsh 2013)

3.2.5 Backfill Zone

The pile cap was pushed into the backfill zone, located on the north end of the pile cap as shown in Figure 3.12. The area was approximately 24 ft (7.3 m) wide and 24 ft (7.3 m) long. The backfill next to the pile cap face extended to a depth approximately 1 to 2 ft (0.3 to 0.6 m) below the base of the pile cap. The backfill zone gradually inclined over approximately 8 ft (2.4 m), until the backfill extended to a depth roughly level with the bottom of the pile cap. This area was filled with the test material to 3 ft (0.91 m) and 5.5 ft (1.68 m), whereas the area was limited to 11 ft (3.35 m), or the width of the pile cap, when MSE walls were used.

Backfill material was placed in lifts approximately 6 to 8 in (150 to 200 mm) in height. Water was added to the material during placement to aid in compaction. A vibratory roller and vibrating plate compactor were used to compact each lift. To ensure proper compaction and to determine the soil unit weight and moisture content, two nuclear density tests were performed for each lift. The water table at the test site is approximately 5.5 ft (1.68 m) below the ground surface. To keep the water from interfering with test procedures, two automated sensor pumps were provided which continuously pumped the water out of the test pit.

Figure 3.12: Test site backfill zone

3.3 Geotechnical Backfill Properties

This section describes the laboratory and field test results of the backfill soil used during testing. Included are the soil gradation, relative density, dry and moist unit weights, and water content for each of the zero skew tests.

3.3.1 Backfill Gradation and Relative Density

Approximately 250 tons (227 metric tons) of sand at 7% moisture content was purchased for this project, see Figure 3.13. The sand was classified as poorly graded (SP type soil according to the Unified Soil Classification System or an A-1-b type soil according to the AASHTO Classification System) and was used as backfill material for all tests. Pre- and post-testing gradation plots are shown in Figure 3.14. Initial soil conditions fall within the gradation limits of washed concrete sand (ASTM C33), though additional fines picked up during testing caused the particle size distribution to fall outside the gradation limits of a washed concrete sand towards the end of testing. Table 3.1 provides the soil gradation parameters for the soil particle size analyses conducted before and after the abutment tests. Changes in gradation during testing were likely due to contamination of the backfill material with the native material located at the bottom and sides of the test pit. However, because the zero skew tests were completed first, the gradation likely stayed within the washed concrete sand limits.

Table 3.1: Soil gradation characteristics, pre- and post-test

	Sand	Fines	D_{60}		D_{50}		D_{30}		D_{10}		C_u	C_c
	[%]	[%]	[in]	[mm]	[in]	[mm]	[in]	[mm]	[in]	[mm]		
Pre-Test	98.0	2.0	1.22	(31.0)	0.9	(22.9)	0.4	(10.2)	0.16	(4.1)	7.6	0.8
Post-Test	96.1	3.9	1.26	(32.0)	0.92	(23.4)	0.34	(8.6)	0.13	(3.3)	9.7	0.7

Figure 3.13: Delivered backfill sand (SP)

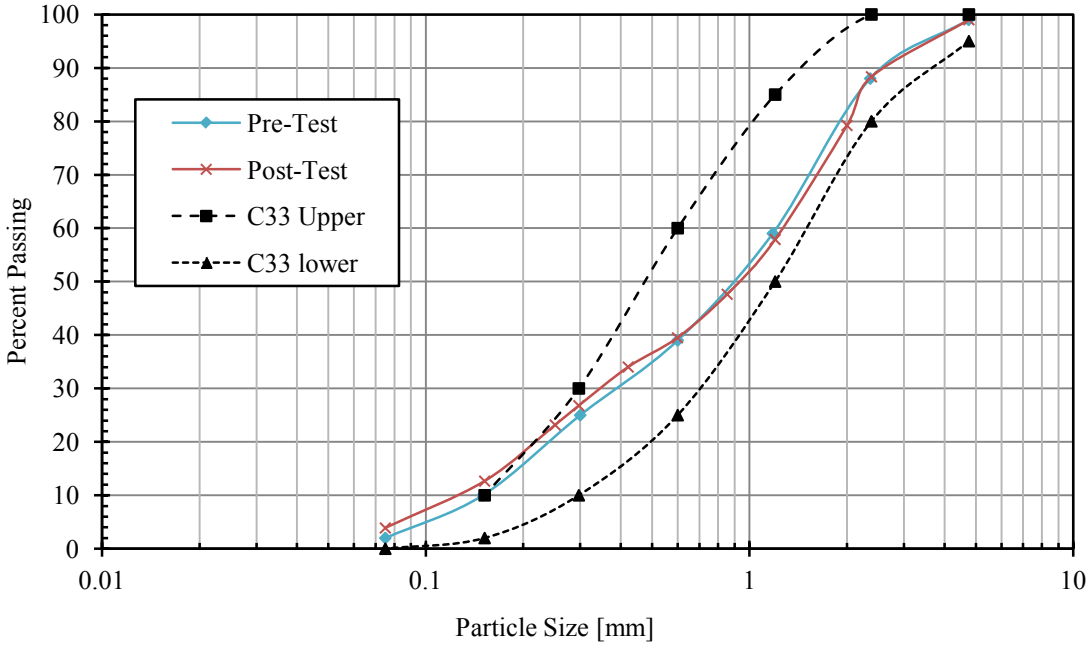

Figure 3.14: Particle size distribution of backfill soil, pre- and post-test (Marsh 2013)

3.3.2 Lift Compaction Properties

The compaction properties were measured in two various locations of the backfill per each lift using a nuclear gage test. The maximum dry density according to the modified Proctor compaction lab test (ASTM D1557) was 111.5 pcf (17.52 kN/m^3) with optimum moisture content of 7.1%. The achieved average relative compaction for all zero skew tests considered herein was 97.2% of the modified proctor maximum, which was higher than the target on-site compaction level of 95%.

Histograms showing the frequency of backfill dry unit weight occurrences for the 3ft fill, the 5.5ft fill, and the MSE wall tests are shown in Figures 3.15, 3.16, and 3.17, respectively. Figure 3.18 and Table 3.2 summarize the dry unit weight characteristics of all three zero skew tests. The average dry unit weights for the 3ft, 5.5ft, and MSE wall zero skew tests were found to be 107.0 pcf (16.81 kN/m^3), 107.0 pcf (16.81 kN/m^3), and 108.3 pcf (17.02 kN/m^3), respectively. The average dry unit weight of all zero skew tests was 107.2 pcf (16.84 kN/m^3) with an average relative compaction of 96.2%. The similar unit weights and relative compaction suggest that the backfill material is comparable for the zero skew tests.

Relative density was calculated using a correlation developed by Lee and Singh (1971) between relative density and relative compaction of granular soils, shown as Equation (3.1).

$$R = 80 + 0.2D_r \quad \textbf{(3.1)}$$

Calculated relative densities, D_r, and relative compaction, R, for each of the three zero skew tests are summarized in Table 3.3. The 0° skew average relative density was calculated to be 81.0%.

Other nuclear gage parameters determined during each test were recorded and analyzed. Scatter plots of moisture content, relative compaction, dry unit weight, and moist unit weight with respect to elevation above the base of the pile cap for all three zero skew tests are shown in

Figures 3.19, 3.20, 3.21, and 3.22, respectively. All values were determined from two nuclear gage tests per lift for each test. The average moisture content for each fill height hovered around 9%. As before stated, relative compaction averaged at 96.2% for all zero skew tests. The average dry and moist unit weights were 107 pcf (16.81 kN/m^3) and 117 pcf (18.38 kN/m^3), respectively. The tight scatter suggests the lifts were similar throughout the backfill for each of the zero skew tests. The average values are similar between each test, again suggesting the testing methods allowed for reliable comparisons of the data.

Table 3.2: Summary of backfill dry unit weight characteristics for all 0° tests

	3ft Test		*5.5ft Test*		*MSE Wall Test*	
Dry Unit Weight	*[pcf]*	*[kN/m^3]*	*[pcf]*	*[kN/m^3]*	*[pcf]*	*[kN/m^3]*
Minimum	105.7	16.6	105.4	16.6	104.8	16.5
Maximum	108.2	17.0	109.9	17.3	110.0	17.3
Average	107.0	16.8	107.0	16.8	107.5	16.9
Median	106.8	16.8	106.9	16.8	107.4	16.9

Table 3.3: Backfill relative compaction and relative densities for 0° tests

	3ft Test	*5.5ft Test*	*MSE Wall Test*
Relative Compaction [%]	96.0	96.0	96.4
Relative Density [%]	79.9	79.8	82.2

Table 3.4: Average of measured field parameters with respect to depth for each backfill

Average Soil Parameters	0° Skew		
	3ft	5.5ft	MSE
Moisture Content [%]	9.3	8.9	9.1
Relative Compaction [%]	96	96	97
Dry Unit Weight [pcf]	107	107	108
Moist Unit Weight [pcf]	117	117	117

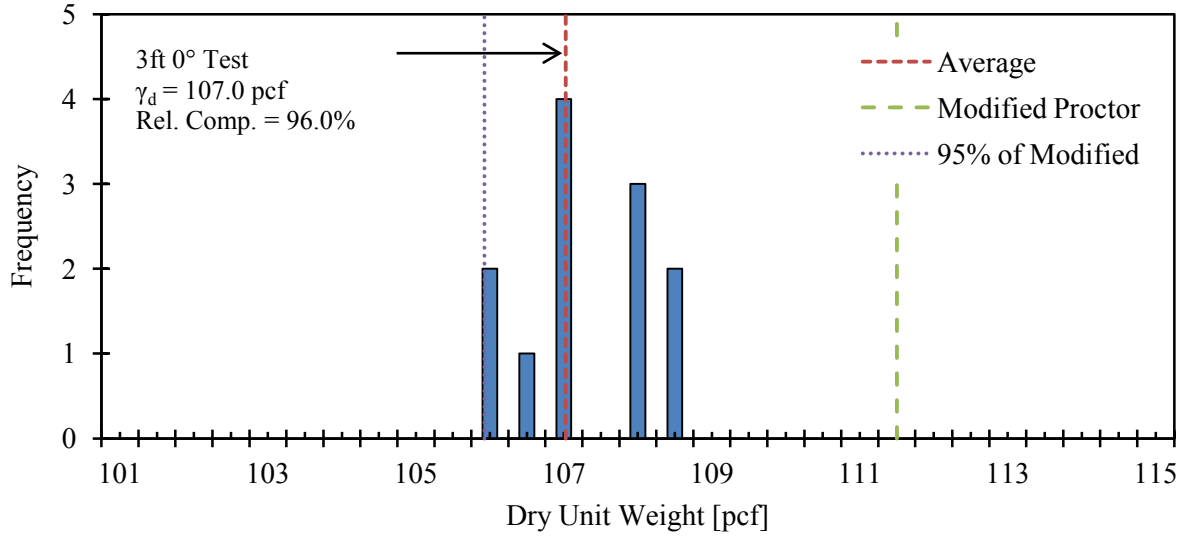

Figure 3.15: Backfill dry unit weight histogram for 3ft fill test

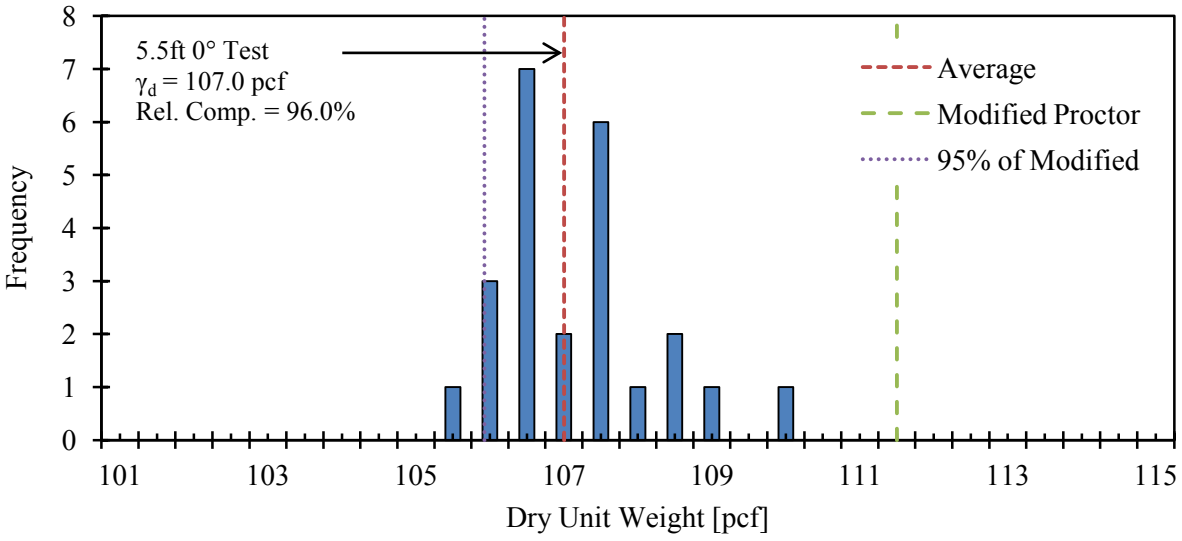

Figure 3.16: Backfill dry unit weight histogram for 5.5ft fill test

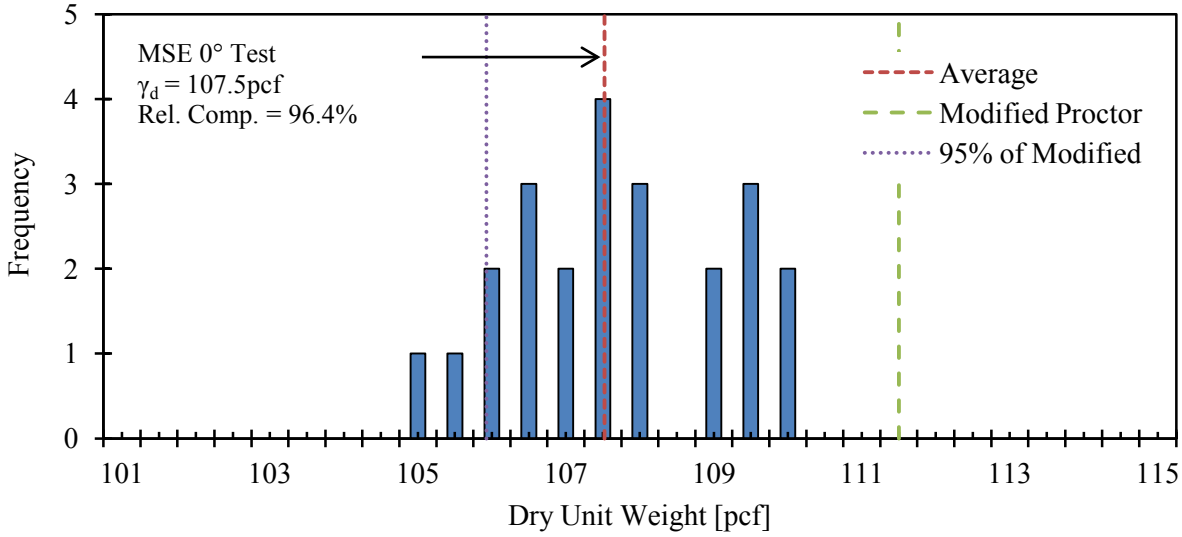

Figure 3.17: Backfill dry unit weight histogram for MSE wall test

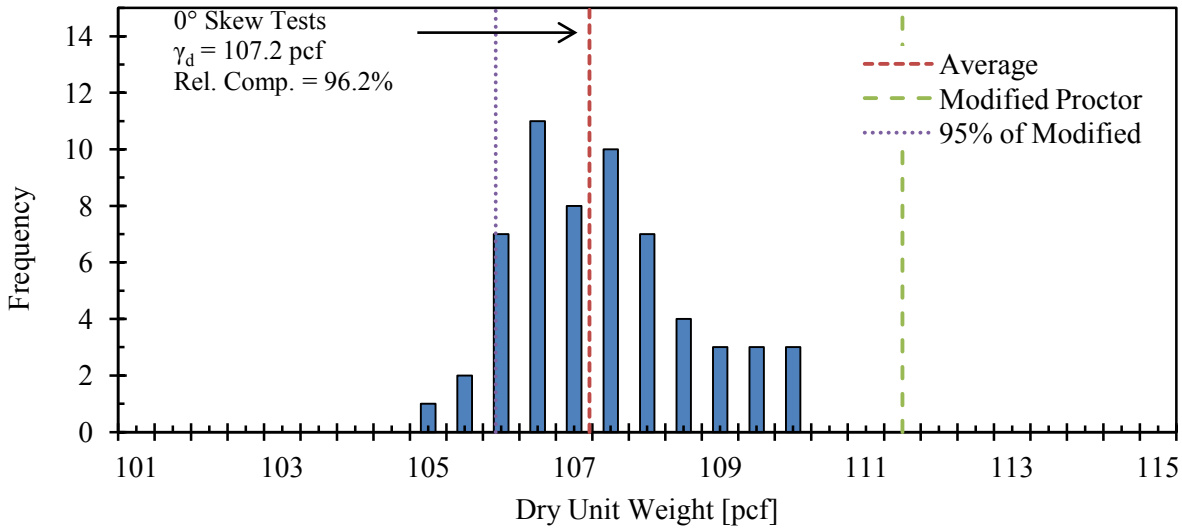

Figure 3.18: Backfill dry unit weight histogram for all 0° skew tests

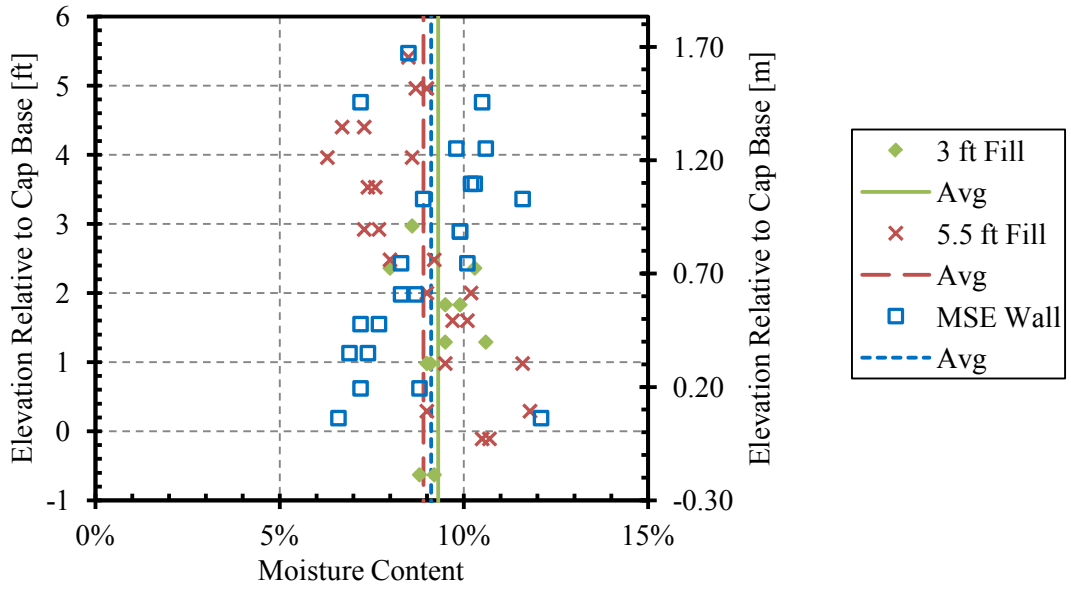

Figure 3.19: Moisture content with respect to depth for all 0° tests

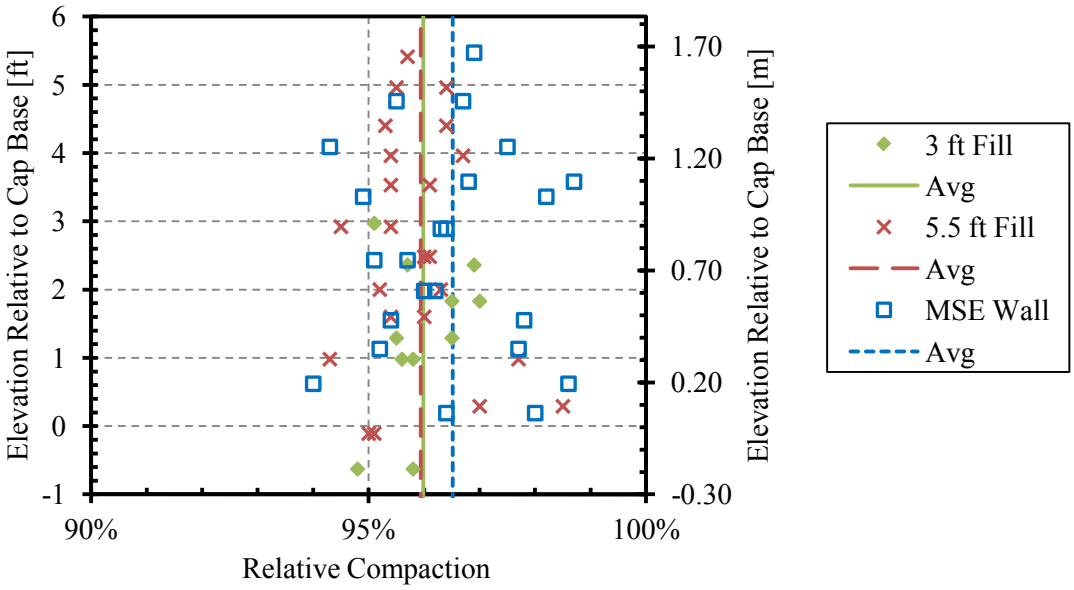

Figure 3.20: Relative compaction with respect to depth for all 0° tests

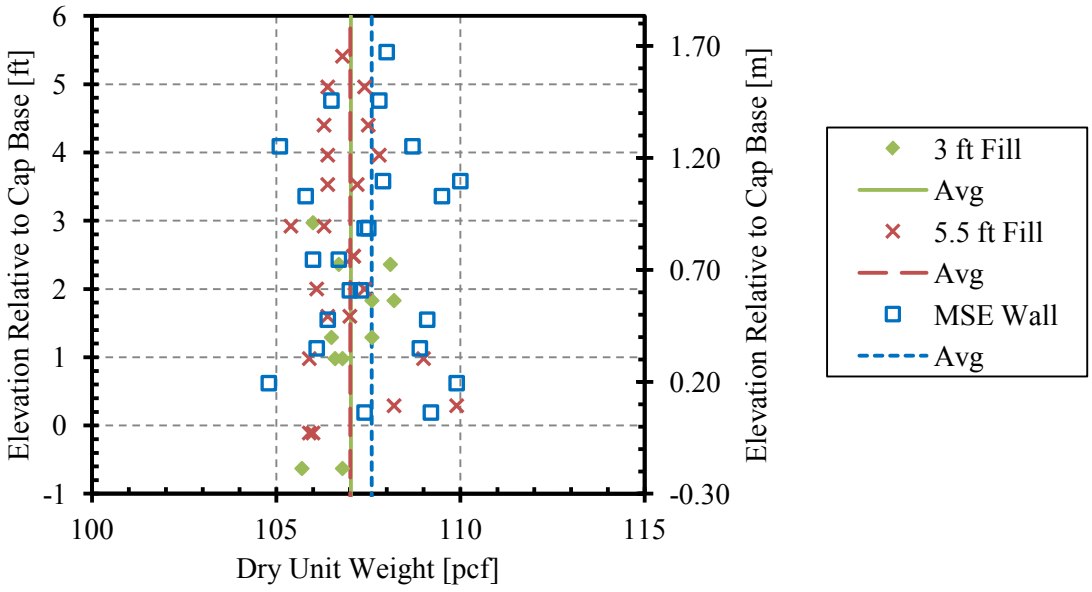

Figure 3.21: Dry unit weight with respect to depth for all 0° tests

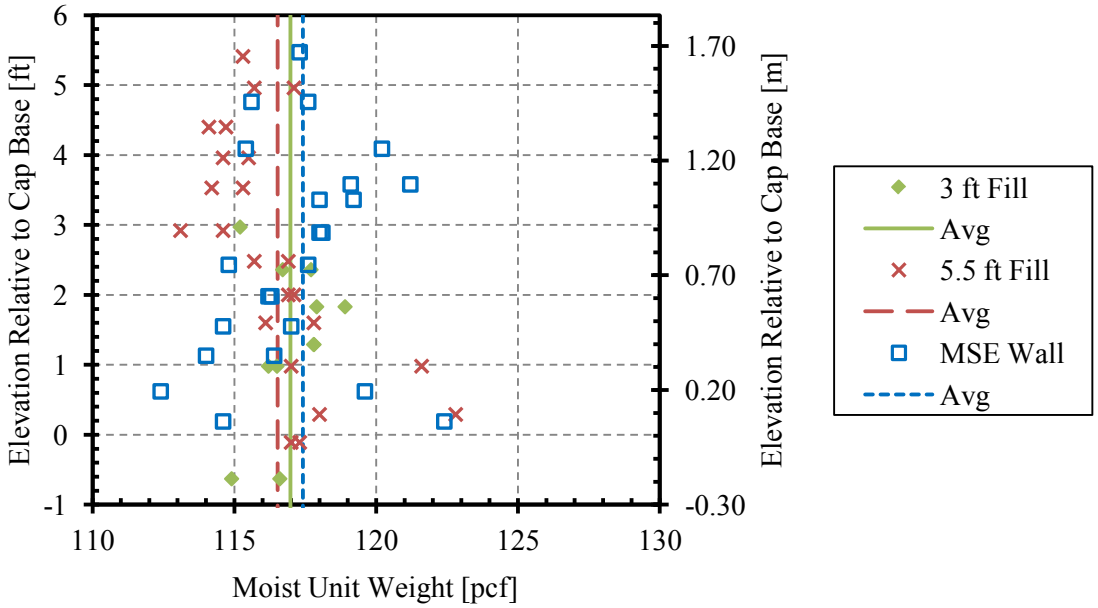

Figure 3.22: Moist unit weight with respect to depth for all 0° tests

3.3.3 Backfill Shear Strength

Direct shear tests (ASTM D 3080) were conducted in the BYU soils laboratory to determine the friction angle φ and cohesion c of the backfill material. The results are presented fully in Marsh (2013), and only summarized here.

A large range of normal stresses were tested to match the vertical stresses in the field tests. The typical field moisture contents were also used for direct shear testing, as well as submerged. The backfill strength parameters are included in Table 3.5.

Table 3.5: Backfill strength parameters (Marsh 2013)

Source of Test Result	*Peak*		*Ultimate*	
	φ (deg)	*c (psf)*	*φ (deg)*	*c (psf)*
Direct Shear (full range, dry)	46.7	161.6	40.4	113.8
Direct Shear (full range, dry, zero cohesion)	48.3	0	41.8	0
Direct Shear (full range, submerged)	42.7	92.9	41.4	78.8
Direct Shear (full range, sub., zero cohesion)	43.8	0	42.3	0

3.4 Instrumentation

Four independent pieces of instrumentation were used to measure pile cap and wall displacement: string potentiometers, linear variable differential transformers (LVDTs), an inclinometer, and shape accelerometer arrays (SAA). Independence of the instrumentation allowed each device to be compared for accuracy. The string pots and LVDTs measured longitudinal and/or lateral displacement, while the inclinometer and SAAs were equipped to measure both directions of displacement. Longitudinal load was measured by pressure transducers in the actuators throughout the duration of each test. For this series of tests, vertical

movement of the pile cap was not monitored because the piles and weight of the cap were assumed to hold the cap in place.

3.4.1 String Potentiometers

An independent reference frame was placed between the reaction foundation and the pile cap, shown in Figure 3.23 as the highlighted frame stretching across the test pit. Six string potentiometers were attached to this reference frame with C-clamps. Approximate string pot attachment locations are shown in Figure 3.23 as the dashed lines. Four string pots measured the deflection of the four corners of the pile cap and two measured the deflection of the reaction foundation. The four pile cap string pots were used to measure the longitudinal movement and, if any, rotation of the pile cap during testing. The two reaction foundation string pots attached to the center of the I-beam at the same level of the actuators. The numerical locations, described as coordinates, follow in Table 3.6, which remained constant for each of the tests.

Seven additional string pots mounted to the top north end of the pile cap measured the backfill strain, as shown in Figure 3.24. For the zero skew tests, the seven string pots were located 10 in (254 mm) behind the north face of the cap. Each potentiometer was attached to a stake in the backfill at the distances from the cap face shown in Table 3.7. The distance of the string pot from the centerline of the backfill is also included as the instruments could not be placed in the same centerline location. Values with a negative distance indicate the string pot was located on the west side of the backfill centerline.

Figure 3.23: String pot locations and reference frame

Figure 3.24: String pot arrangement for zero skew backfill deflection measurements

Table 3.6: String pot locations on south end of pile cap

String Pot ID	String Pot Distance [in (cm)]	
	From Top of Pile Cap	*From West Side of Pile Cap*
SP 965 (top west)	3 (7.62)	3 (7.62)
SP 963 (bottom west)	51 (130)	3 (7.62)
SP 964 (top east)	3 (7.62)	129 (328)
SP 962 (bottom east)	51 (130)	129 (328)
SP 967 (west reaction)	33 (83.8)	-10.5 (-277)
SP 966 (east reaction)	36 (91.4)	145.5 (370)

Table 3.7: String pot distances from pile cap face for zero skew tests

String Pot ID	*Dist. from Face [ft (m)]*	*Dist. from Center [ft (m)]*
SP25	2 (0.61)	0.58 (0.18)
SP968	4 (1.22)	-0.25 (-0.08)
SP18	6 (1.83)	1.42 (0.43)
SP10	10 (3.05)	-1.08 (-0.33)
SP11	14 (4.27)	2.25 (0.69)
SP969	18 (5.49)	-1.75 (-0.53)
SP2	22 (6.71)	-2.50 (-0.76)

3.4.2 Linear Variable Differential Transformers (LVDTs)

For the 0° skew tests, LVDTs were only used during the MSE test. Assuming similar movement of the walls due to symmetry, the LVDTs were only used on the east wall. The locations are included in Table 3.8. The instrumentation setup for the zero skew MSE wingwalls is shown in Figure 3.25. Other recorded tests used LVDTs to measure both the east and west MSE walls, and pile cap movement; specifics can be found in Franke (2013), Marsh (2013), and Palmer (2013).

Figure 3.25: MSE wall instrumentation setup for 0° test

Table 3.8: Instrument locations on 0° skew MSE wall

String Pot ID	*Distance [in (cm)]*	
	From Top of MSE Wall	*From North Side of MSE wall*
SP 971 (top south)	2 (5.08)	259 (658)
SP 973 (top mid-south)	2 (5.08)	180 (457)
SP 972 (top mid-north)	2 (5.08)	109 (277)
SP 970 (top north)	2 (5.08)	51 (130)
LVDT ID	*Distance [in (cm)]*	
	From Bottom of MSE Wall	*From North Side of MSE wall*
SR 1 (bottom south)	5.5 (14.0)	262 (665)
SR 2 (bottom mid-south)	9 (22.9)	182 (462)
SR 5 (bottom mid-north)	7 (17.8)	109 (277)
SR 3 (bottom north)	6 (15.2)	53 (135)

3.4.3 Inclinometer

As seen in Figure 3.26, two inclinometer pipes are located in the longitude center of the pile cap on both the north and south ends, 146 in (371 cm) apart with the south pipe 18 in (46 cm) from the south edge of the pile cap. The pipes are installed within the center pile of both pile rows of the pile group. Each pipe runs to a depth of approximately 43 ft (13.1 m), or to the bottom of the piles. The pipes extend above the pile cap by 12 in (0.31 m), making the top-most inclinometer reading at 1.1 ft (0.34 m) level with the top of the pile cap. The grooved inclinometer pipes have an outside diameter of 2.75 in (70 mm) and an inside diameter of 2.32 in (60 mm).

The Digitilt inclinometer probe, manufactured by SlopeIndicator, is 2 ft (0.61 m) long with sensors at the top and bottom of the probe. Data is recorded by calculating movement based on the relative angle between the two sensors. The probe consists of spring-pressured wheels to securely run through the pipe grooves. The cord length was used to 43.1 ft (13.1 m) and 41.1 ft

(12.5 m) on the north and south ends, respectively. For recording purposes, every 2 ft (0.61 m) on the cord is marked with yellow tape and every 10 ft (3.05 m) is marked with red tape and length value. The probe was lowered to the bottom of the pipe, careful not to strike the bottom which would cause damage to the probe sensor. A pulley system attached to the top of the pipe was used to provide an accurate measurement datum, and to easily raise and lower the probe. While the instructions recommended letting the probe acclimate for at least five minutes at the bottom of the pipe, the suggestion was not always followed which may have led to some slight discrepancies in the data. A cooler temperature due to water towards the bottom of the inclinometer pipe could also have affected the readings.

Inclinometer readings were recorded with a DataMate II portable data acquisition unit. Using the pulley system, each reading was taken when the yellow tape was pulled just past the pulley catch. Each side of the pile cap was measured twice, first facing north and then again with a 180° rotation facing south. These recorded values were averaged during data reduction to reduce error in recording. This data provided information on both longitudinal and lateral movement of the pile cap versus depth. This procedure occurred both before pushing began and after the pile cap had reached its maximum displacement.

Figure 3.26: Inclinometer locations on top of pile cap

3.4.4 Shape Accelerometer Arrays (SAA)

A 1.1-in (27-mm) inside diameter schedule 40 PVC electrical conduit was tied alongside the north and south inclinometer pipes. The PVC pipe was originally installed to a depth of 50.2 ft (15.3 m) below the top of the pile cap. The electrical conduit extends upward through the pile cap and terminates approximately 3 in (75 mm) above the cap. However, over time, some sand appears to have accumulated within the pipe, thus reducing the effective length. For this study, a 48-ft (14.6-m) array was installed into the north pipe to a depth of 38.7 ft (11.8 m) below the top of the pile cap. A 24-ft (7.32-m) array was installed in the south pipe to a depth of 23.1 ft (7.04 m) below the top of the cap.

The arrays connected to a data concentrator which in turn connected to the field computer. Both arrays provided triaxial static and dynamic accelerations for each joint along the length of the arrays. Application software ("SAARecorder") calculated positional data at the vertices of the arrays using the static components. For static or slowly-changing deformations, the accelerometers measure tilt angles of each segment, similar to conventional inclinometers. However, azimuth in the SAA is resolved by performing 3D joint-angle calculations using the bend-without-twist joint construction as a constraint (Measurand Inc. 2011), rather than the grooves in the inclinometer casing. The bottom (FAR) node for the north array was considered deeper than any expected lateral movement and was thus set as an absolute zero reference point. Assuming the rigid pile cap to move as a block, the shorter south array was adjusted to match the uppermost longitudinal movement of the array in the north end of the pile cap. This adjustment allowed the south array to more accurately describe the south pile movement.

Both arrays were also adjusted to align their x- and y-axes with the north and east movements of the pile cap. More information on these adjustments can be found in Franke

(2013), Marsh (2013), and Palmer (2013). The shape array data included in the results portion of this thesis has been adjusted according to the judgment of the researchers, similar to those outlined in the given papers.

3.4.5 Instruments for Backfill Heave and Shear Displacement

For each zero skew test, the backfill vertical heave was measured with use of a 2-ft (0.61-m) grid painted on the backfill surface. The relative elevation of each grid intersection was measured with a survey level before and after each test. The observed surface cracks in the backfill were also marked with paint following the completion of each test. Refer to Figure 3.27 to see the backfill instrumentation setup.

Holes to measure shear failure within the backfill were also included during testing. A hand auger was used to drill 2-in (51-mm) diameter, vertical holes at various locations throughout the backfill to determine the location of the internal failure surfaces. These columns were then refilled and compacted with red-dyed sand. After the final displacement was reached, the soil adjacent to the shear holes was excavated to reveal the failure locations in each red sand column. For specific locations of the shear columns for each test refer to Marsh (2013) and Palmer (2013). Results of the shear failure locations are included in Section 4.1.2.

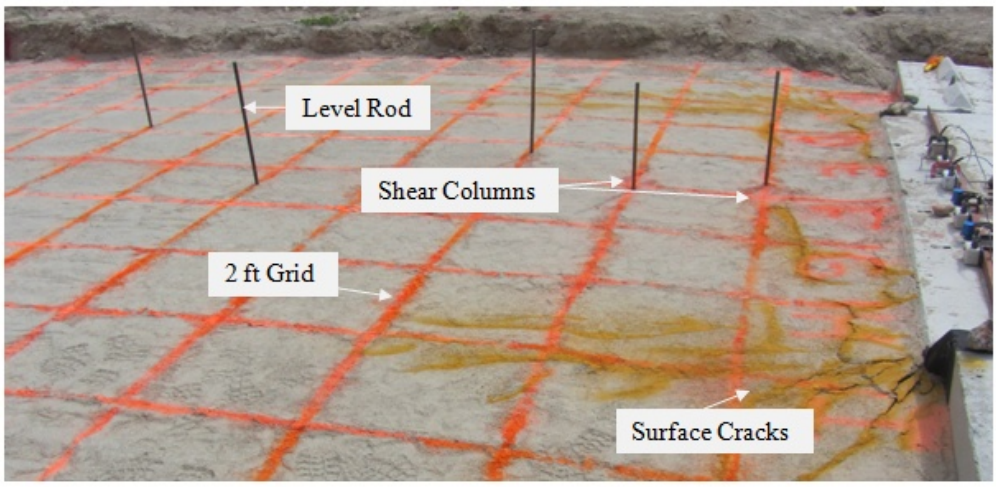

Figure 3.27: General view of backfill instrumentation

3.5 General Test Procedure

This section describes the general test procedure in relation to the 0° skew tests. This includes which tests will be discussed, test set up, and test and measurement operation.

3.5.1 Summary of Tests

There were a total of 16 large-scale tests conducted during the testing time period (April to June 2012) including six baseline tests. All tests are summarized in Table 3.9 organized by the date performed. Tests 3, 4, and 6 correspond with the zero skew tests that will be discussed and compared in detail within this thesis. These include the 0° skew tests at backfill heights of 3 ft (0.91 m), 5.5 ft (1.68 m), and MSE wingwalls with 5.5 ft (1.68 m) backfill. The 0° skew tests were conducted on the existing pile cap before the skew wedges were constructed and attached.

The general testing procedure occurred as follows. Prior to testing each skew angle, a lateral load test was performed to determine the "baseline" resistance of the pile cap and attached wedges. Following the baseline test, the sand was compacted adjacent to the cap so a lateral load

test could be performed to obtain the total resistance. Following backfill installation, the surface grid and shear columns were applied and appropriate initial measurements were recorded.

To run the test, the pile cap was pushed longitudinally into the backfill zone using the two hydraulic actuators. The cap was pushed in 0.25-in (6.35-mm) increments to final displacements of 3.25 in to 3.75 in (8.30 cm to 9.53 cm) to prevent failure of the supporting piles. At each 0.25-in (6.35-mm) displacement increment the load was held for approximately 2 minutes to observe the reduction in longitudinal force against the backwall as a function of time. Intermediate measurements were recorded at each incremental push. After the last push, final measurements were recorded. The pile cap was pulled by the actuators back to its initial starting position, and the backfill soil was removed. The backfill material was completely excavated and recompacted for each individual test.

Table 3.9: 2012 Testing Summary

Test Number	Test Date	Test Description	
		Skew Angle	*Backfill*
1	4/25/2012	0°	Baseline
2	4/25/2012	0°	Baseline Retest
3	4/30/2012	0°	3.0 ft (0.91 m)
4	5/3/2012	0°	5.5 ft (1.52 m)
5	5/3/2012	0°	Baseline Retest
6	5/8/2012	0°	MSE Wall
7	5/14/2012	30°	Baseline
8	5/15/2012	30°	Baseline Retest
9	5/18/2012	30°	MSE Wall
10	5/24/2012	30°	5.5 ft (1.52 m)
11	5/30/2012	30°	3.0 ft (0.91 m)
12	5/31/2012	15°	Baseline
13	6/4/2012	15°	5.5 ft (1.52 m)
14	6/6/2012	15°	3.0 ft (0.91 m)
15	6/8/2012	15°	3.0 ft (0.91 m) Retest
16	6/13/2012	15°	MSE Wall

3.5.2 Backfill Installation

In general, backfilling began between 6 to 12 in (15.2 to 30.5 cm) below the bottom of the pile cap. Underneath the backfill consisted of native clay material. Each lift was placed in approximately 6-in (15.2-cm) increments until the desired height for each test was reached. Each lift was filled and leveled by a backhoe and by hand with shovels for the corners and edges. The lift was then compacted with a vibrator roller compactor for deep compaction and a walk-behind plate compactor for shallow compaction, edges, and corners. Figure 3.28 shows the compactor instrumentation in action. Each lift was tested in two random locations by a nuclear density gage, as shown in Figure 3.29, to ensure that a density greater than or equal to 95% of the modified proctor value was achieved. The average soil properties for each test are given and summarized in Section 3.3. After reaching the desired height, the backfill was smoothed and leveled by taking random level rod readings along the top of the soil surface.

Figure 3.28: Compaction instruments with vibrator roller compactor on left and plate compactor on right

Figure 3.29: Testing soil with nuclear gage

3.5.3 Instrumentation Measurements

After each backfill was leveled adequately, a 2 x 2 ft^2 (0.61 x 0.61 m^2) grid was spray painted on the surface parallel to direction of push and to the cap face a shown in Figure 3.30. The grid lines helped to measure and locate soil surface cracking and failure. Dimensions of the grid equaled approximately 22 ft (6.7 m) wide and 24 ft (7.3 m) long for the 3ft and 5.5ft tests. The MSE walls limited the backfill to 11.5 ft (3.5 m) wide. During testing, surface cracking often appeared first on the spray painted lines.

At each intersection of the grid, a relative elevation measurement was taken with a surveying level and rod. These measurements were recorded, and new measurements were taken and recorded at the end of the test to determine the vertical displacement of the backfill. String pots were also set up near the face of the pile cap to read the longitudinal displacement of the soil. Each string pot was attached to a rod at varying positions along the grid as presented in

Section 3.4.1. Before pushing the cap, inclinometer and shape array readings were taken at both the north and south ends of the pile cap. Results for backfill movement are given in Section 4.1.

Figure 3.30: General backfill surface grid

3.5.4 Procedures During Test

For each test, the actuators pushed the pile cap into the backfill at a rate of 0.05 inches per minute (1.27 mm per minute) Each push was limited to approximately 0.25-in (6.4-mm) increments. After each push, an SAA reading was recorded for approximately 10 seconds. String pot values were also recorded and averaged to determine the actual push distance. These values helped calculate the next applied load of the actuators. Surface cracking was marked throughout the test with a spray paint color different from the grid. Each test was pushed at least 3.25 in (82.6 mm) not exceeding 3.75 in (95.3 mm) to prevent failure of the supporting piles.

At the end of the test, final SAA and inclinometer readings were taken. The crack locations were recorded as shown in Figure 3.31. Final heave measurements were taken with the surveying level and rod. During final measurements, the actuators were held at a constant load. Before excavation of the backfill, the pile cap was pulled back to its starting position.

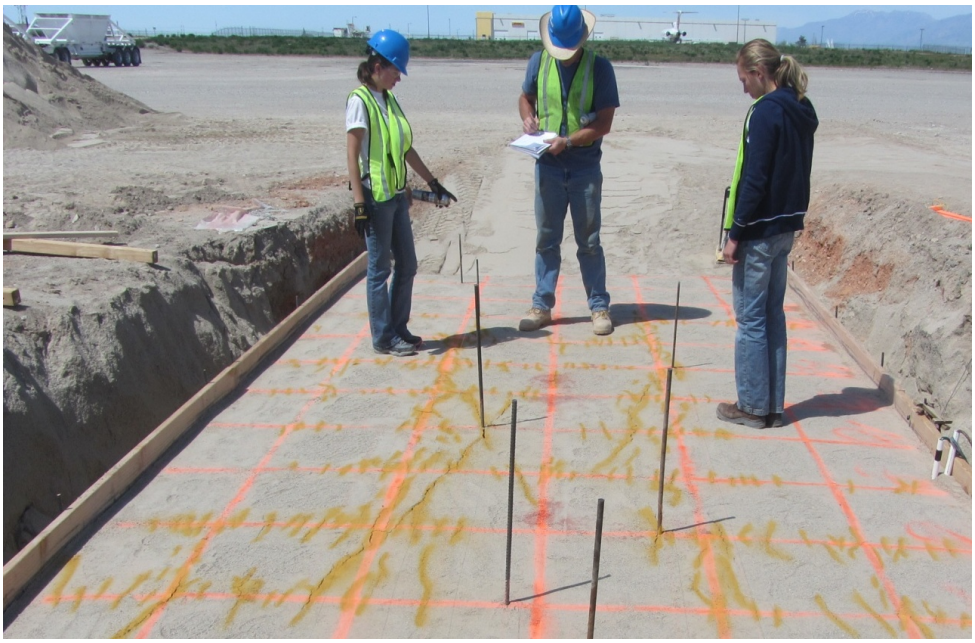

Figure 3.31: Marking and recording crack patterns in backfill

3.5.5 Shear Locations and Excavation

For the 3ft and 5.5ft zero skew tests, shear columns were placed along the middle of the grid at 2, 4, 6, and 8 ft (0.61, 1.22, 1.83, and 2.44 m) perpendicular to the pile cap face. These were constructed by hand auguring each hole to below the bottom of the pile cap, then refilling and compacting each hole with red-dyed sand. To find the shear plane, the lengths of the holes were excavated by backhoe and shovel; an example is shown in Figure 3.32. After the depths of the shear plane were measured and recorded, the pile cap was returned to its initial position, and the backfill was excavated by backhoe to the bottom clay layer boundary.

Figure 3.32: Discovering shear plane

4 0° SKEW TEST RESULTS AND ANALYSIS

This section compares the results of the different backfills for the 0° skew tests. Most often, the comparisons are between the unconfined 3ft and 5.5ft tests and between the 5.5ft unconfined and MSE confined tests. The displacement, strain, and failure zones of the backfills are first discussed along with the deflections of the tested pile cap. The passive force - deflection curves are subsequently discussed and analyzed.

4.1 Backfill Displacement, Strain, and Failure

The shear failure wedge for each test was determined by mapping the vertical displacement and cracking patterns observed on the surface of the backfill and using sand columns placed within the backfill. The strain in the backfill was also recorded.

4.1.1 Backfill Heave and Surface Cracking

Displacement of the backfill for each of the zero skew tests was an interesting comparison. Figure 4.1 provides a side-by-side comparison of ground surface heave and crack patterns for each test. Figure 4.2 provides side-by-side photographs of the crack patterns observed for each test. Lastly, Figure 4.3 provides photos and contour plots side-by-side for each of the three tests.

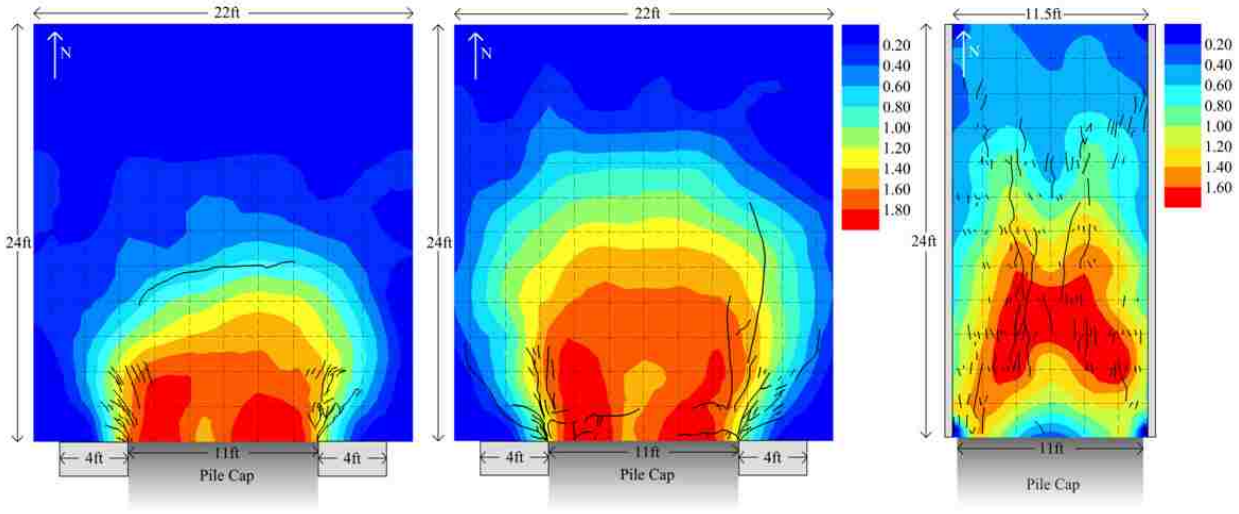

(a) **(b)** **(c)**

Figure 4.1: Plotted heave and crack patterns for 0° skew tests for (a) 3ft, (b) 5.5ft, (c) MSE

(a) **(b)** **(c)**

Figure 4.2: Heave and crack patterns for 0° skew for (a) 3ft, (b) 5.5ft, (c) MSE

As shown in Figure 4.1, the maximum heave values were 2.4 in (61 mm) near the face of the cap, 1.8 in (46 mm) near the face of the cap, and 1.8 in (46 mm) between 4 and 10 ft (1.2 and 3.0 m) behind the face of the cap for the 3ft, 5.5ft, and MSE wall tests, respectfully. These heave values amount to 6.7%, 2.7%, and 2.7% of each respective backfill height. The larger heave values for the 3ft test could be partially attributed to the lesser amount of soil being pushed and the reduction in vertical confining pressure. The soil had less resistance above and therefore

compressed and rose at the face of backwall with greater ease. More likely, the larger heave may be attributable to the fact that the normalized longitudinal displacement for the 3ft test was about three times greater than that for the 5.5ft test. Greater longitudinal displacement would be expected to result in more heave.

The maximum heave values near the outside edges of the pile cap are similar to observations from previous tests (Cummins 2009, Douglas and Davis 1964). Larger vertical displacement values and cracking of the backfill indicate higher pressures at those locations. Heaving and cracking release the pressure. The failure surface can be identified by heave contours and visible cracks at the surface. Figure 4.1 shows the shear failure surfaces of the 3ft and 5.5ft tests form a bulb-like shape, where the most pressure has been released. The MSE wall test, discussed subsequently, most likely failed with a different governing failure mechanism than the other two tests.

Each heave surface is relatively symmetrical about the centerline of the backfill. Heave and cracking of the unconfined 3ft and 5.5ft tests are similar in shape, with a larger failure bulb existing in the 5.5ft test. The defining boundary line of the failure zone is generally located where heave values are between 0.4 to 0.6 in (10.2 to 15.2 mm) (Franke 2013). This is generally exhibited in both the 3ft and 5.5ft tests by comparing the cracks and heave contour values. Based on 0.6 in (15.2 mm) heave criteria, the heave zones extended out from the backwall face by 10 ft (3.1 m), 17 ft (5.2 m), and 18 ft (5.5 m) for the 3ft, 5.5ft, and MSE backfills, respectively. The length of the heave zone increased by about 70% as the height of the backfill increased about 80% from 3 ft (0.91 m) to 5.5 ft (1.68 m). The ratio of failure surface length to wall height was relatively consistent with a value between about 3.1 and 3.3.

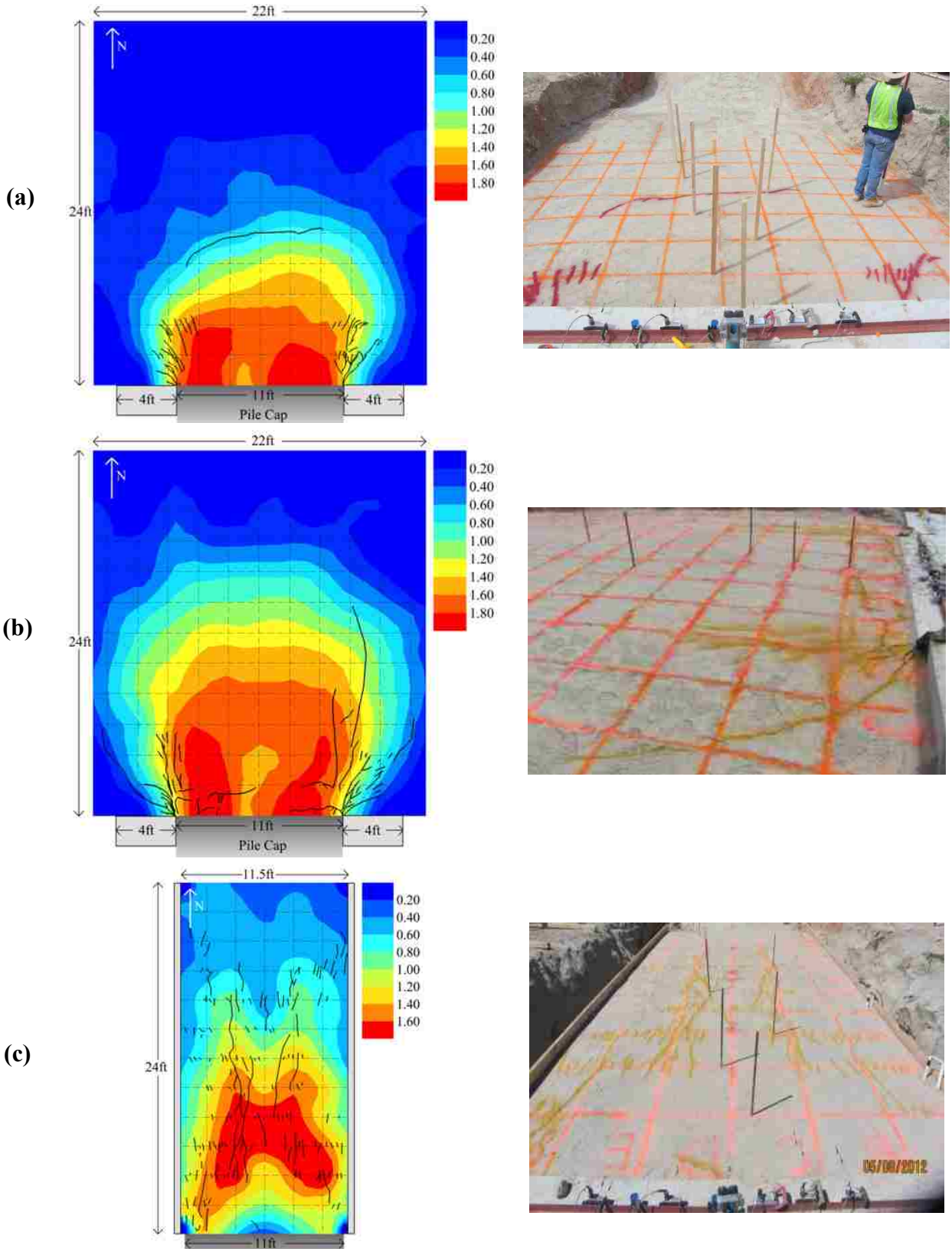

Figure 4.3: Heave and crack patterns for 0° skew tests for (a) 3 ft, (b) 5.5 ft, (c) MSE wall

For the unconfined backfills, the failure planes extend beyond the edges of the pile cap and increase the "effective width" of the pile cap. The effective widths, measured parallel to the cap face and between failure surfaces, were estimated as 17 ft (5.2 m), 21 ft (6.4 m), and the confined 11.5 ft (3.5 m) for the 3ft, 5.5ft, and MSE wall backfills, respectively. These effective widths correspond to 1.54B, 1.91B, and 1.05B, respectively, where B is the 11 ft (3.35 m) width of the pile cap. The "effective width" to wall height ratios were also relatively consistent remaining between about 3.6 and 3.8 for both unconfined tests.

The confined MSE wall test shows an "X" shape crack pattern and maximum vertical deformation farther from the cap face. This is most likely due to the attached grids and MSE walls, which helped the backfill act together as a unit as the pile cap was pushed (Franke 2013). Heave values are seen to remain high along the MSE walls. The longitudinal cracking pattern suggests that the MSE wall panels are moving outward transverse to the direction of loading. The greatest transverse wall deflection occurs at about 12 ft (3.7 m) back from the pile cap face (Franke 2013).

4.1.2 Shear Failure

Both the 3ft and 5.5ft backfills failed along a log spiral curve surface as illustrated in Figure 4.4. The observed shear locations for each soil column were measured and plotted as shown in Figure 4.5. Both the 3ft and 5.5ft tests exhibited a shear failure zone as described by Terzaghi (1943), consisting of both the Prandtl and Rankine zones. The base of the Prandtl zone has a curved (log-spiral) shape while the base of the Rankine zone is linear. A downward trending shear plane separates the two zones. The Prandtl zone wedge, adjacent to the face of the backwall, seems to displace the most moving forward and down. The farther and downward movement of the Prandtl zone is seen in both Figures 4.4a and 4.4b for the 3ft and 5.5ft backfills,

respectively. The Rankine zone, which incorporates the soil wedge beneath the surface of the backfill, is forced upwards by the Prandtl zone and forward by the Prandtl zone and pile cap displacement. The portion of the soil columns below the log spiral shear plane are outside the shear zone. Heave is limited to the zone inside the failure mass.

(a)

(b)

Figure 4.4: Shear failure zone for (a) 3ft test and (b) upper 5.5ft test

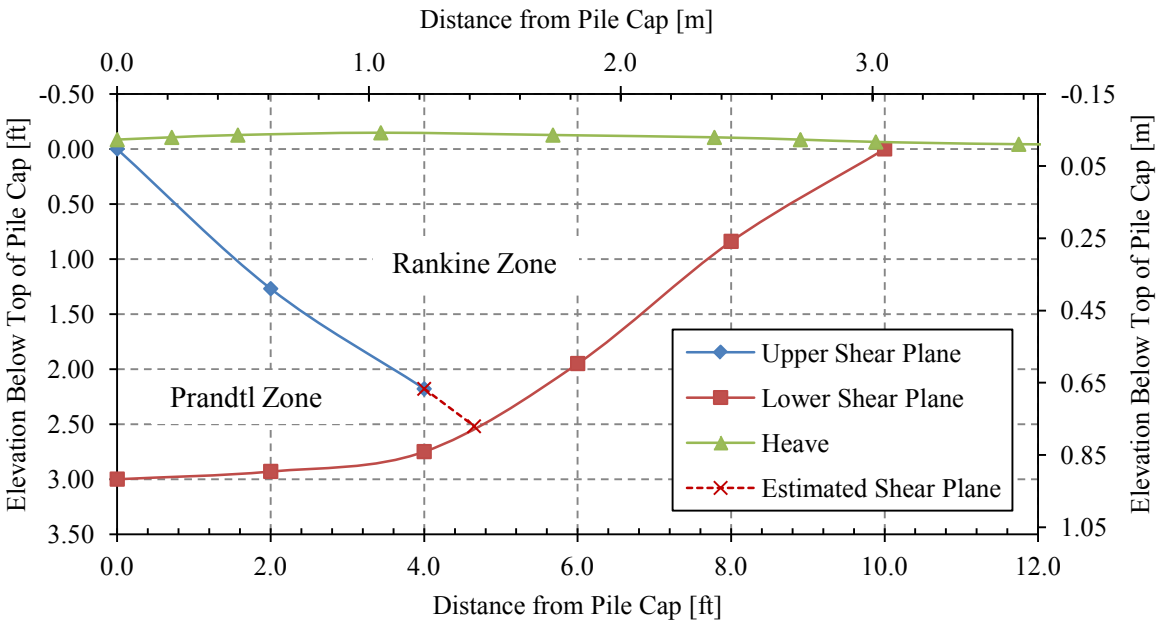

(a)

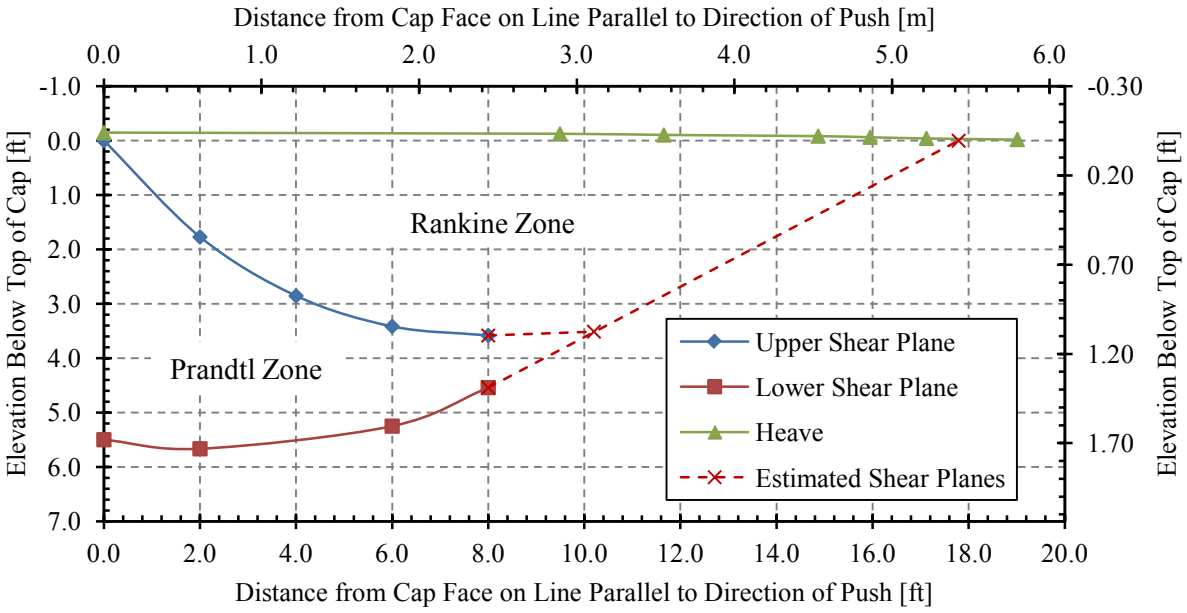

(b)

Figure 4.5: Profile plot of failure geometry for (a) 3ft (Palmer 2013) and (b) 5.5ft (Marsh 2013) tests

4.1.3 Backfill Displacement

The measurements from the string pots located longitudinally along the backfill grid for each of the zero skew tests are displayed in Figure 4.6, with the final displacements summarized in Figure 4.7. String pot setup is discussed in Section 3.4.1. Displacement versus distance curves for incremental pushes of the pile cap are shown with different line styles. Curves are shown at longitudinal pile cap deflection of 0.5 in (12.7 mm), 1.0 in (25.4 mm), 2.0 in (50.8 mm), and the final push at 3.25 in (82.6 mm). The displacements at various locations in the three backfills are similar up to the 2.0 in (50.8 mm) push.

At the 2.0 in (50.8 mm) push, the 3ft test displacement drops significantly lower than the other tests at approximately 12 ft (3.7 m) from the backwall. With the shear failure wedge daylighting at 10 ft (3.0 m) and the peak passive force occurring at 1.53 in (38.9 mm), it can be assumed the 12 and 14 ft (3.7 and 4.3 m) measurements were outside the shear failure zone and thus experienced a smaller amount of displacement. Neither the 5.5ft nor MSE wall tests show the same distinctive drop in displacement, or daylighting of the shear wedge in the zero skew tests. Rather the displacement pattern showed a relatively linear trend with distance from the backwall. In Figure 4.7, the 5.5ft test exhibits a rather significant drop in displacement immediately behind the backwall, suggesting significant heave and compression of the soil between the face of the cap and the 2.0-ft (0.61-m) string pot measurement. This type of drop in displacement is also seen in the 2.0 in (50.8 mm) and the last push of each of the tests, though not as dramatic. Due to the resisting force from the larger amount of backfill, the 5.5ft test reasonably compresses more than the other tests. As the soil compressed during loading, the amount of displacement proportionally decreased with distance from the pile cap face. The MSE

test curve has a similar shape through each of the pushes, suggesting that the MSE walls effectively held the soil together as a unit.

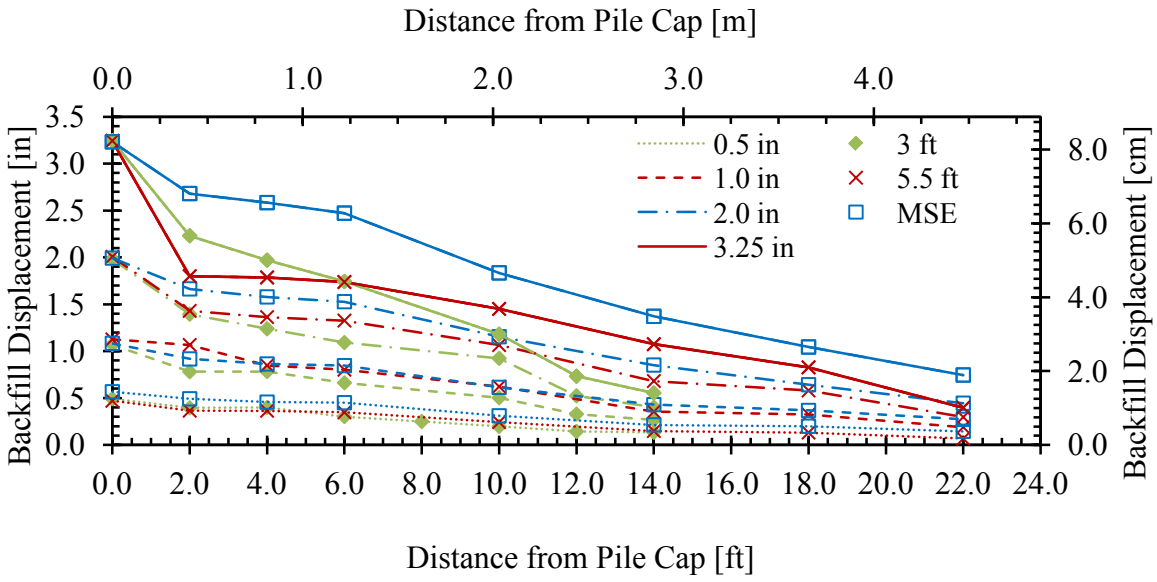

Figure 4.6: Backfill displacement measurements at various locations beyond the pile cap for 0° skew tests

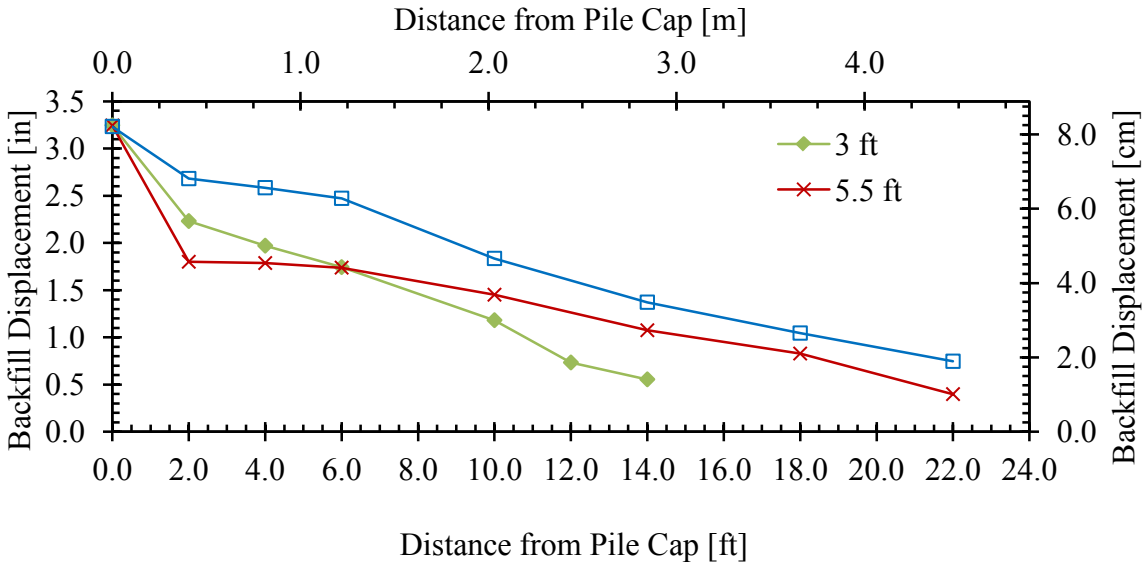

Figure 4.7: Final backfill displacement of 0° skew tests

4.1.4 Backfill Compressive Strain

The longitudinal compressive strain in each of the backfills was calculated from the measured displacements in Figures 4.6 and 4.7 and is plotted as a function of distance from the back of the pile cap in Figure 4.8. For simplicity, Figure 4.8 compares the final compressive strain for each of the 0° skew tests. All three strain profiles are reasonably comparable. The greatest amount of compressive strain is located within the first 2 ft (0.61 m) of the backwall with strain values of 2 to 6%. The 5.5ft backfill produced the greatest strain while the MSE produced the least. Beyond about 3 ft (0.91 m), the strain levels drop and remain typically between 0.5% and 1.5% along the rest of the backfill distance. The lower and constant strain suggests that the soil mass is displacing more or less as a block. Some evidence of increased strain for the 3ft test occurred where the failure surface daylights at around 11 ft (3.4 m) indicating that the soil behind the failure wedge was likely being compressed (Palmer 2013). Without a daylighted failure wedge in either the 5.5ft or MSE wall 0° skew tests, the compressive strain shows little evidence of the failure surfaces. Perhaps the grid spacing is too coarse to resolve the increased strain around the failure surface which may be rather localized. The lower strain in the MSE test could also be attributed to the presence of the MSE walls and grids which reinforce the soil, preventing soil compressibility. The rise in compressive strain between 8 and 16 ft (2.4 and 4.9 m) occurs within the unreinforced section of the MSE walls (Franke 2013). Also, outward movement of the MSE wall panels could have relieved pressure and reduced the compressive strain.

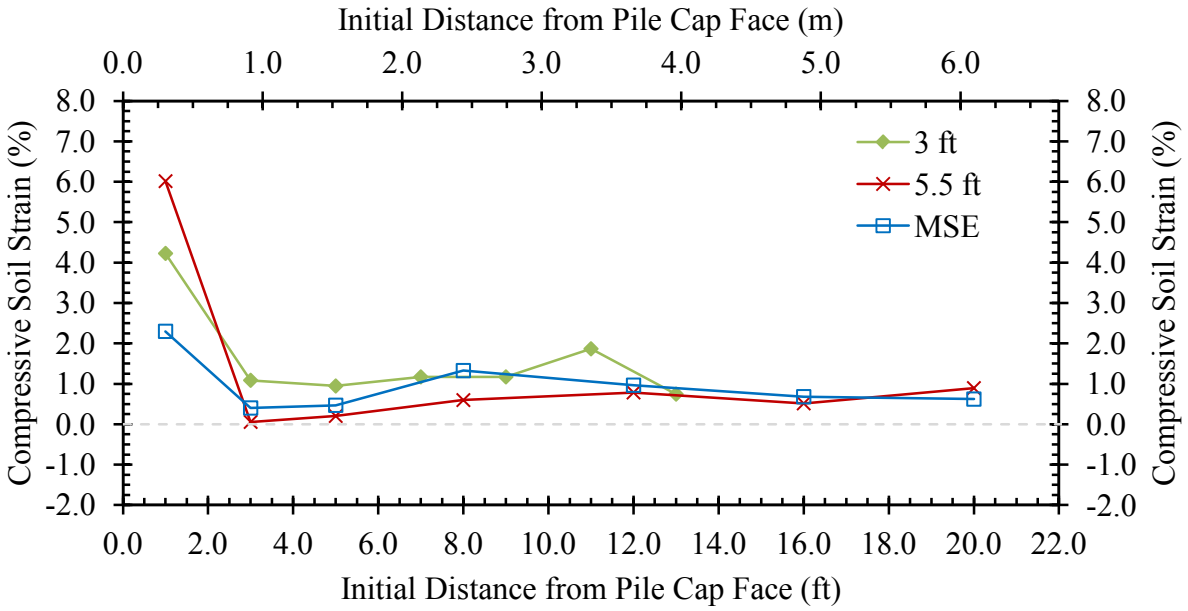

Figure 4.8: Final compressive strain of backfill for 0° skew tests

4.2 Passive Force vs. Deflection Comparison

As the surface and internal behavior of the backfill was recorded, the force required to accomplish displacement was also measured. The passive resistance of each backfill exhibited comparable reactions. Peak passive forces were recorded at displacement values within previously observed ranges. Each test required different loads due to the mass of each backfill and the shear failure zones. Effective width and cohesion are also seen to attribute significantly to the measured passive force and deflection values. This section compares the results between the unconfined tests with different backwall heights (3ft vs. 5.5ft), and between the unconfined and confined backfills (5.5ft vs. MSE).

4.2.1 Baseline Tests

Six baseline tests were conducted throughout the testing program. The baseline tests provided means to compare the backfill resistance of the different heights and skews for the tests performed. To summarize, the pile cap was pushed three separate times with no skew wedge attached, twice with the 30° wedge, and once with the 15° wedge. The individual baseline tests chosen for the zero skew analyses were determined for the 3ft, 5.5ft and MSE wall tests in the Palmer (2013), Marsh (2013), and Franke (2013) theses, respectively. To accurately compare their results, the same chosen baseline tests were used for this analysis. The reader may refer to their theses for further discussion on the baseline choices. For the 0° skew, the 3ft test used the first 30° skew baseline test (Palmer 2013), the 5.5ft test used the first 0° baseline test (Marsh 2013), and the MSE wall test also used the first 0° baseline test (Franke 2013). The baseline results used for each of the 0° skew tests are shown in Figure 4.9. As expected, the results are all very similar which allows the computed backfill resistance to be compared.

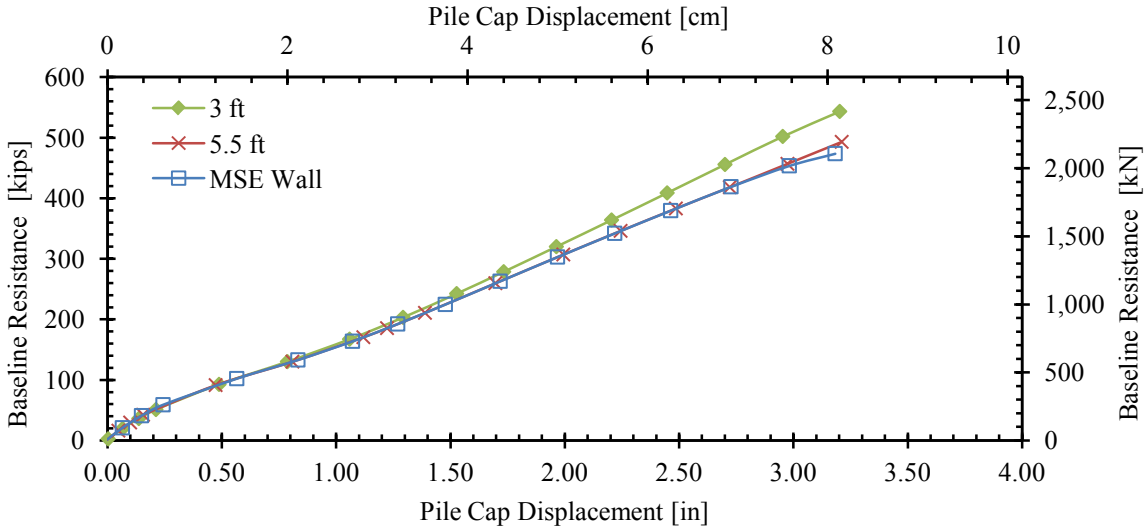

Figure 4.9: Baseline resistance for each of the 0° skew tests

4.2.2 Passive Force – Deflection Curve

Figure 4.10 provides the resulting backfill resistance for each of the 0° skew tests. The peak passive forces for the 3ft, MSE wall, and 5.5ft unconfined fill tests were 167.6 kips (745.5 kN), 453.7 kips (2018 kN), and 480.5 kips (2137 kN), respectively. The associated deflections for the peak forces occurred at 1.53 in (38.9 mm), 3.18 in (80.8 mm), and 2.97 in (75.4 mm), respectively. Although actual peak resistance may not have been fully achieved, concerns about exceeding pile resistance with further displacement necessitated that the peak passive force for the MSE wall test be defined at the maximum displacement (Franke 2013). Thus, the peak resistance and deflection may have actually been somewhat higher than the values reported for the MSE wall test. As previously mentioned in Section 4.1, the lack of failure may have occurred because the MSE wall boundaries prevented shear zones from extending beyond the edges of the pile cap. The normalized deflection at the peak passive force for the 3ft, 5.5ft, and MSE wall tests, with H as the height of the backwall, correspond to 0.043H, 0.045H, and 0.048H, respectively. Each of these values are comparable and fall within the previously observed ranges of 0.03H to 0.05H for zero skew tests by Rollins and Cole (2006). Table 4.1 summarizes the passive force and deflection values for easy reference.

Table 4.1: Peak passive force and deflection values for the 0° skew tests

Test	*Peak Passive Force [kips] (kN)*	*Deflection [in] (cm)*	*Deflection Equation*
3ft	167.6 (745.5)	1.53 (3.89)	0.043H
5.5ft	480.5 (2137)	2.97 (7.54)	0.045H
MSE wall	453.7 (2018)	3.18 (8.08)	0.048H

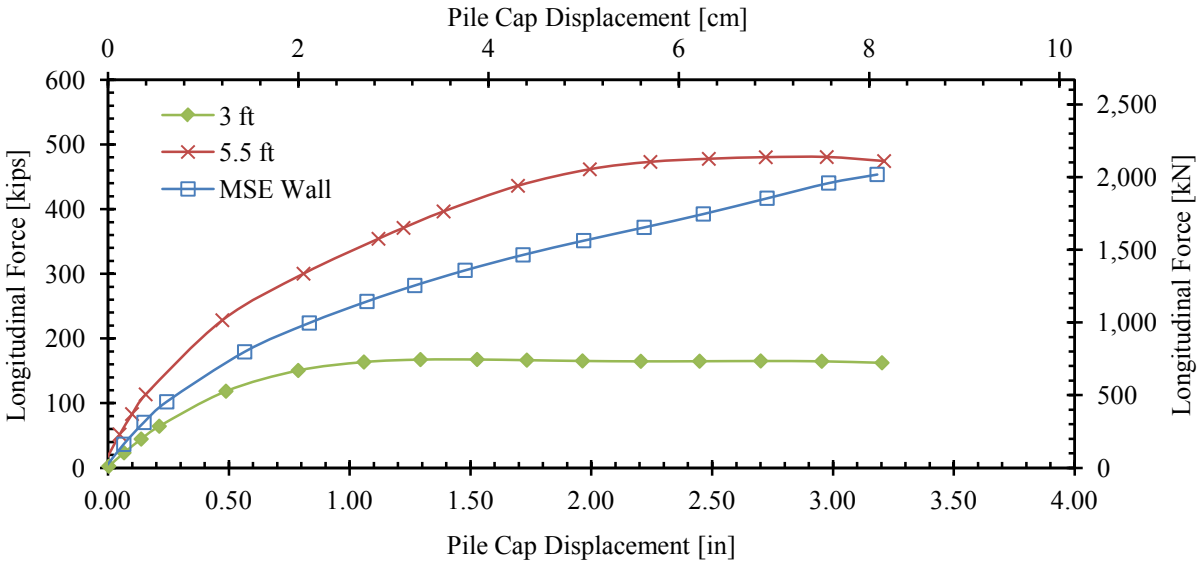

Figure 4.10: Backfill resistance for each 0° skew test

As the mass of the backfill increased, the amount of force required to move the pile cap increased. The total volume of the backfill for the 3ft and 5.5ft unconfined tests were approximately 2000 ft^3 (57 m^3) and 4000 ft^3 (113 m^3), respectively. The volume of the 5.5ft MSE backfill, confined within the MSE walls, measured approximately 2000 ft^3 (57 m^3) not including the weight of the walls and grids. When the pile cap was pushed, each backfill failure zone contributed to the force needed to move the pile cap. The estimated volumes within the shear failure zones for the 3ft, MSE wall, and 5.5ft tests were calculated to be 420 ft^3 (11.9 m^3), 1265 ft^3 (35.8 m^3), and 1760 ft^3 (49.8 m^3). With the dry unit weights listed in Section 3.3.2, the weight of the soil within the failure zones come to 45 kips (200 kN), 137 kips (609 kN), and 188 kips (837 kN), respectively. Table 4.2 shows the percent increase in both mass and load for the larger backfills. Although there is not a direct correlation between the percentages, a definite increase is observed in both load and mass. Because the weight of the walls and grids were not

included in the comparison, only a slight load increase is seen compared to the larger mass increase between the MSE wall and 5.5ft tests.

Table 4.2: Percent increase in mass and load between 0° skew tests

Test	*Applied Load [kips (kN)]*	*Mass Resistance [kips (kN)]*	*Increase in Load (%)*		*Increase in Mass (%)*	
			From 3ft	*From MSE*	*From 3ft*	*From MSE*
3ft	167.6 (745.5)	45 (200)	-	-	-	-
MSE	453.7 (2018)	137 (609)	171	-	204	-
5.5ft	480.5 (2137)	188 (837)	187	6	318	37

Except for the zero skew MSE wall, each test exhibited a hyperbolic load-displacement curve as seen in previous large scale tests (Rollins and Cole 2006, Shamsabadi, et al. 2006). The hyperbolic shape occurs when the backfill soil mass shears and resistance peaks or flattens out. The maximum passive force is the load that occurs just before shear failure is reached. The leveling out of the load results in the formation of 3-dimensional shear surfaces within the soil mass. Shear planes for the various tests are discussed in Section 4.1.2. The 3ft test, with a smaller passive force, sheared at an earlier deflection than the other two tests as seen in Table 4.1. The 5.5ft test took nearly twice the displacement of the 3ft test to shear. Compared to the unconfined 5.5ft test, the MSE about 7% more displacement was needed to reach the peak resistance.

Between the three tests, width of the failed soil (3D plane) was seen to affect the force resisted by the soil. Estimated from the shear failure zones, as shown in Section 4.1.1, effective widths for the MSE wall, 3ft, and 5.5ft tests are 11.5 ft (3.5 m), 17 ft (5.2 m), and 21 ft (6.4 m), respectively. The ratios of effective width to actual width are 1.55 and 1.91, respectively for the 3ft and 5.5ft walls. The ratio appears to increase as the wall width to height ratio decreases. When passive force is divided by effective width, the efficiency of a given abutment geometry

can be better understood. The results in Figure 4.11 clearly show that the passive force per width is greater for the backfill with MSE walls than for the unconfined test. The peak passive force for the MSE wall is 72% higher relative to the unconfined 5.5ft test as described in Table 4.3. This observation may be explained by at least three reasons. First, the failure geometry of the MSE case is a 2D or plane strain condition, whereas the failure for the unconfined backfill is closer to a 3D or triaxial shear geometry. As discussed in more detail in Section 5.1, greater soil strength is generally obtained with a plane strain geometry. In addition, the presence of the bar mats and MSE wall panels can potentially increase the lateral pressure on the failure mass and thereby increase shear strength. Finally, reinforcing mats may create a volume which simply compresses longitudinally and expands laterally rather than allowing a conventional log spiral shear surface to form. Even if the failure surface did form, it would have to pass through the reinforcing layers which would then increase shear strength.

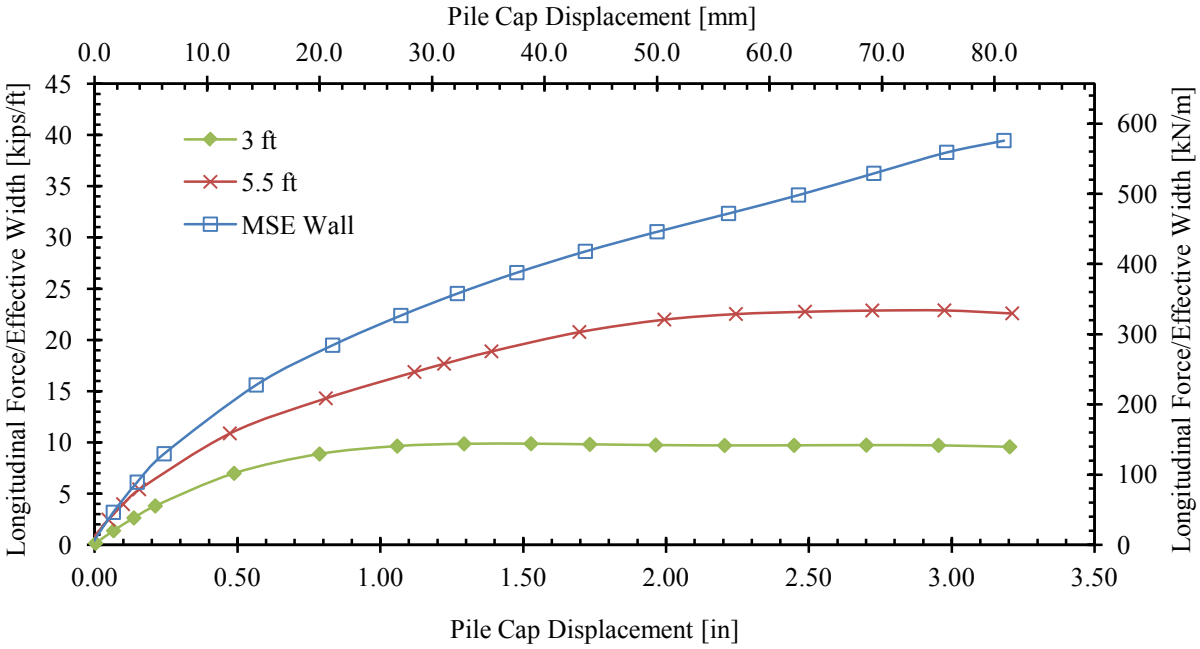

Figure 4.11: Backfill resistance normalized with effective width for each 0° skew test

Table 4.3: Comparison of passive force/width between confined and unconfined 5.5ft tests

Test	*Peak force/Measured width [kips/ft (kN/m)]*	*MSE/5.5ft (% increase)*
5.5ft	22.9 (332)	72
MSE	39.5 (577)	

The previous discussion and the results in Figure 4.11 clearly show that both the effective width and the total passive force for the unconfined backfills vary with backfill height. As described in Section 2.1, the effect of backfill height is not seen as a linear trend. Based on the classical passive force theories, the passive force should increase proportionally to the square of the height ratio. The square of the height ratio between the 3ft and 5.5ft tests equals 3.36, which is greater than the passive force ratio of 2.87. Therefore, the increase in passive force is not as great as expected based on the height ratio. There are two possible explanations for the differing values. First, the 3D effects for the two wall heights are different as addressed in Section 4.1 and more fully analyzed in Section 5.1. The 3ft test has a smaller effective width than the 5.5ft test. Second, small amounts of cohesion can have a pronounced effect on the passive force contributed by the soil. Discussed in more detail in Section 5.1, the cohesive term is only a linear function of the height ratio. As a result, a lower passive force ratio than expected by the squared height ratio is likely. Without considering cohesion or effective width differences, the raw test results suggest an exponent of 1.74 for the height in the passive force equation. Another study conducted by Shamsabadi, et al. (2010) also found that the squared height ratio was not an accurate comparison to the passive force ratio for dense sand. Section 5.1 discusses the effects of removing the 3D and cohesion force contributions using Duncan and Mokwa's (2001) PYCAP program, and lowering the squared height ratio.

In Figures 4.10 and 4.11, the initial stiffness clearly increases as the wall height increases and also seems to depend on the amount of backfill placed behind the wall in each test. However, all three tests have a similar initial stiffness when force is normalized by peak force and displacement is normalized by wall height. Initial stiffness comparisons of the 0° skew tests are included in Figure 4.12. Initially, the 5.5ft test has the highest stiffness, but decreases at about 0.01H. The 3ft test has the most consistent slope and peaks much earlier than the other two tests. Because of the smaller load and height associated with the 3ft test, normalized displacement extends the curve to 0.09H. The curve remains relatively flat after the peak is reached although there is a small decrease (<5%) in resistance. The MSE wall test has the softest response, likely due to transverse movement of the wingwalls as longitudinal force is applied. Taking out the normalized effects of displacement in Figure 4.13, the locations of peak passive force are more clearly seen. In terms of absolute displacement, the 3ft test peaked first, then the 5.5ft test, with the MSE wall test reaching its peak at the farthest displacement.

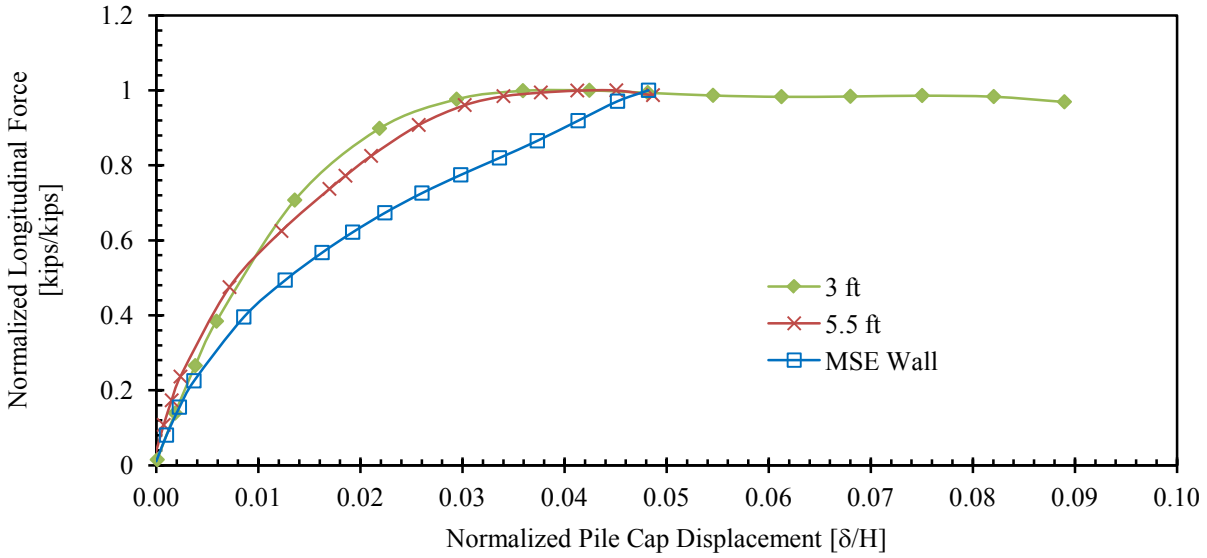

Figure 4.12: Normalized backwall resistance vs. normalized pile cap displacement for 0° skew tests to compare initial stiffness values

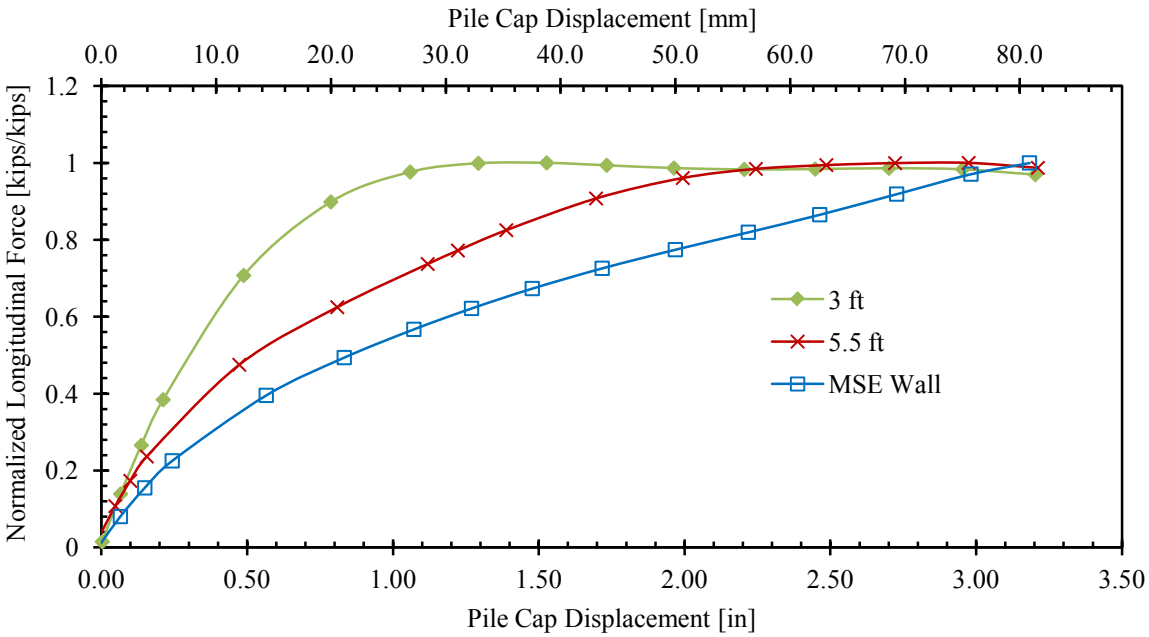

Figure 4.13: Normalized backwall resistance vs. displacement for 0° skew tests to compare peak force locations

4.3 Pile Cap Deflection and Rotation

Following the movement of the pile cap and piles helped to understand the way a bridge abutment would behave under applied static loading. For the zero skew tests, forward movement is as expected. Unexpected transverse displacement and rotation of the pile cap was also observed and is described in the following section. Comparisons of the tests also indicate consistent and repeatable testing methods.

4.3.1 Inclinometer and Shape Array Profiles

The pile cap was pushed at 0.25-in (6.4-mm) increments to a maximum forward or longitudinal deflection of approximately 3.5 in (89 mm). Between each increment the cap was held in place to secure recordings and measurements. Before each test and at the maximum

forward deflection for each test, inclinometer readings were taken of the pile cap deflection. Figure 4.14 provides plots of longitudinal deflection versus depth curves at the maximum forward displacement for each zero skew test side by side for easy comparison. Good agreement is seen between all instruments in each test for both the measured north and south ends of the pile cap, which gives validation to the repeatability of the tests. The final displacements of each of the tests are also similar, resulting in comparable attributes. In each case, the deflections within the pile cap itself indicate that the cap largely translated under the lateral loading but some forward rotation was also evident in each case. Below the base of the cap within the piles, the deflection rapidly decreased to zero at a depth of about 20 ft (6.1 m) which did not vary much with the backfill type.

Transverse deflection was also recorded for the north and south ends of the pile cap. Comparisons are shown in Figure 4.15. Reasonable agreement is seen between the shape array and inclinometer readings; however, the transverse movements are very small. The cap shifted slightly to the left (west) during both the 3ft and MSE wall tests, whereas for the 5.5ft test the cap generally stayed close to the original centerline but did rotate out to the right (east and counterclockwise) on the south end. More discussion of rotation is provided in the following section. Movement is seen in the uppermost 20 ft (6.1 m) of the piles in both the longitudinal and lateral deflections.

4.3.2 Rotation

Transverse displacement at the top of the pile cap are plotted to show and aerial view of the rotation in Figure 4.16. The transverse displacements were obtained from the top points of both the inclinometer and shape arrays on the north and south sides of the pile cap for each zero skew test. The transverse deflection measurements of the pile cap for both north and south sides

revealed small amounts of counterclockwise rotation even during the zero skew test as shown in Figure 4.16. The rotation is likely accounted for by the two actuator components during the pushing of the pile cap and small discrepancies in the displacement for each actuator. The differences in rotation are assumed to be due to the backfill properties. For comparison, the zero skew baseline test is also included and shows slight counterclockwise rotation without much of a lateral shift.

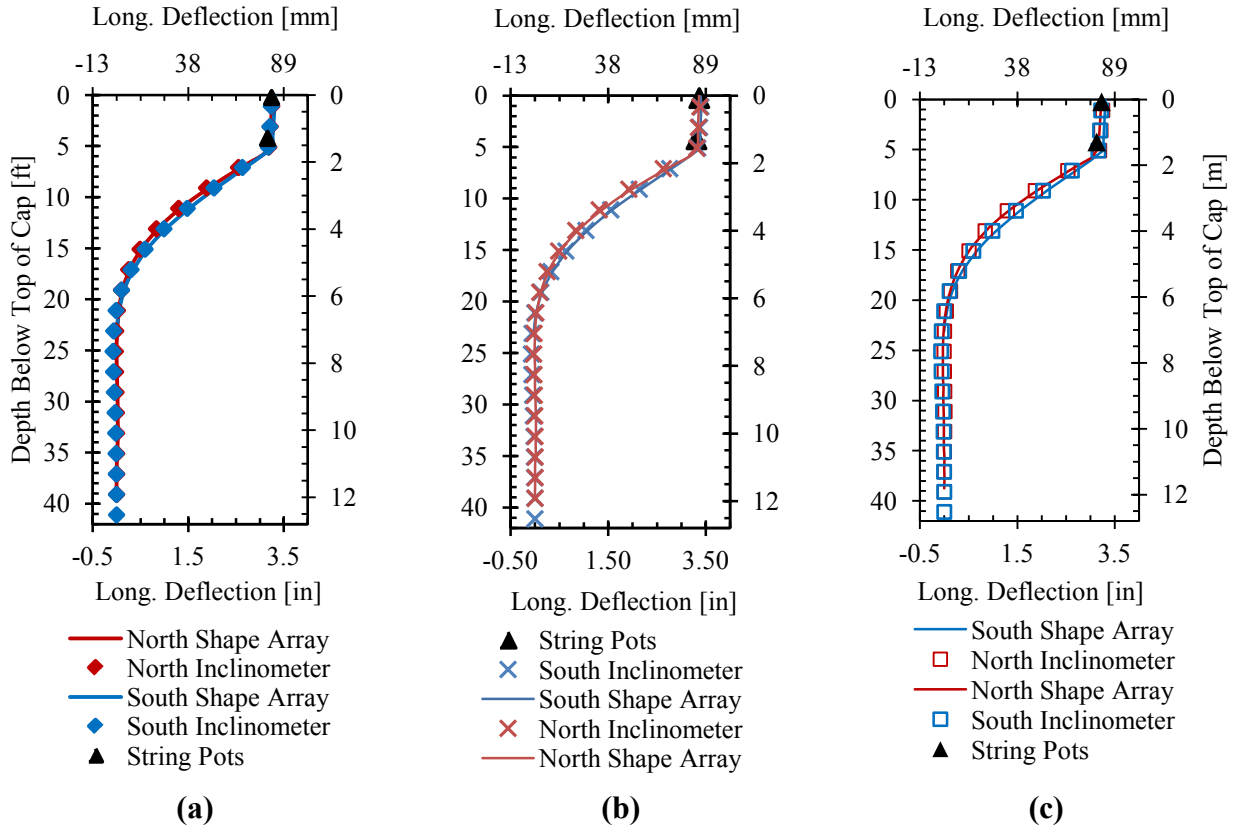

Figure 4.14: Longitudinal pile deflection as measured by the north and south shape arrays, inclinometers, and string pots for (a) 3ft, (b) 5.5ft, and (c) MSE wall tests

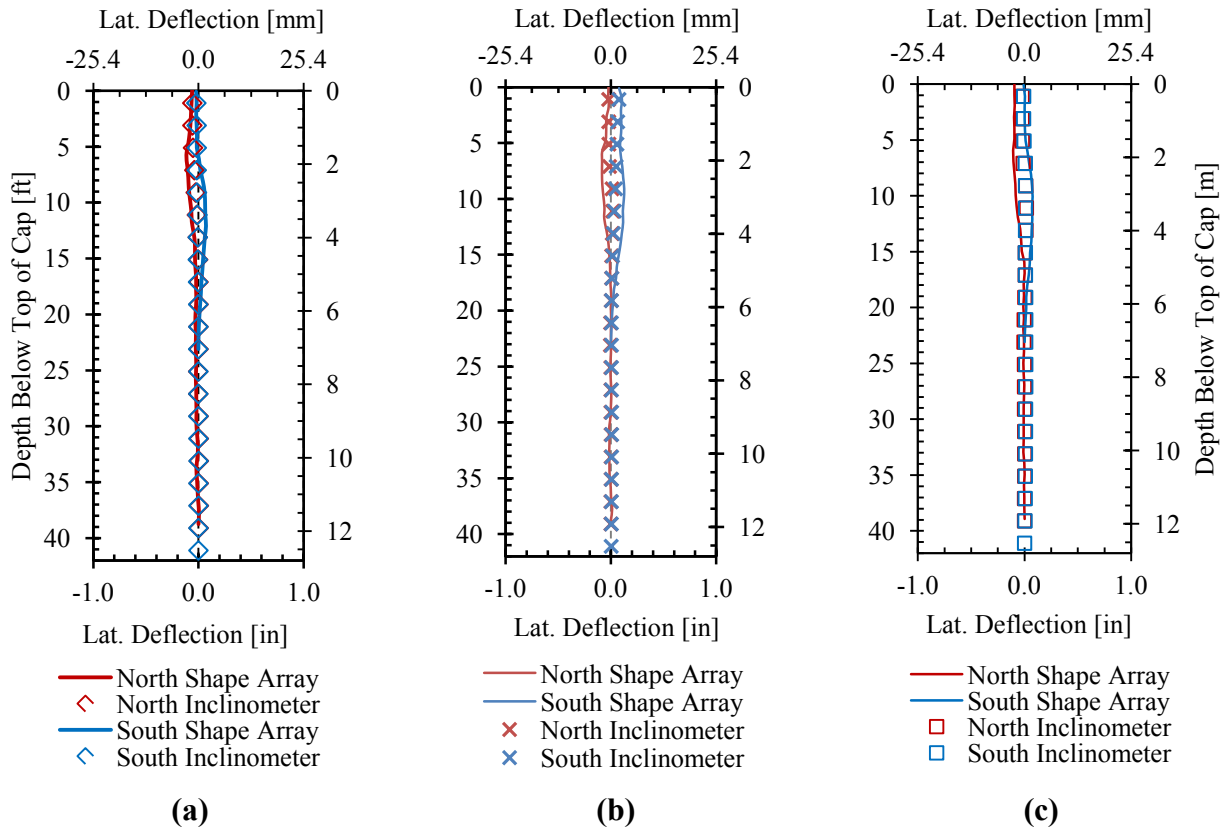

Figure 4.15: Transverse pile deflection as measured by the shape arrays and inclinometers for the (a) 3ft, (b) 5.5ft, and (c) MSE wall tests

Slight forward rotation of pile cap was also observed with all measurement devices for all 0° skew tests as shown in Figure 4.17. The rotations are very slight with typical measurements of about 1.2 degrees at the end of the test. This coupling effect has been attributed to the piles beneath the cap resisting the actuator load at the center of the cap which produces a moment on the pile cap (Palmer 2013).

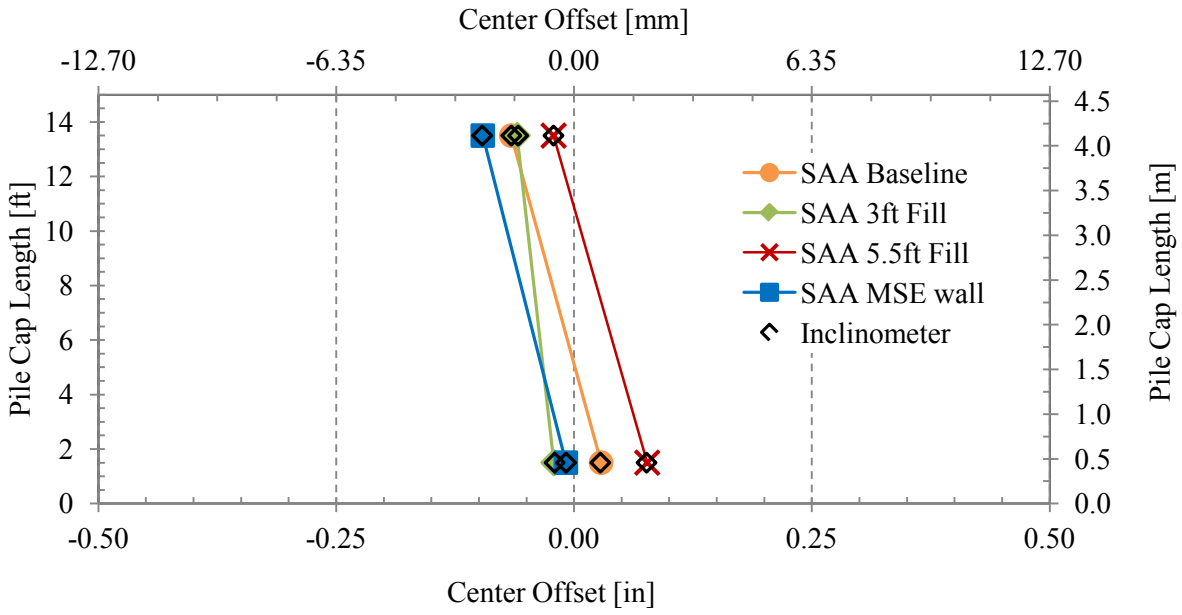

Figure 4.16: Final pile cap rotation for each 0° skew test

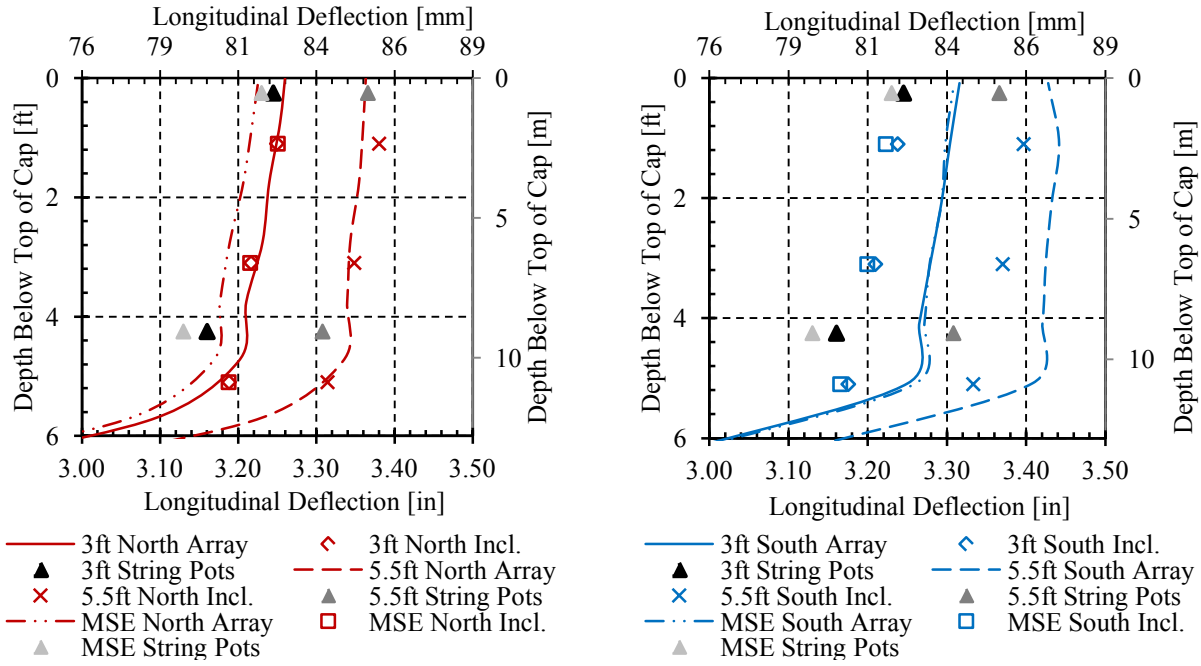

(a) **(b)**

Figure 4.17: String pot, shape array, and inclinometer measurements of pile cap for both (a) north and (b) south sides showing slight forward rotation

5 PASSIVE FORCE ANALYSIS AND COMPARISON

This section compares the results of various passive force theories and predictive methods described in Section 2 to the field results of the 0° skew tests.

5.1 Comparison of Results with Various Passive Force Prediction Approaches

The design methods for passive force - deflection curves described in Section 2.2 were used to make comparisons with the measured field test results. To provide comparable results, the soil backfill parameters were generally held constant for each design method. The back-calculated PYCAP parameters, determined from the two different zero skew backfill heights were used to compute the design curves. In most cases, the design curves were not accurate. In addition, best-fit parameters were also back calculated for each method.

5.1.1 PYCAP Design Curve

Duncan and Mokwa's (2001) PYCAP Excel spreadsheet was used to back calculate the optimum parameters for each test which were then used in calculating the other design curves. The optimum parameters determined by Palmer (2013), Marsh (2013), and Franke (2013) are listed in Table 5.1 and the curve comparisons are shown in Figure 5.1. The optimum soil parameters found for the 3ft and 5.5ft tests were similar, but many of the values for the MSE wall test parameters needed to be increased to fit the actual curve. The Brinch-Hansen (1966) 3D effects were disregarded for the MSE wall curve. In each thesis, the passive force curve was

optimized for the individually analyzed backfill, which prohibited a realistic estimate of the potential error found in the PYCAP predictions.

Table 5.1: Parameters used with PYCAP approach to compare passive force – deflection curves for individual 3ft, 5.5ft, and MSE wall tests [Adapted from Palmer (2013), Marsh (2013), and Franke (2013)]

Parameter	*3ft*	*5.5ft*	*MSE*	*Units*
Cap Width, b	11 (3.35)	11 (3.35)	11 (3.35)	ft (m)
Cap Height, H	3.0 (0.91)	5.5 (1.68)	5.5 (1.68)	ft (m)
Cohesion, c	100 (4.79)	85.0 (4.07)	137.7 (6.59)	psf (kN/m^2)
Soil Friction Angle, ϕ	42	40	47.2	degrees
Wall Friction Angle, δ	28.8	28	32.0	degrees
Friction Ratio, δ/ϕ	0.686	0.700	0.678	–
Initial Soil Modulus, E_i	415 (19.87)	415 (19.87)	520 (24.90)	kip/ft^2 (kN/m^2)
Poisson's Ratio, ν	0.25	0.33	0.25	–
Soil Unit Weight, γ_m	117 (18.4)	116.5 (18.3)	117.4 (18.4)	pcf (kN/m^3)
Adhesion Factor, α	1.00	1.00	1.00	–
Δ_{max}/H at Failure	0.032	0.032	0.065	–

To more fully compare the backfills, an attempt was made to determine how well one set of consistent PYCAP parameters would fit the measured test results for all tests. The Brinch-Hansen (1966) 3D correction equation was used to account for the effective width. Values for the 3D factor are tabulated in Table 5.2. These values are typically about 5% lower than observed in the field tests discussed previously. However, in computing the passive force for the MSE test the Brinch-Hansen (1966) correction factor was removed because the failure surface could not extend beyond the edge of the cap owing to the presence of the MSE wingwalls. Parameters were found that suited both the 3ft and 5.5ft tests within about 10% of the measured field curves. These values can be found in Table 5.4 and the computed and measured passive force-displacement curves are plotted in Figure 5.2. However, with these same parameters the

predicted curve for the MSE test significantly underestimates the measured load-deflection curve as shown in Figure 5.2. This is consistent with previous tests using MSE walls and appears to be a result of the 2D or plane strain loading condition (Bingham 2012, Rollins, et al. 2010, Strassburg 2010). The MSE curve in Figure 5.2 suggests that use of a triaxial, or 3D, friction angle in backwall design leads to a substantially conservative estimate.

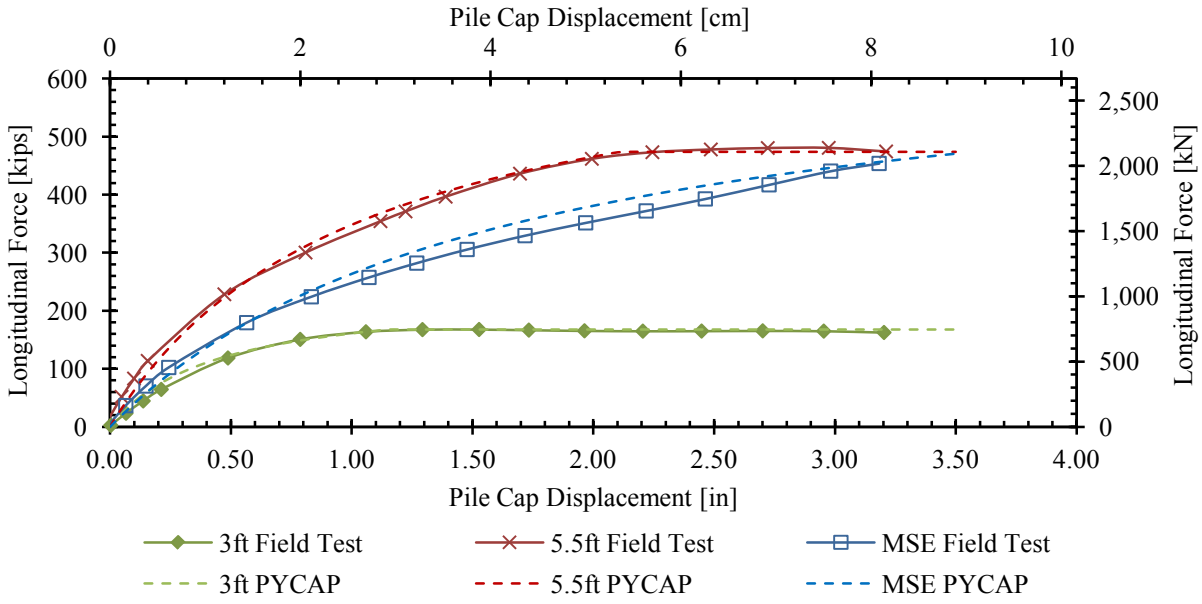

Figure 5.1: Comparison of PYCAP design curve with the passive force vs. backwall deflection curve for the individual 3ft, 5.5ft, and MSE wall tests [adapted from Palmer (2013), Marsh (2013), and Franke (2013), respectively]

Table 5.2: Comparison of measured and calculated 3D end effects

	3ft		5.5ft	
	Effective Width [ft (m)]	3D Factor	Effective Width [ft (m)]	3D Factor
Measured	17 (5.18)	1.55	21 (6.40)	1.91
PYCAP	16.1 (4.91)	1.47	20.0 (6.10)	1.82
% Error	5.3	5.2	4.8	4.7

Table 5.3: Parameters used with PYCAP approach to compare passive force – deflection curves for 3ft, 5.5ft, and MSE wall tests

Parameter	*3ft*	*5.5ft*	*MSE*	*Units*
Cap Width, b	11 (3.35)	11 (3.35)	11 (3.35)	ft (m)
Cap Height, H	3.0 (0.91)	5.5 (1.68)	5.5 (1.68)	ft (m)
Cohesion, c	100 (4.79)	100 (4.79)	100 (4.79)	psf (kN/m^2)
Soil Friction Angle, ϕ	41.2	41.2	41.2	degrees
Wall Friction Angle, δ	27.0	27.0	27.0	degrees
Friction Ratio, δ/ϕ	0.654	0.654	0.654	–
Initial Soil Modulus, E_i	450 (21.6)	450 (21.6)	450 (21.6)	kip/ft^2 (kN/m^2)
Poisson's Ratio, ν	0.25	0.25	0.25	
Soil Unit Weight, γ_m	117.0 (18.4)	116.5 (18.3)	117.4 (18.4)	pcf (kN/m^3)
Adhesion Factor, α	1.00	1.00	1.00	–
Δ_{max}/H at Failure	0.035	0.035	0.035	–

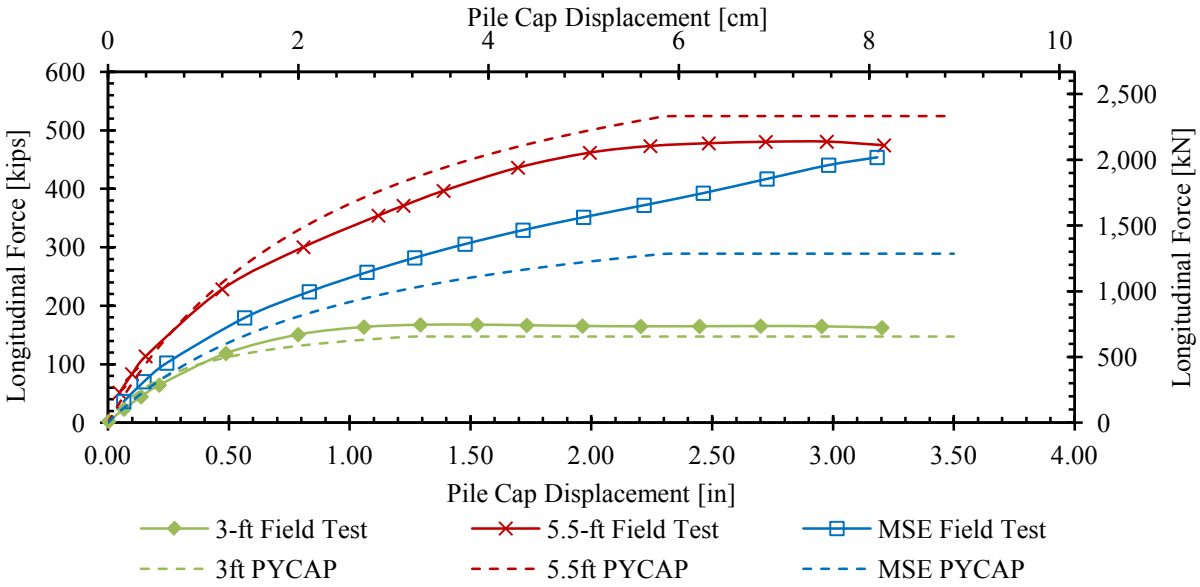

Figure 5.2: Comparison of PYCAP design curves with the passive force vs. backwall deflection curve for the combined 3ft, 5.5ft, and MSE wall tests with same soil parameters

While trying to preserve the parameters found with the 3ft and 5.5ft, some MSE test parameters were increased to better fit the field curve as shown in Table 5.4. While keeping the ratio similar to the unconfined tests, the soil and interface friction angles were increased. To make the plane strain condition compatible, an approximate 10% increase over the triaxial friction angle was needed. This increase is consistent with laboratory tests results which indicate that the plane strain friction angle is typically about 10% higher than the triaxial friction angle (Bingham 2012, Rollins, et al. 2010, Strassburg 2010). Figure 5.3 compares the effectiveness of using a plane strain friction angle rather than the commonly used triaxial angle. The plane strain parameters much more closely match the measured passive force-deflection curve, particularly up to a displacement of about 2.5 in (6.4 cm) after which the measured curve diverges upward. However, both cases assume the peak force occurred at a deflection 3.5% of the backfill height, which does not match the observed MSE field curve. The divergence at large deflections call into question the baseline curve used to define the MSE wall passive force, but no obvious errors in the baseline curve could be determined. Based on the shape of the measured curve, failure of the backfill is assumed to have occurred after the final measured displacement. Therefore, the Δ_{max}/H value was increased to 0.065 for which the curve follows a more comparable path. The final values used in the analysis can be found in Table 5.4 and the resulting computed passive force-deflection curve in Figure 5.4.

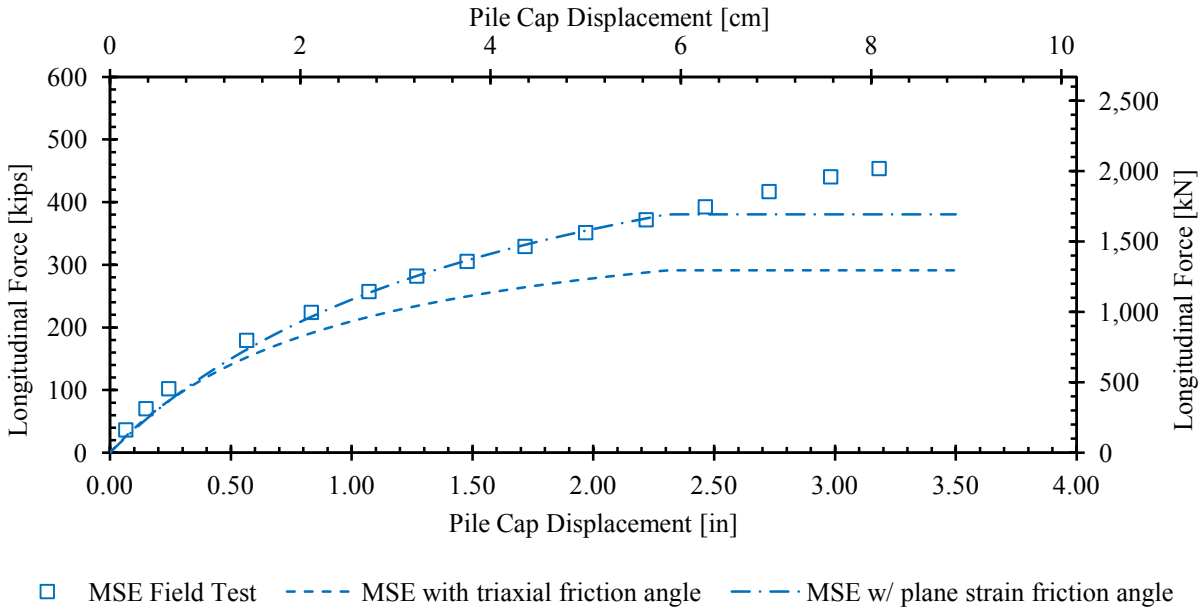

Figure 5.3: Comparison of MSE field test with unconfined PYCAP parameters using triaxial and plane strain friction angles

Table 5.4: Final parameters used with PYCAP approach for 3ft and 5.5ft tests with adjusted MSE test parameters

Parameter	*3ft*	*5.5ft*	*MSE*	*Units*
Cap Width, b (ft)	11 (3.35)	11 (3.35)	11 (3.35)	ft (m)
Cap Height, H (ft)	3.0 (0.91)	5.5 (1.68)	5.5 (1.68)	ft (m)
Cohesion, c	100 (4.79)	100 (4.79)	100 (4.79)	psf (kN/m^2)
Soil Friction Angle, ϕ	41.2	41.2	45.3	degrees
Wall Friction Angle, δ	27.0	27.0	29.6	degrees
Friction Ratio, δ/ϕ	0.654	0.654	0.654	–
Initial Soil Modulus, E_i	450 (21.6)	450 (21.6)	450 (21.6)	kip/ft^2 (kN/m^2)
Poisson's Ratio, ν	0.25	0.25	0.25	
Soil Unit Weight, γ_m	117.0 (18.4)	116.5 (18.3)	117.4 (18.4)	pcf (kN/m^3)
Adhesion Factor, α	1.00	1.00	1.00	–
Δ_{max}/H at Failure	0.035	0.035	0.065	–

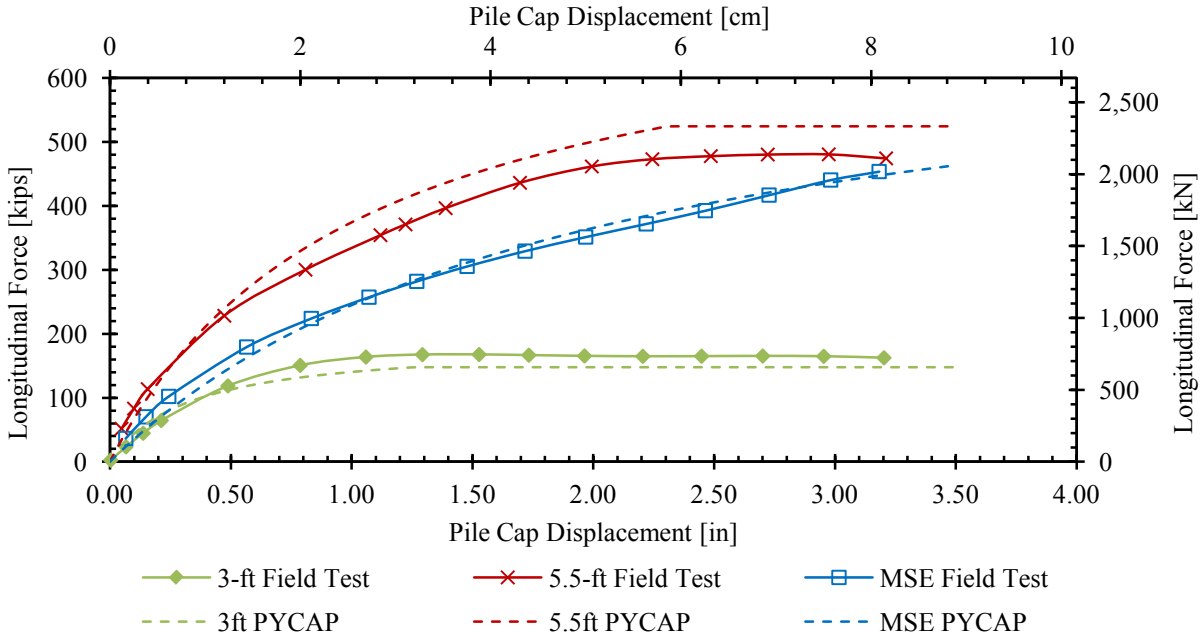

Figure 5.4: Comparison of PYCAP design curves with the passive force vs. backwall deflection curve for the combined 3ft, 5.5ft, and MSE wall tests with similar soil parameters

The shape of the MSE passive force-deflection curve is similar in comparison with previous studies of MSE wingwalls, as shown in Figure 5.5. Each of the compared tests consisted of a dense sand with field compaction averaging between 95% and 96% of modified Proctor target. While the backfill heights were similar at 5.5 ft (1.68 m), the loads varied due to various testing methods as described in Bingham (2012), Rollins, et al. (2010), and Strassburg (2010), and were thus normalized with the maximum force values. Conveniently, each test was pushed to approximately the same deflection. These similar curves suggest that the MSE tests are valid and that the wingwalls do affect the passive resistance and deflection of the backfill. The compared MSE tests also increased the soil friction angle and percent deflection to match the calculated PYCAP curves to the field curves (Bingham 2012, Rollins, et al. 2010, Strassburg 2010).

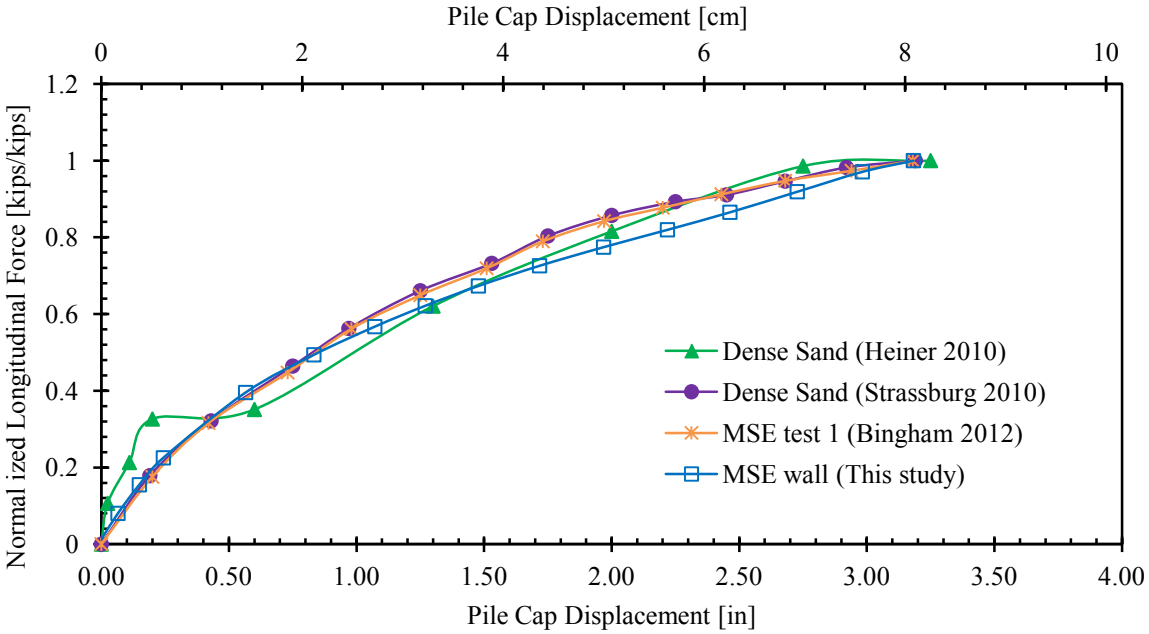

Figure 5.5: Comparison of MSE tests [adapted from Rollins, et al. (2010), Strassburg (2010), Bingham (2012)]

To evaluate the height effects for passive resistance of backfills, the 3ft and 5.5ft 0° skew tests were analyzed and compared using the PYCAP program. As discussed in Section 4.2.2, using the measured total passive resistance caused an apparent discrepancy between the passive force and squared height ratios. The lower passive force ratio between the tests is likely due to the 3D effects and cohesion contribution to the passive resistance. When the cohesion and 3D effects are removed, the passive forces can be more appropriately compared. After removal of 3D effects and the contribution of cohesion, the ratio of the square of the heights should correspond with the ratio between passive force for the two wall heights as shown in Equation (2.1). PYCAP was used to determine the force contributions for each unconfined test and Table 5.5 provides the results. The included forces were calculated by using the parameters in Table 5.4. The total passive forces calculated for the 3ft and 5.5ft tests were 147.6 kips (657 kN) and

524.2 kips (2332 kN), respectively. Table 5.14 in Section 5.2 reports that the PYCAP values used are within 12% of the measured results and can logically be related to the field results. As such, the measured peak passive forces and the calculated PYCAP components were used in the calculations. After removing the edge shear effects with the Brinch-Hansen (1966) 3D correction factor, the 2D passive forces came to 114.2 kips (508 kN) and 215.8 kips (960 kN) for the 3ft and 5.5ft backfills, respectively. The cohesion contributions of 33.7 kips (150 kN) and 62.4 kips (278 kN) for the respective 3ft and 5.5ft tests were removed from the 2D passive forces to determine a comparable cohesionless 2D passive force for each of the unconfined backfills. The forces for the 3ft and 5.5ft tests were determined to be 80.5 kips (358 kN) and 202.3 kips (900 kN), respectively.

In Table 5.6, the passive force contributions provided by the 3D edge effects and cohesion are listed as a percentage of the total passive force. The combined percent contribution is slightly higher for the 5.5ft test at 58% than that of the 3ft test at 53%, which suggests the lower backwall is more influenced by the friction angle. The amount of force supplied by each variant between the different components is also insightful. The 3ft test is only slightly more influenced by the 3D factor than the cohesion. The 5.5ft test is influenced almost five times more by the 3D effects than the cohesion factor. Relatively, cohesion provided slightly more force to the 3ft test than the 5.5ft test, with 20% and 13% respective contributions. These percentages suggest that the passive force is increasingly influenced by the friction angle, and simultaneously less affected by cohesion as the height of the backwall increases. In addition, for a given wall width, the 3D edge effects become more pronounced as the wall height increases. The effects of the cohesion and 3D edge effects on the measured passive force - deflection curves are shown in Figure 5.6. As demonstrated, removing the cohesion variable affects the 3ft passive force

relatively more than the 5.5ft curve. While removing the 3D effects lowers the 5.5ft passive force relatively more than with the 3ft force. The similar effect of each contribution on the 3ft curve is also seen. Although the error between the measured curves and the calculated PYCAP curves may cause the contributions and percentages to vary, the results support that a trend between backfill height and passive force contributions exists.

Table 5.5: Comparison of passive force contributions for the 0° skew 3ft and 5.5ft tests using PYCAP parameters

	3ft	*5.5ft*
Total measured passive force [kip (kN)]	167.6 (746)	480.5 (2137)
3D correction factor	1.468	1.815
3D effect contribution [kip (kN)]	53.4 (238)	215.8 (960)
2D passive force [kip (kN)]	114.2 (508)	264.7 (1177)
Cohesion contribution [kip (kN)]	33.7 (150)	62.4 (278)
Cohesionless 2D passive force [kip (kN)]	80.5 (358)	202.3 (900)

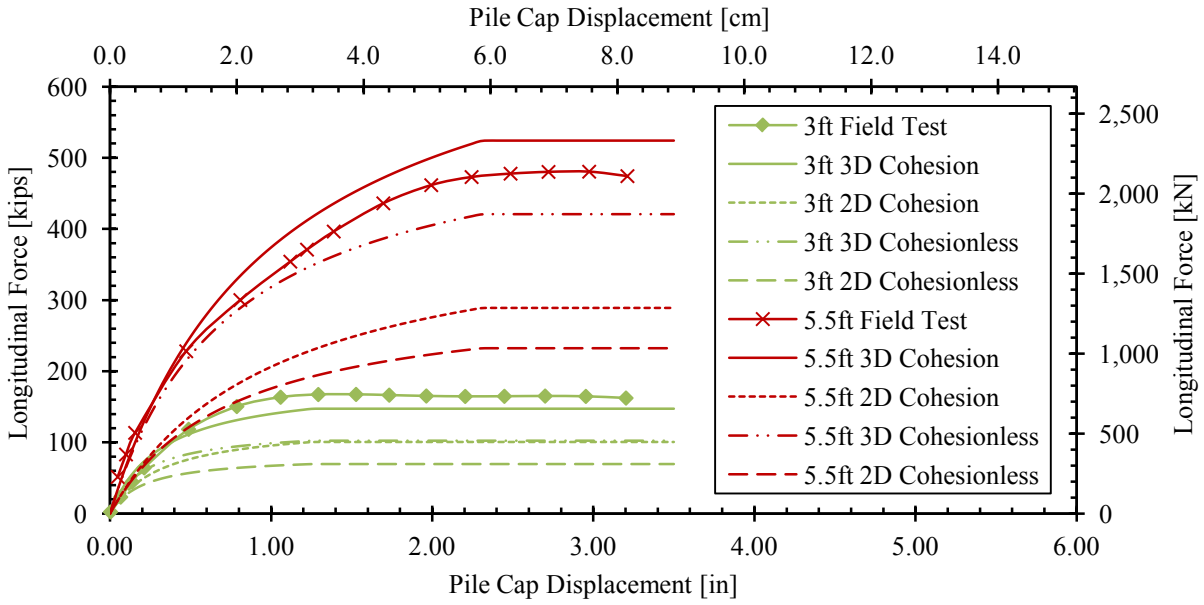

Figure 5.6: Effects of cohesion and Brinch-Hansen (1966) 3D correction factor on passive force for 3ft and 5.5ft unconfined tests using PYCAP

Table 5.6: Percent contribution of passive forces for 3ft and 5.5ft tests

	Percent Contribution [%]	
	3ft	*5.5ft*
3D effects	32	45
Cohesion	20	13
Combined 3D and cohesion	52	58

The comparison of the height and force ratios are presented in Table 5.7. Based on a ratio of $(H_1/H_2)^2$ with H_1 and H_2 being respectively 5.5 ft (1.68 m) and 3 ft (0.91 m), the passive resistance ratio should match 3.36. Using the calculated cohesionless 2D forces from Table 5.5, the ratio comes to a smaller value of 2.51. The exponent on the height ratio has been previously proposed to give a closer estimate of the force ratio with a value closer to 1.5 for sand backfills (Shamsabadi, et al. 2010). To scale the height for backfills with both cohesion and friction, an exponent between 1 and 2 is suggested (Stewart, et al. 2011). In this case, exponents of 1.4 or 1.5 for 2D passive force with cohesion or frictional resistance, respectively, fall within this more suitable range. As seen in Table 5.4, the soil properties between the two field tests are the same besides the backfill height and the unit weight of the soil. Even so, the soil unit weights are within 0.5 pcf (0.1 kN/m^3) of each other and do not cause great difference when calculated with the PYCAP program. Some amount of error could also possibly be attributed to potential variations in soil properties between the two tests. Because the PYCAP program was used to match both field tests, neither result exactly followed the measured field curves, as shown in Figure 5.2, which could also contribute some error. Error could also be because the measured field curves were used to calculate the forces, using the PYCAP values which did not completely match the curves.

Table 5.7: Passive force and height ratio comparison

Ratio	*(5.5ft/3ft)*
Height $(H/H)^2$	3.36
Passive force (corrected for 3D effects)	2.32
Passive force (based on frictional resistance)	2.51

5.1.2 AASHTO Design Method

Using the design parameters included in Table 5.8, the AASHTO curves for each test were plotted in Figure 5.7. The values for K_p were estimated using Figure 3.5.11.4-2 in section 3.11.5.4 of the 2011 specifications (AASHTO 2011). For the 3ft and 5.5ft tests, the K_p value was estimated to be 21 with a reduction factor R of 0.720. The MSE test K_p was estimated to be 35 with a reduction factor of 0.659. The peak displacement for each test was estimated as 2% of the backwall height as recommended in the AASHTO (2011) design manual. The peak values for the 3ft, 5.5ft, and MSE wall tests were 137 kips (609 kN), 515 kips (2292 kN), and 442 kips (1966 kN), respectively. Compared to field peak resistance, the AASHTO design curves underestimated the 3ft peak passive force by 22%, and overestimated the 5.5ft by 7% and MSE test by 24.3%. Error for both the unconfined tests is within a reasonable range. The 3ft AASHTO curve seems to best follow the shape of the field curve, but misinterprets the stiffness of both the 5.5ft tests. The 5.5ft and MSE wall AASHTO curves peak at an earlier horizontal displacement than the field curves show, thus giving false force estimations at earlier displacements.

Table 5.8: Parameters used with AASHTO approach to compare passive force – deflection curves for 3ft, 5.5ft, and MSE wall tests

Parameter	*3ft*	*5.5ft*	*MSE*	*Units*
Soil Friction Angle, ϕ	41.2	41.2	45.3	degrees
Soil Unit Weight, γ_s	117.0 (18.4)	116.5 (18.3)	117.4 (18.4)	pcf (kN/m^3)
Abutment Width, w_2	11 (3.35)	11 (3.35)	11 (3.35)	ft (m)
3D Width Corr. Factor	1.468	1.815	N/A (2-D failure)	–
Effective Width of Failure Wedge, w_1	16.1 (4.92)	20.0 (6.09)	11.0 (3.35)	ft (m)
Soil Cohesion, c	100.0 (4.79)	100.0 (4.79)	100.0 (4.79)	psf (kN/m^2)
Abutment Height, H	3.0 (0.91)	5.5 (1.68)	5.5 (1.68)	ft (m)
Interface Friction Angle, δ	27.0	27.0	29.6	degrees
Interface/Soil Friction Angle Ratio, δ/ϕ	0.654	0.654	0.654	
Coefficient of Passive Earth Pressure, K_p	15.1	15.1	23.1	–

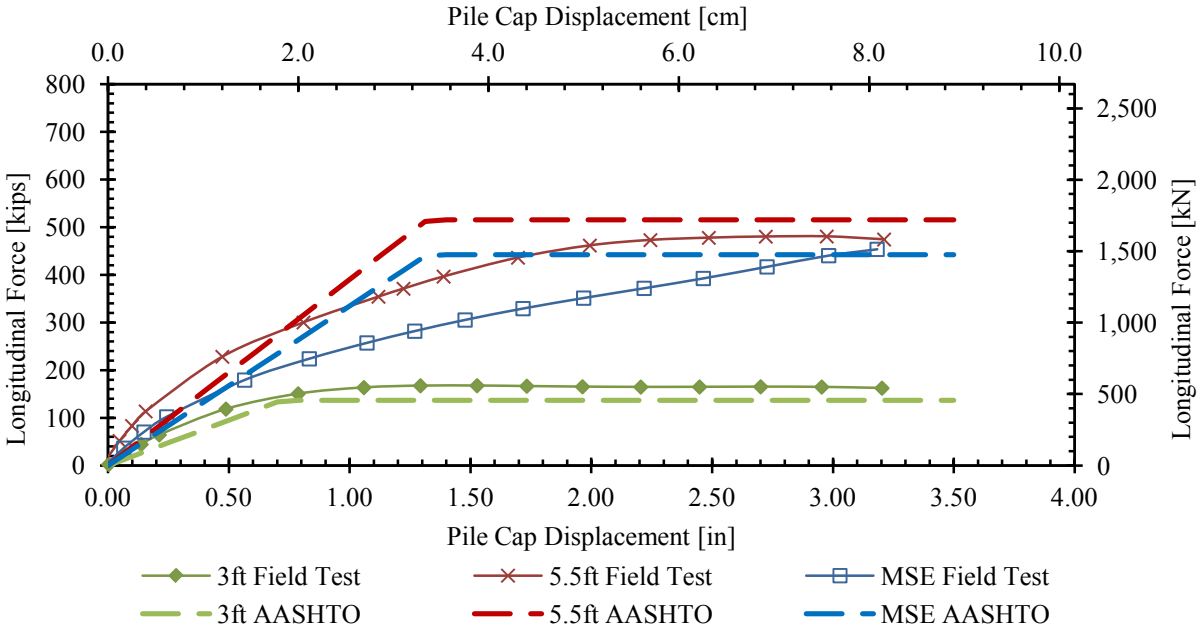

Figure 5.7: Comparison of AASHTO design curve with the passive force vs. backwall deflection curve for the 3ft, 5.5ft, and MSE wall tests

5.1.3 Caltrans Design Method

As outlined in Section 2.1.6, the Caltrans predictive method uses generalities based on previous passive force testing. Equation (2.7) calculates the passive force based on the effective area of the backwall, the maximum passive force found with previous tests, and is adjusted with the backwall height from the conducted tests. The abutment stiffness is calculated with Equation (2.6) and based on appropriate soil conditions to determine the initial stiffness value used. The Caltrans approach parameters were determined from soil type and wall geometry, and are summarized in Table 5.9. The Brinch-Hansen (1966) 3D correction factors were calculated through PYCAP.

To find the backwall area, the effective widths of the unconfined backfills were used to account for the 3D end effects. Because the MSE test was assumed to fail with a plane strain condition, the actual width of the backwall was used. Assuming the backfills met the soil conditions listed in the Caltrans (2010) Standard Specifications, the higher initial stiffness parameter was used, and these results are shown in Figure 5.8. Both the 5.5ft and MSE wall tests did not need the height adjustment as they both matched the 5.5 ft (1.68 m) backwall height of the Caltrans tests. The 3ft test was reduced with a linear height ratio according to the Caltrans (2010) Specifications. However, a closer fit to the 3ft field curve was achieved by increasing the height ratio with a 0.75 exponent rather than an exponent of 1.0. The curve using the 0.75 exponent is shown in Figure 5.9.

The calculated peak force values for the 3ft, 5.5ft, and MSE wall tests are 132 kip (587 kN), 549 kip (2442 kN), and 303 kip (1348 kN), respectively. Peak field data for each test compare with values of 168 kips (746 kN), 481 kips (2137 kN), and 454 kips (2018 kN), respectively. The Caltrans method overestimates the 5.5ft peak resistance by only 14.1%.

Comparatively, it underestimates the 3ft and MSE wall peaks by 21.4% and 33.3%, respectively. For the 5.5ft and MSE tests, more error is seen at smaller displacements due to the higher stiffness. In Figure 5.8, the 5.5ft Caltrans curve reaches the peak at a much lower displacement assuming the field resistance to be almost twice as much as actually recorded. However, the agreement with the 3ft test seems reasonable. The shape of the MSE field curve compared with the Caltrans prediction seems to defy the Caltrans assumptions. As described in Section 4.2.2, the MSE test may not have reached a peak passive force. The Caltrans method does not account for the increased resistance of the MSE walls and grids within the backfill, which only assumes a plane strain failure similar to the 5.5ft test. More research on MSE passive force would be useful in adjusting the Caltrans method to more appropriately address the increased force that MSE walls and grids provide.

Table 5.9: Parameters used with Caltrans approach to compare passive force – deflection curves for 3ft, 5.5ft, and MSE wall tests

Parameter	*3ft*	*5.5ft*	*MSE*	*Units*
Most Appropriate Initial Backfill Stiffness, K_i	50 (28.7)	50 (28.7)	50 (28.7)	kip/in/ft (kN/mm/m)
Projected Wall Width, w	11 (3.35)	11 (3.35)	11 (3.35)	ft (m)
3D Width Correction Factor	1.468	1.815	1.000	–
Effective Wall Width, w_e	16.1 (4.9)	20.0 (6.1)	11 (3.35)	ft (m)
Abutment Stiffness, K_{abut}	453 (79.4)	491 (86.1)	275 (48.2)	kip/in (kN/mm)
Wall Height, h	3.0 (0.91)	5.5 (1.68)	5.5 (1.68)	ft (m)
Effective Backwall Area, A_e	47.1 (4.38)	105.6 (9.81)	60.5 (5.62)	ft^2 (m^2)

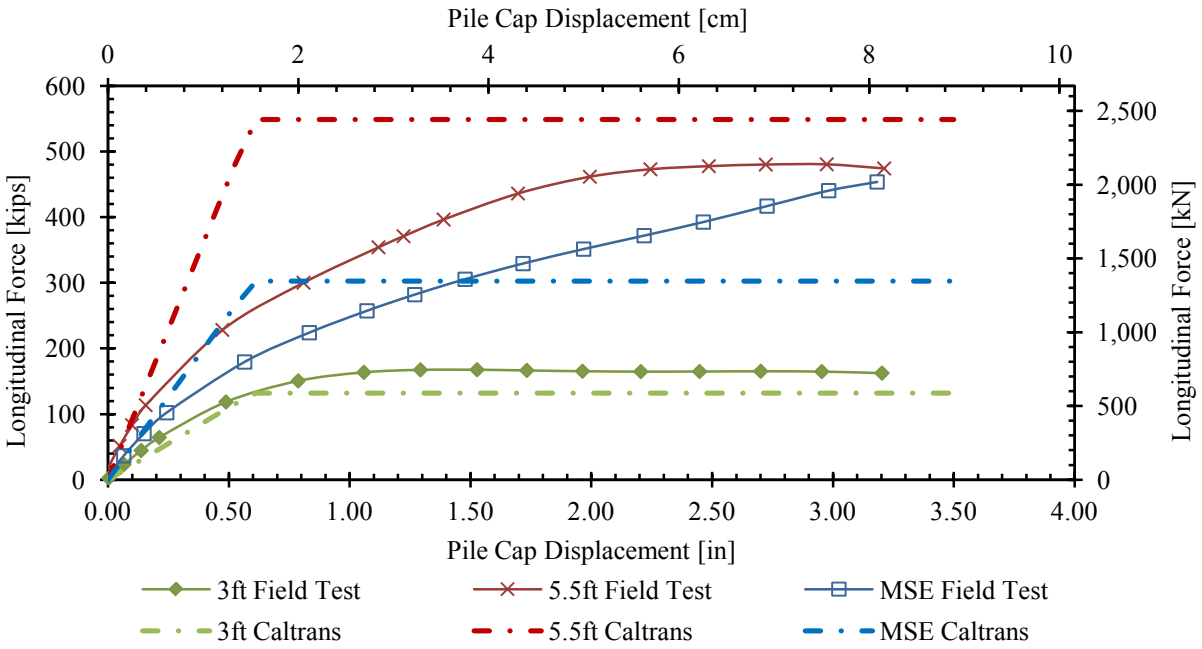

Figure 5.8: Comparison of Caltrans design curve with the passive force vs. backwall deflection curve for 3ft, 5.5ft, and MSE wall tests

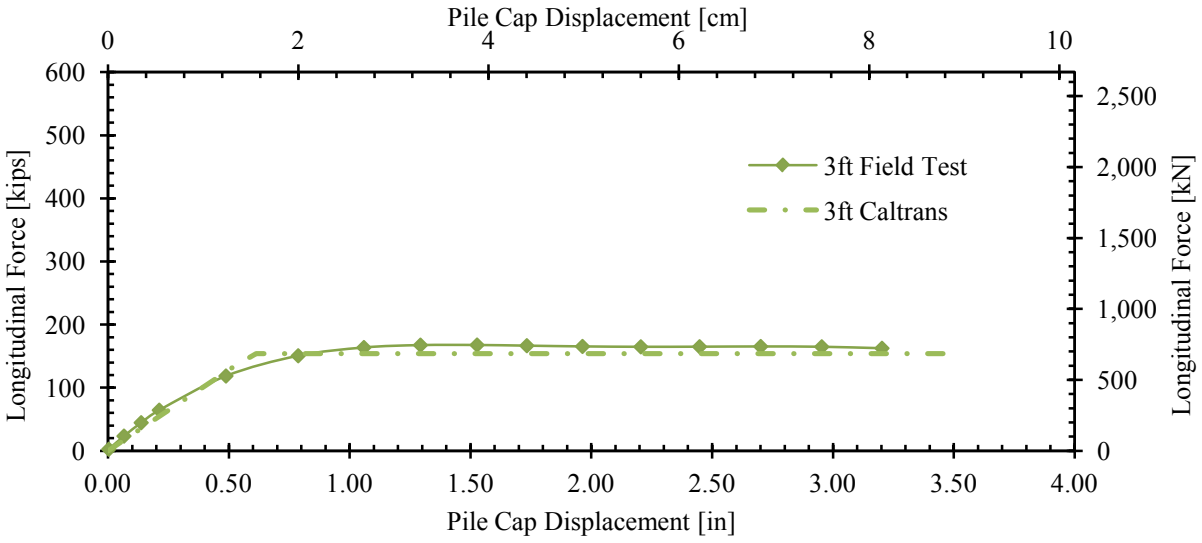

Figure 5.9: Comparison of the Caltrans predicted curve using a height ratio of (3ft/5.5ft)$^{0.75}$

5.1.4 ABUTMENT Design Curve

The curves derived from Shamsabadi's (2007) ABUTMENT program are plotted in Figure 5.10. The soil parameters initially used in the analyses are listed in Table 5.10 and are the same values used in the PYCAP analyses. Recommended values for ε_{50} are listed in Table 5.11 and typical R_f values should be between 0.94 and 0.98 (Shamsabadi, et al. 2007). For the tests in this study, the recommended ε_{50} and R_f values were not high enough to achieve agreement with the field curves. Other comparisons have also needed to increase the ε_{50} to match the field curves (Bingham 2012, Marsh 2013, Palmer 2013, Rollins, et al. 2010, Strassburg 2010). In Figure 5.10, the MSE test has a higher ε_{50} value and a lower R_f to match the measured curve, which was also done by Franke (2013). Within ABUTMENT, the peak passive force was computed using the "Log Spiral – Modified Moment Method". The MSE wall test was analyzed using a 2D failure plane, while the 3ft and 5.5ft tests were considered 3-dimensional with edge effect corrections using the Brinch-Hansen (1966) equation.

The computed passive force-deflection curves for both the unconfined tests are overestimated using the initial parameters. At the peak resistance of the field tests the 3ft, MSE, and 5.5ft predicted peak forces were estimated to be 192 kips (854 kN), 415 kips (1846 kN), and 655 kips (2914 kN), respectively. These values correspond to percent errors of 14%, 8.6%, and 136% from the measured peak passive forces for the 3ft, MSE, and 5.5ft tests, respectively. Increasing the ε_{50} strain increased the amount of displacement needed to reach the peak value, which also lowered the curve. Based on the measured field curves, higher strain values have been quite typical (Bingham 2012, Rollins, et al. 2010, Strassburg 2010). Although the ABUTMENT curves continuously increase in force, the rounded shape of the curves more closely follow the field curves as opposed to the AASHTO and Caltrans design curves. The MSE

curve most likely aligns better with the field curve because of the individually adjusted parameters.

Table 5.10: Parameters used with ABUTMENT approach to compare passive force – deflection curves for 3ft, 5.5ft, and MSE wall tests

Soil Parameter	*3ft*	*5.5ft*	*MSE*	*Units*
Friction Angle, ϕ	41.2	41.2	45.3	degrees
Interface Friction Angle, δ	27.0	27.0	29.6	degrees
Soil Density, γ	117.0 (18.4)	116.5 (18.3)	117.4 (18.4)	pcf (kN/m^3)
Cohesion, c	100 (4.79)	100 (4.79)	100 (4.79)	psf (kN/m^2)
Strain at 50% of Max Load, ε_{50}	0.0035	0.0035	0.014	–
Poisson's Ratio, ν	0.25	0.25	0.25	–
Failure Ratio, R_f	0.98	0.98	0.90	–

Table 5.11: Range of values for ε_{50} [taken from Shamsabadi, et al. (2007)**]**

	ε_{50}	
Predominant soil type	Range	Presumptive value
Gravel	0.001–0.005	
Clean sand (0–12% fines[a])	0.002–0.003	0.0035
Silty sands (12–50% fines[a])	0.003–0.005	
Silt	0.005 (nonplastic)–0.007 (plastic)	
Clay	0.0075	0.007

[a]Fines is the percentage by weight of soil grain sizes smaller than 0.075 mm.

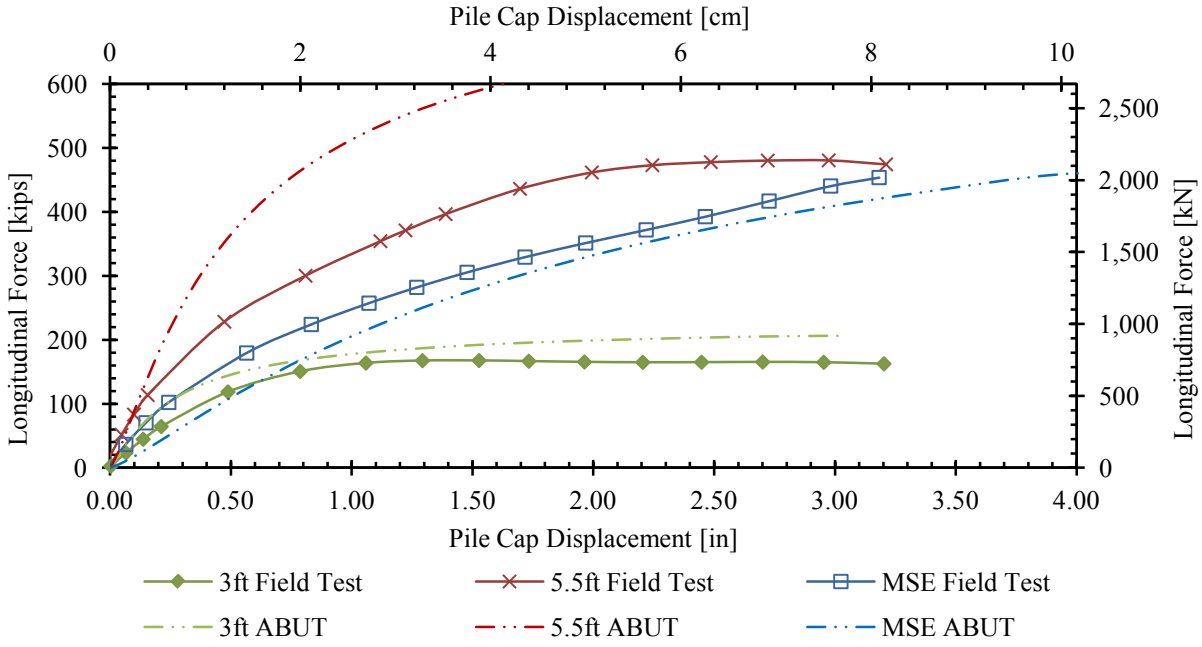

Figure 5.10: Comparison of ABUTMENT design curves with the passive force vs. backwall deflection curves for the 3ft, 5.5ft, and MSE wall tests

5.2 Comparison of Results with Rankine, Coulomb, and Log Spiral Methods

The ultimate horizontal passive force predicted by the Rankine, Coulomb, and Log Spiral methods, as described in Section 2.1, was calculated and compared to the measured field values for each zero degree skew test. Table 5.12 summarizes the calculated passive force per width and the total passive force values determined by each predictive method. Values used in the predictive equations were determined using the best-fit PYCAP curves and are summarized in Table 5.13. The 3D correction factors were calculated using the Brinch-Hansen (1966) equation and applied for the 3ft, 5.5ft, and MSE wall tests, respectively. As compared to the measured failure wedges, listed in Section 4.1.1, the determined widths were within 9% and 10% for the 3ft and 5.5ft tests, respectively. The total passive forces listed in Table 5.12 were divided by the effective widths to calculate the passive forces per unit width. The estimated values predicted by

the Coulomb, Rankine, and Log Spiral methods and field comparisons are as expected based on previous testing (Duncan and Mokwa 2001, Franke 2013, Lemnitzer, et al. 2009, Marsh 2013, Palmer 2013, Rollins and Cole 2006, Rollins and Sparks 2002). As seen by the percentages in Table 5.14, the Coulomb method significantly overestimated the passive force in each test; the Rankine method significantly underestimated the passive force in each test; and the Log Spiral method was the closest to predicting the measured passive force in each test.

By comparing the percent error values with the error determined by Franke (2013), Marsh (2013), and Palmer (2013) in Table 5.15, the Log Spiral is again seen as the most accurate with an even smaller amount of error. The values in both tables also roughly emulate the margin of error between the PYCAP curves when matched to the field curves. In the results from each individual thesis, the PYCAP curves were optimized using the maximum passive force for each curve. In Figure 5.1, the values were optimized individually for each test, and therefore have a much smaller amount of error. The overestimation of the Log Spiral passive force for the MSE wall test is most likely attributed to the test not reaching a peak passive force value (Franke 2013). In Figure 5.2, the values were optimized to the 3ft and 5.5ft tests together, introducing a ±12% margin of error. As illustrated in both in Figure 5.2 and Table 5.14, the Log Spiral curve underestimated the 3ft curve and overestimated the 5.5ft curve. The smaller percent error for the MSE wall test is most likely due to individually optimizing the PYCAP values. As seen in these examples, the high degree of accuracy of the Log Spiral method was due to the previously optimized input parameters. However, PYCAP is still a useful tool in estimating the field performance and in conducting sensitivity studies.

Table 5.12: Calculated passive force for Coulomb, Rankine, and Log Spiral methods

Test	*Method*	*Passive Force per ft kip/ft (kN/m)*	*Total Passive Force kips (kN)*
3ft	Coulomb	11.37 (166)	183.1 (814)
	Rankine	2.56 (37.3)	41.2 (183)
	Log Spiral	9.40 (137)	147.6 (657)
	Field Results	10.68 (156)	167.6 (746)
5.5ft	Coulomb	38.06 (554)	761.2 (3386)
	Rankine	8.56 (125)	171.3 (762)
	Log Spiral	27.30 (398)	524.2 (2332)
	Field Results	25.05 (366)	480.5 (2137)
MSE	Coulomb	81.13 (1182)	892.4 (3970)
	Rankine	10.50 (153)	115.5 (514)
	Log Spiral	40.32 (180)	463.7 (2063)
	Field Results	39.48 (176)	453.7 (2018)

Table 5.13: Parameters used with predictive methods for 3ft, 5.5ft, and MSE tests

Parameter	*3ft*	*5.5ft*	*MSE*	*Units*
Cap Width, b	11 (3.35)	11 (3.35)	11 (3.35)	ft (m)
Cap Height, H	3.0 (0.91)	5.5 (1.68)	5.5 (1.68)	ft (m)
Soil Friction Angle, ϕ	41.2	41.2	45.3	degrees
Wall Friction Angle, δ	27.0	27.0	29.6	degrees
Soil Unit Weight, γ_m	117.0 (18.4)	116.5 (18.3)	117.4 (18.4)	pcf (kN/m^3)
Brinch-Hansen (1966) 3D Correction Factor	1.468	1.815	1.000	-
Effective Widths	16.1 (4.9)	20.0 (6.1)	11.0 (3.35)	ft (m)

Table 5.14: Comparison of predicted total passive force values to measured total passive force in percent error

Test	*Total Passive Force Percent Error (%)*		
	Coulomb	*Rankine*	*Log Spiral*
3ft	9.2	-75.5	-11.9
5.5ft	158.4	-64.3	9.1
MSE	196.7	-74.5	2.2

Table 5.15: Comparison of predicted total passive force values to measured total passive force in percent error [Adapted from Franke 2013, Marsh 2013, and Palmer 2013]

Test	*Total Passive Force Percent Error (%)*		
	Coulomb	*Rankine*	*Log Spiral*
3ft	75.0	-61.3	-0.10
5.5ft	47.0	-60.0	-1.50
MSE	115.0	-63.0	10.0

6 CONCLUSIONS AND RECOMMENDATIONS

This thesis presents results from a series of laterally loaded tests on a large-scale pile cap including unconfined backfill heights of 3 ft (0.91 m) and 5.5 ft (1.68 m), and a 5.5 ft (1.68 m) backfill with MSE wall supports. The purpose of this study is to determine the effects of the wall heights and of the MSE support on passive pressure and backfill failure, and compare the field results with various predictive methods. Based on the results and analysis on this series of tests, a number of conclusions and recommendations can be made. Further research is recommended to compare test results between backfill heights for skewed abutments to see if the differences are similar when a skew angle is introduced

6.1 Conclusions Relative to Failure Geometry

1. The failure surface for the unconfined backfills exhibited a more 3D geometry with failure surfaces extending beyond the edge of the cap, increasing the "effective width", and producing a failure "bulb". In contrast, the constraint provided by the MSE wingwalls produced a more 2D failure geometry.
2. The "effective width" of the failure surface increased as the width to height ratio decreased. The effective width predicted using the Brinch-Hansen (1966) equation was typically about 5% less than the measured effective width.

3. For each test, the length of the passive failure wedge was typically about 3.2 times the wall height for the sand tested.
4. Both the 3ft and 5.5ft unconfined backfills shear failure zones were similar to a log spiral failure geometry. However, the MSE walls and grids seemed to hold the soil mass together so a traditional failure "bulb" was complicated by outward movement of the walls. Nevertheless, the heave patterns suggest a similar length of the failure surface.
5. Compressive strain for all tests was highest in the first 2 ft (0.61 m) of the failure zone behind the pile cap and then decreased significantly within the failure mass. This suggests that most of the failure surface is moving as a block. The MSE walls and grids presumably reduced the strain on the soil mass as the reinforcements kept the backfill from compressing.

6.2 Conclusions Relative to Measured Passive Force

1. As the wall height for the unconfined backfill increased from 3ft to 5.5ft, the passive force increased by 2.87 times in displacing about 2 times the mass. If 3D geometry and cohesion contributions are ignored, this increase can be explained using a height ratio with an exponent of 1.75 rather than 2.0 as in classical theories.
2. In terms of total passive force, the unconfined 5.5ft wall provided about 6% more resistance than the 5.5ft MSE wall. However, in terms of passive force/width the MSE wall provided about 70% more resistance than the unconfined wall. Most likely, the MSE test failed with a plane strain, or 2-dimensional, geometry which

generally contributes to a greater soil strength than a triaxial, or 3-dimensional, failure geometry.

3. The peak passive pressures occurred at normalized deflections of 0.043H, 0.045H, and 0.048H for the 3ft unconfined fill, the 5.5ft unconfined fill, and the 5.5ft MSE fill, respectively. All values fell within the high end of the previously suggested range (Rollins and Cole 2006). However, the MSE test might have exceeded the range if pushed beyond the assumed peak value. Further testing is recommended to discover and compare an actual peak force and displacement for tests including MSE walls.

6.3 Conclusions Relative to Computed Passive Force

1. The passive force computed using the Log Spiral approach produced the best agreement (<12% error) with the measured passive force for the three tests. In contrast, the Rankine method significantly underestimated the resistance (≈70% low), while the Coulomb method significantly overestimated the passive resistance (over 100% high).
2. To match the measured passive force for the MSE wall test using the Log Spiral method, it was necessary to use a plane strain friction angle which was about 10% higher than the triaxial friction angle which produced acceptable agreement for the unconfined wall tests. These results suggest that a plane strain friction angle should be used in computing the passive force for walls where the failure geometry is close to a 2D geometry.

3. The predicted peak passive forces from the AASHTO approach overestimated the 5.5ft unconfined test by only 7% and the 5.5ft MSE test by 24%, while the 3ft test was underestimated by 22%.
4. The Caltrans method overestimates the 5.5ft peak resistance by only 14.1%. Comparatively, it underestimates the 3ft peak by 21.4% and significantly underestimates the MSE wall peak 33.3%. The Caltrans method does not account for the increased resistance of the MSE walls and grids within the backfill, which only assumes a plane strain failure similar to the 5.5ft test.
5. As the height of the backwall increased for the unconfined tests, the passive force was influenced more by frictional resistance and less by the cohesion. Relatively, cohesion provided 20% of the total passive force for the 3ft test but only 13% of the passive force for the 5.5ft test.
6. As the wall height increased from 3ft to 5.5ft, the wall width to height ratio decreased and the effective width increased. This led to a higher 3D correction factor for the 5.5ft wall than the 3ft wall.
7. After removing the 3D edge and cohesion effects, the field tests for the 3ft and 5.5ft walls indicate that the exponent for the height term is between 1.0 and 2.0 as indicated in classical passive pressure equations.

6.4 Conclusions Regarding Computed Load-Deflection Relationships

1. The bi-linear passive force-displacement curves proposed by Caltrans were unable to consistently match the measured curves using the 50 k/in/ft criteria.
2. Using the same PYCAP parameters, Shamsabadi's (2007) ABUTMENT program had higher curves. As seen in previous comparisons, an increased ε50 value better

matches the field curves. The rounded shape of the ABUTMENT curves more completely match the measured field curves as opposed to the AASHTO and Caltrans design curves.

3. The AASHTO design method had relatively good agreement with the unconfined field tests, but overestimated the stiffness of the 5.5ft and MSE field tests.
4. For the MSE curve, the Caltrans prediction significantly underestimated the passive force curve. Further research would be useful in adjusting the Caltrans method to more appropriately address the increased resistance that MSE walls and grids provide. While with a steeper abutment stiffness, the Caltrans design curve followed the 5.5ft field test relatively well. The 3ft Caltrans design curve fit the field curve more closely with a non-linear height adjustment of $(H/5.5\ ft)^{0.75}$. More research is recommended to validate this type of height adjustment.

REFERENCES

AASHTO (2011). Guide Specifications for LRFD Seismic Bridge Design.

Apirakyorapinit, P., Mohammadi, J. and Shen, J. (2012). "Analytical Investigation of Potential Seismic Damage to a Skewed Bridge." *Practice Periodical on Structural Design and Construction*, 16(1), 5-12.

Bingham, N. G. (2012). "Passive Resistance of Abutments with MSE Wingwalls." Master of Science, Department of Civil and Environmental Engineering, Brigham Young University, Provo, UT.

Brinch Hansen, J. (1966). "Resistance of a Rectangular Anchor Slab." *Bullentin No. 21*, Danish Geotechnicl Institute, Copenhagen, 12-13.

Caltrans (2010). "Seismic Design Criteria Version 1.6." California Department of Transportation, Sacramento, California.

Christensen, D. S. (2006). "Full Scale Static Lateral Load Test of a 9 Pile Group in Sand." M.S., Department of Civil and Environmental Engineering, Brigham Young University,

Clough, G. W. and Duncan, J. M. (1991). *Foundation engineering hand-book.* Chapman and Hall, New York.

Cole, R. T. and Rollins, K. M. (2006). "Passive earth pressure mobilization during cyclic loading." *Journal of Geotechnical and Geoenvironmental Engineering, ASCE*, 132(9), 1154-1164.

Coulomb, C. A. (1776). "Essai sur une application des regles des maximis et minimis a quelques problemes de statique relatifs a l'architecture." *Memoires de l'Academie Royale pres Divers Savants*, 7.

Cummins, C. R. (2009). "Behavior of a Full-Scale Pile Cap with Loosely and Densely Compacted Clean Sand Backfill Under Cyclic and Dynamic Loadings." Master of Science, Civil and Environmental Engineering, Brigham Young University, Provo, UT.

Das, B. M. (2010). *Principles of Geotechnical Engineering.* Cengage Learning, Connecticut.

Douglas, D. J. and Davis, E. H. (1964). "The Movement of Buried Footings due to Moment and Horizontal Load and the Movement of Anchor Plates." *Geotechnique*, 14(2), 115-132.

Duncan, J. M. and Mokwa, R. L. (2001). "Passive Earth Pressures: Theories and Tests." *Journal of Geotechnical and Geoenvironmental Engineering*, 127(3), 248-257.

Elnashai, A. S., Gencturk, B., Kwon, O., Al-Qadi, I. L., Hashash, Y., Roesler, J. R., Kim, S. J., Jeong, S., Dukes, J. and Valdivia, A. (2010). "The Maule (Chile) Earthquake of February 27, 2010: Consequence Assessment and Case Studies." Department of Civil and Environmental Engineering, University of Illinois at Urbana-Champaign,

Franke, B. (2013). "Passive Force of Skewed Abutments with Mecanically Stabilized Earth (MSE) Wingwalls Based on Large-Scale Tests." Master of Science, Department of Civil and Environmental Engineering, Brigham Young University, Provo, UT.

Johnson, S. R. (2003). "Static lateral load testing a full-scale pile group spaced at 5.65 pile diameters." M.S., Department of Civil and Environmental Engineering, Brigham Young University, Provo, UT.

Kunin, J. and Alampalli, S. (1999). "Integral Abutment Bridges: Current Practice in the United States and Canada (N. Y. S. D. o. Transportation, Trans.)." Albany, New York: Transportation Research and Development Bureau.

Lee, K. L. and Singh, A. (1971). "Relative Density and Relative Compaction." *Journal of Soil Mechanics and Foundations Design*, 97(7), 1049-1052.

Lemnitzer, A., Ahlberg, E. R., Nigbor, R. L., Shamsabadi, A., Wallace, J. W. and Stewart, J. P. (2009). "Lateral Performance of Full-Scale Bridge Abutment Wall with Granular Backfill." *Journal of Geotechnical and Geoenvironmental Engineering*, 135(4).

Maroney, B. H. (1995). "Large Scale Abutment Tests to Determine Stiffness and Ultimate Strength Under Seismic Loading." Ph.D., Civil & Environmental Engineering, University of California, Davis, Davis, CA.

Marsh, A. K. (2013). "Evaluation of Passive Force on Skewed Bridge Abutments with Large-Scale Tests." M.S., Department of Civil and Environmental Engineering, Brigham Young University, Provo, UT.

Measurand, Inc. (2011). "ShapeAccelArray (SAA) Installation Guide." http://measurandgeotechnical.com/Installation_Guide_2011.pdf, 02/08/2013.

Mokwa, R. and Duncan, J. (2001). "Experimental Evaluation of Lateral-Load Resistance of Pile Caps." *Journal of Geotechnical and Geoenvironmental Engineering*, 127(2), 185-192.

Nasr, M. and Rollins, K. M. (2010). "Numerical Analysis of Limited Width Dense Gravel Backfills for Plane Strain Conditions."

Ovesen, N. K. (1964). "Anchor slabs, calculation methods, and model tests." *Bulletin No. 16*, Danish Geotechnical Institute(Copenhagen), 5-39.

Palmer, K. N. (2013). "Large-Scale Testing of Passive Force Behavior for Skewed Abutments with High Width-Height Ratios." M.S., Department of Civil and Environmental Engineering, Brigham Young University, Provo, UT.

Peterson, K. T. (1996). "Static and Dynamic Lateral Load Testing a Full-Scale Pile Group in Clay." M.S., Department of Civil and Environmental Engineering, Brigham Young University,

Potyondy, J. G. (1961). "Skin Friction between Various Soils and Construction Materials." *Geotechnique*, 11(4), 339-353.

Rankine, W. J. (1857). "On the Stability of Loose Earth." *Philosophical Transactions of the Royal Society of London*, 147, 29-42.

Rollins, K. M. and Cole, R. T. (2006). "Cyclic Lateral Load Behavior of a Pile Cap and Backfill." *Journal of Geotechnical and Geoenvironmental Engineering, ASCE*, 132(9), 1143-1153.

Rollins, K. M., Gerber, T. M. and Heiner, L. (2010). "Passive Force-Deflection Behavior for Abutments with MSE Confined Approach Fills." Brigham Young University Department of Civil & Environmental Engineering, Salt Lake City, UT.

Rollins, K. M. and Jessee, S. (2012). "Passive Force-Deflection Curves for Skewed Abutments." *Journal of Bridge Engineering*, 17(5).

Rollins, K. M. and Sparks, A. E. (2002). "Lateral Load Capacity of a Full-Scale Fixed-Head Pile Group." *Journal of Geotechnical and Geoenvironmental Engineering, ASCE*, 128(9), 711-723.

Sandford, T. C. and Elgaaly, M. (1993). "Skew Effects on Backfill Pressures at Frame Bridge Abutments."

Shamsabadi, A., Kapuskar, M. and Zand, A. (2006). "Three-Dimensional Nonlinear Finite-Element Soil-Abutment Structure Interaction Model for Skewed Bridges." *5th National Seismic Conference On Bridges and Highways*, San Francisco, CA.

Shamsabadi, A., Khalili-Tehrani, P., Stewart, J. P. and Taciroglu, E. (2010). "Validated simulation models for lateral respnse of bridge abutments with typical backfills." *J. Bridge Eng.*, 15(3), 302-312.

Shamsabadi, A., Rollins, K. M. and Kapaskur, M. (2007). "Nonlinear Soil-Abutment-Bridge Structure Interaction for Seismic Performance-Based Design." *Journal of Geotechnical and Geoenvironmental Engineering, ASCE*, 133(6), 707-720.

Snyder, J. L. (2004). "Full-scale lateral-load tests of a 3x5 pile group in soft clays and silts." M.S., Department of Civil and Environmental Engineering, Brigham Young University, Provo, UT.

Stewart, J. P., Taciroglu, E., Wallace, J. W., Lemnitzer, A., Hilson, C. H., Nojoumi, A., Keowan, S., Nigbor, R. L. and Salamanca, A. (2011). "Nonlinear Load-Deflection Behavior of Abutment Backwalls with Varying Height and Soil Density." University of California, Los Angeles, Los Angeles, CA.

Stewart, P. S., Taciroglu, E., Wallace, J. W., Ahlberg, E. R., Lemnitzer, A., Rha, C. and Tehrani, P. K. (2007). "Full Scale Cyclic Testing of Foundation Support Systems for Highway Bridges, Part II: Abutment Backwalls." Department of Civil and Environmental Engineering, University of California, Los Angeles, CA,

Strassburg, A. N. (2010). "Influence of Relative Compaction on Passive Resistance of Abutments with Mechanical Stabilized Earth (MSE) Wingwalls." Department of Civil and Environmental Engineering, Brigham Young University, Provo, UT.

Terzaghi, K. (1943). *Theoretical soil mechanics.* J. Wiley & Sons, Chapman and Hall, New York.

Terzaghi, K., Peck, R. B. and Mesri, G. (1996). *Soil mechanics in engineering practice.* Wiley, New York.

Toro, F., Rubilar, F., Hube, M. A., Santa-Maria, H. and Cabrera, T. (2013). "Statistical Analysis of Underpasses Damaged During 2010 Chile Earthquake." *Paper presented at the National Seismic Conference on Highways and Bridges*.

Unjohn, S. (2012). "Repair and Retrofit of Bridges Damaged by the 2010 Chile, Maule Earthquake." Tokyo, Japan.

Walsh, J. M. (2005). "Full scale lateral load test of a 3x5 pile group in sand." M.S., Department of Civil and Environmental Engineering, Brigham Young University, Provo, UT.